An Investigation Into The Characterisation Of The Spalling Behaviour Of Polycrystalline Diamond Compact (PDC) Cutters Under Impact Loading Conditions

By Justin Craig Williams

A Dissertation Submitted As Partial Requirements
For The Degree M.Sc. (Engineering)

Department Of Mechanical Engineering
University Of Cape Town
Cape Town, 2002

DECLARATION

I declare that this dissertation contains only my original work, except where reference is made with acknowledgements to contributions from others. I also declare that this material has not been submitted for any other purpose or examination to any other Department or University.

Signed by candidate

Signed this ..... day of .. July 2002...

Signed by candidate

Justin Craig Williams

ACKNOWLEDGEMENTS

This project has been an invaluable learning experience that would not have been possible without the help and support of the entire *Department of Mechanical Engineering* at the *University of Cape Town.* I would like to thank each and every person involved but especially:

- Prof. Gerald Nurick, my supervisor, for his openness, advice and direction.
- Trevor Cloete for the generous sharing of his knowledge.
- Stephen Marais for his guidance while using the experimental apparatus.
- The workshop staff for their assistance and endless encouragement.
- The secretaries for their cheerful support.
- My family and friends for their help and understanding.

TERMS OF REFERENCE

A contractor's brief was received outlining an investigation into the characterisation of the spalling behaviour of polycrystalline diamond compact (PDC) cutters under impact loading conditions. It stated that the project was to be performed using the split-Hopkinson pressure bar (SHPB) apparatus with the specific purpose of providing recommendations for the testing procedures of PDC cutters. This would be done by subjecting the cutter to an impulse and monitoring the response by means of a high-speed oscilloscope or similar apparatus.

The objectives of the project are to:

1. Determine whether spalling of the PDC cutters can be achieved using the SHPB apparatus.
2. Identify the mechanism / mechanisms responsible for the spalling phenomenon.
3. Evaluate the degree of spalling due to the loading conditions experienced.
4. Complete a statistical analysis of the repeatability of the spalling behaviour.

ABSTRACT

An experimental investigation into the identification of the spalling mechanisms of polycrystalline diamond compact (PDC) cutters and the effect of stress wave shape on the degree of spalling was performed using the split-Hopkinson pressure bar (SHPB) apparatus. The PDC cutters were loaded under specific impact conditions and their reactions monitored and characterised.

In order to isolate and identify the mechanism responsible for the spalling of the PDC cutters required them to be tested for compression waves, reflected tensile waves, contact stresses, resultant forces and normal forces. It was determined that the spalling phenomenon observed in PDC cutters was due to the application of excessive normal forces.

The results obtained during the impact testing of the PDC cutters were of projected damage area and mass losses, which were converted to volume losses and average crack depth measurements. The loading conditions were characterised as the peak force, average force and impulse experienced by the PDC cutters which were then plotted as a function of each other as well as of the damage measurements. It was found that the degree of spalling is dependent on the amplitude of the applied stress wave and independent of the period.

For this reason traditional drop testing methods cannot be used to describe the impact behaviour of PDC cutters and the SHPB apparatus therefore offers an alternative experimental technique.

TABLE OF CONTENTS

LIST OF FIGURES

LIST OF TABLES

GLOSSARY AND LIST OF SYMBOLS

PCD	Polycrystalline diamond
PDC	Polycrystalline diamond compact
SHPB	Split-Hopkinson pressure bar
WC	Tungsten carbide
Co	Cobalt
WC-Co	Tungsten carbide cobalt

F	Force
u	Displacement
t	Time
v	Velocity
c	Wave speed
a	Acceleration
m	Mass
ρ	Density
A	Cross-sectional area
E	Youngs modulus
σ	Stress
ε	Strain
$\dot{\varepsilon}$	Strain Rate
I	Impulse

1 INTRODUCTION

This report describes an experimental investigation into the identification of the spalling mechanisms of polycrystalline diamond compact (PDC) cutters and the effect of stress wave shape on the degree of spalling. Using the split-Hopkinson pressure bar (SHPB) apparatus the PDC cutters were loaded under specific impact conditions and their reactions monitored and characterised.

A PDC cutter is a round composite disc comprised of a thin layer of sintered polycrystalline diamond (PCD) bonded to a tungsten carbide cobalt (WC-Co) substrate. PCD is formed by sintering a mass of fine diamond crystals in the temperature range of 1500-2000 °C. The process of PDC cutter manufacture requires the use of a WC-Co disc placed onto diamond powder followed by high pressure and high temperature conditions.

PDC cutters are widely used today as drag bit cutters to drill oil and gas wells. PDC cutters offer significant advantages over conventional roller cone drill bits, although they are limited to drilling in weak rock formations because they are much more susceptible to brittle fracture than are the cutting elements on conventional bits.

The wear and failure of PCD and PDC cutters has long been the subject of concern and research attention, especially with regard to the spalling phenomenon. Gross fracturing or spalling occurs when a crack nucleates on the curved surface of the PCD table of the cutter and propagates towards the centre, removing a more or less circular chip. This takes place over a short period of time and usually occurs during the drilling process when the rock formation changes and the cutters run into a hard band.

The objectives of this report are to:

1. Determine whether spalling of the PDC cutters can be achieved using the SHPB apparatus.
2. Identify the mechanism / mechanisms responsible for the spalling phenomenon.
3. Evaluate the degree of spalling due to the loading conditions experienced.
4. Complete a statistical analysis of the repeatability of the spalling behaviour.

The data on which this report is based was gathered using the SHPB apparatus located in the high strain rate laboratory at the *University of Cape Town* while the background information and literature were gathered from published engineering books, journals and papers by recognised researchers in similar fields. Technical data was obtained from the instrumentation suppliers as well as from experts at various educational institutions.

This report begins with a brief review outlining the relevant theory and background information into the subject as well as the results of previous research into the failure mechanisms of PDC cutters. It is then followed by a description of the experimental procedures and equipment used. The results that were obtained are also presented, discussed, conclusions drawn and recommendations made for future work.

2 *BACKGROUND AND LITERATURE REVIEW*

This report investigates the impact characteristics of PDC cutters using the SHPB apparatus. In the chapter that follows the relevant background and literature will be reviewed regarding SHPB apparatus and PDC cutters.

2.1 The Split-Hopkinson Pressure Bar (SHPB)

Standard tensile testing machines are not suitable for conducting material testing and characterisation experiments at high strain rates, due to stress waves that are set up by the rapid loading of the specimen which then propagate through the system and effect transducer readings. To overcome these limitations the SHPB is used for material testing at strain rates of between 10^2 s^{-1} and 10^4 s^{-1}.

2.1.1 History Of The SHPB

The split Hopkinson pressure bar technique is named after Bertram Hopkinson [1] who, in 1914 used the induced wave propagation in a long elastic metallic bar to measure the pressure produced during dynamic effects. Hopkinson studied the shape and evolution of stress waves as they propagated down long metallic rods as a function of time. Based on this pioneering work, the experimental apparatus utilising elastic stress wave propagation in long rods to study dynamic processes was named the Hopkinson pressure bar [2].

Later work by Davies [3] and Kolsky [4] used two Hopkinson pressure bars in series, with the sample sandwiched between, to measure the dynamic stress strain response of materials. This technique thereafter has been referred to as either the split-Hopkinson pressure bar (SHPB), Davies bar or Kolsky bar [2].

Following the original SHPB apparatus developed to measure the compressive mechanical behaviour of a material, alternate SHPB schemes were designed for loading samples in tension [5], torsion [6], and simultaneous compression/tension-torsion [7]. SHPB apparatus have also been utilised to load specimens to measure shear strength and fracture toughness [8].

2.1.2 Principles Of The SHPB

While there is no universal standard design for the compression SHPB, each apparatus shares the following design elements or similar devices and are shown in Figure 2-1 [9]:

- Compressed gas gun and striker bars.
- Pressure bars and mountings.
- Electronics and instrumentation.
- Data acquisition and recording system.

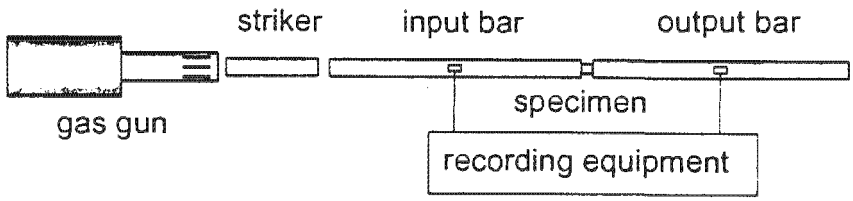

Figure 2-1: Schematic diagram of the SHPB apparatus [10].

The SHPB technique was initially used for specimens loaded in compression. In compression tests the specimen is sandwiched between the two pressure bars. The stress wave travels along the input / incident bar and is partly transmitted to the output / transmission bar by means of the specimen. The compression wave is also partly reflected as a tensile wave back in the incident bar [11].

These three basic waves are recorded using the strain gauges, which are cemented on the pressure bars and the associated data recording instrumentation. This allows for the measurement of strain versus time at the recording positions and thus at the two faces of the specimen. A stress stress-strain relationship for the tested material is then derived by suitable integration [12].

The pressure bars used in a SHPB set-up are traditionally constructed from a high strength structural metal. This is because the upper limits of strain rate and stress are determined by the yield strength of the pressure bars. If plastic deformation takes place in the pressure bars the SHPB analysis no longer applies. This is due to the fact that the position of the interface between specimen and bar can no longer be determined by the elastic equation (Equation (11) – Section 2.1.4) [13].

For proper SHPB operation the pressure bars must be straight, free to move without binding and carefully mounted to ensure optimum axial alignment. Precision bar alignment is required for both uniform and one-dimensional wave propagation within the pressure bars as well as for uniaxial compression within the specimen during loading. Lack of free movement will lead to additional noise in the waveforms measured on the pressure bars. For this reason it is essential to apply precise dimensional specifications during construction and assembly [2].

The most common method of generating an incident wave in the input bar is to propel a striker bar to impact the end of the incident bar. The striker bar is normally fabricated from the same material and is of the same diameter as the pressure bars. The length and velocity of the striker bar are chosen to produce the desired total strain and strain rate within the test specimen. The length of the striker must however always remain less than half the length of the shorter pressure bar. This will ensure a complete unloading before the arrival of any reflected wave and avoid any overlap of incident and reflected waves at the recording positions [14].

2.1.3 One-Dimensional Wave Theory

There are a few assumptions inherent to ensure the one-dimensional theory of wave propagation, which forms the basis for the SHPB technique. In order for the successful application of elementary one-dimensional wave propagation theory [15]:

- The bars need to be free to move without binding.
- The period should be at least six times longer than the typical cross-sectional area of the bar.

Considering an element dx of a long bar of cross sectional area A_0. The equation of motion ($F = m.a$) can be written in the form:

$$-\frac{\partial \sigma_0}{\partial x}.\partial x.A_0 = A_0.\rho_0.\partial x.\frac{\partial^2 u}{\partial t^2} \quad \text{or} \quad \frac{\partial \sigma_0}{\partial x} = -\rho_0.\frac{\partial^2 u}{\partial t^2} \tag{1}$$

The strain in an element of length ∂x is $\partial u/\partial x$. Therefore where E is the Young's Modulus the relationship between stress and strain ($E = \sigma/\varepsilon$) is given by:

$$-\frac{\sigma_0}{\partial u/\partial x} = E \tag{2}$$

Differentiating the equation with respect to x leads to:

$$\frac{\partial \sigma_0}{\partial x} = -E.\frac{\partial u^2}{\partial x^2} \tag{3}$$

This in equation (1) yields:

$$\frac{\partial^2 u}{\partial t^2} = \frac{E}{\rho_0} \cdot \frac{\partial^2 u}{\partial x^2} \quad \text{Where} \quad c_0 = \sqrt{\frac{E}{\rho_0}} \tag{4}$$

Therefore the one-dimensional wave equation is:

$$\frac{\partial^2 u}{\partial x^2} = \frac{1}{c_0^{\,2}} \cdot \frac{\partial^2 u}{\partial t^2} \tag{5}$$

2.1.4 Theory Of The SHPB

From one-dimensional wave theory the wave equation is given by equation (5). The general solution can therefore be written in the form:

$$u = f(x - c_0 t) + g(x + c_0 t) \tag{6}$$

Where f and g are functions describing the incident and reflected wave shapes and c_0 is the wave speed in the pressure bars. Consider then a wave moving in the positive x direction:

$$u = f(x - c_0 t) \tag{7}$$

Differentiating the equation with respect to x and t leads to:

$$\frac{\partial u}{\partial t} = -c_0 . f' \quad \text{and} \quad \frac{\partial u}{\partial x} = f' \tag{8}$$

Substitution of the above equations yields:

$$\frac{\partial u}{\partial t} = -c_0 . \frac{\partial u}{\partial x} \quad \text{or} \quad v = -c_0 . \varepsilon \tag{9}$$

Using the definitions of $\sigma = E.\varepsilon$ and $E = c_0^{\,2} . \rho$ in the equation above gives:

$$v = -c_0 . \frac{\sigma}{E} = \frac{-\sigma}{\rho . c_0} \tag{10}$$

The negative sign indicates that the velocity is in the positive x direction if a tensile wave is being dealt with. It is conventional to take compressive stress as positive in bar wave theory, which leads to the equation:

$$\sigma = \rho.c_0.v \tag{11}$$

Assuming uniaxial stress conditions, relationships can be derived for reflected (σ_R) and transmitted (σ_T) stress waves between bars of different materials and cross-sectional areas at an interface, in terms of an incident stress wave (σ_I). The equilibrium of forces gives:

$$(\sigma_I + \sigma_R).A_1 = \sigma_T.A_2 \tag{12}$$

For continuity of motion and assuming that each of the waves is compressive and that the associated particle velocities in bar 1 and 2 respectively are of equal magnitude and in the same direction ($v_1 = v_2$). Then

$$v_I - v_R = v_T \tag{13}$$

Using this with equation (11) and (12) yields:

$$\sigma_R = \frac{\rho_2.c_2.A_2 - \rho_1.c_1.A_1}{\rho_2.c_2.A_2 + \rho_1.c_1.A_1}.\sigma_I \quad \text{and} \quad \sigma_T = \frac{2.\rho_2.c_2.A_1}{\rho_2.c_2.A_2 + \rho_1.c_1.A_1}.\sigma_I \tag{14}$$

If $\rho_1 = \rho_2 = \rho$ and $c_1 = c_2 = c_0$ then the equations become:

$$\sigma_R = \frac{A_2 - A_1}{A_2 + A_1}.\sigma_I \quad \text{and} \quad \sigma_T = \frac{2.A_1}{A_2 + A_1}.\sigma_I \tag{15}$$

Taking a specimen sandwiched between two long bars and denoting the displacements of the contact faces of the bars as u_1 and u_2, these displacements can be obtained in terms of the incident, transmitted and reflected strains. Equation (9) can also be written as:

$$\frac{\partial u}{\partial t} = c_0.\varepsilon \quad \text{or} \quad u = c_0.\int \varepsilon.dt \tag{16}$$

Where $t = 0$ corresponds to the prime arrival of the head of the incident wave at the interface. The displacement u_1 of the face of the incident bar is the result of both the incident and reflected travelling waves and the displacement u_2 of the face of the transmitter bar in contact with the specimen are:

$$u_1 = c_0.\int_0^t \varepsilon_I.dt + (-c_0).\int_0^t \varepsilon_R.dt = c_0.\int_0^t (\varepsilon_I - \varepsilon_R).dt \quad \text{and} \quad u_2 = c_0.\int_0^t \varepsilon_T.dt \tag{17}$$

The velocities of the face of each of the bars in contact with the specimen are:

$$v_1 = c_0.(\varepsilon_I - \varepsilon_R) \quad \text{and} \quad v_2 = c_0.\varepsilon_T \tag{18}$$

The applied forces F_1 and F_2 on each of the face of the specimen are:

$$F_1 = E.A.(\varepsilon_I + \varepsilon_R) \quad \text{and} \quad F_2 = E.A.\varepsilon_T \tag{19}$$

Assuming that the stress is across the specimen is constant and if A_0 and l_0 are the initial cross-sectional area and length of the specimen respectively, and with:

$$F_1 \cong F_2 \quad \text{and} \quad \varepsilon_I + \varepsilon_R \cong \varepsilon_T \tag{20}$$

Then the average stress in the specimen σ_s is determined as:

$$\sigma_s = \frac{F_1 + F_2}{2.A_0} = \pm\frac{1}{2}.\frac{E.A.(\varepsilon_I + \varepsilon_R + \varepsilon_T)}{A_0} \tag{21}$$

or

$$\sigma_s \cong \pm E.(\frac{A}{A_0}).\varepsilon_T \tag{22}$$

The average strain in the specimen ε_s is determined as:

$$\varepsilon_s = \frac{u_1 - u_2}{l_0} = \pm\frac{c_0}{l_0}.\int_0^t(\varepsilon_I - \varepsilon_R - \varepsilon_R).dt \tag{23}$$

or

$$\varepsilon_s \cong \pm\frac{2.c_0}{l_0}.\int_0^t \varepsilon_R.dt \tag{24}$$

The average strain rate in the specimen $\dot{\varepsilon}$ is determined as:

$$\dot{\varepsilon} = \frac{v_1 - v_2}{l_0} = \pm\frac{c_0.(\varepsilon_I - \varepsilon_R - \varepsilon_T)}{l_0} \tag{25}$$

or

$$\dot{\varepsilon} \cong \pm\frac{2.c_0}{l_0}.\varepsilon_R \tag{26}$$

2.2 *Polycrystalline Diamond Compact (PDC) Cutters*

PDC cutters are widely used today as drag bit cutters to drill oil and gas wells. PDC cutters offer significant advantages over conventional roller cone drill bits, although they are limited to drilling in weak rock formations because they are much more susceptible to brittle fracture. In the section that follows the manufacture, material properties and failure mechanisms of PDC cutters will be reviewed.

2.2.1 Manufacture Of PDC Cutters

A PDC cutter is a round disc comprising of a thin layer of sintered PCD bonded to a WC-Co substrate. Commercially available PCD thicknesses vary between 0.5 mm and 1.0 mm. The total thickness of the PDC blanks varies from a few millimetres to more than a centimetre. The standard diameter of PDC cutters is 12.5 mm (½ in), although 19.6 mm (¾ in) and 25.4 mm (1 in) diameter are now common. Cutters as large as 50.8 mm (2 in) are also currently available. A diagram of a PDC cutter is shown in Figure 2-2 [16].

PCD is formed by sintering together a mass of fine diamond crystals in the temperature range of 1500-2000 °C. The process of PDC cutter manufacture requires the use of a WC-Co disc placed onto diamond powder followed by high pressure and high temperature conditions [17].

The PDC sintering technology involves the technique of infiltrating molten WC-Co material from the substrate into the diamond feed powder. The infiltrating material wets diamond particles and provides a liquid phase medium to facilitate inter-grain diamond bonding. Therefore the metallic phase in the microstructure is retained in the final product and has a significant influence on the fracture toughness properties compared to those of diamond [18].

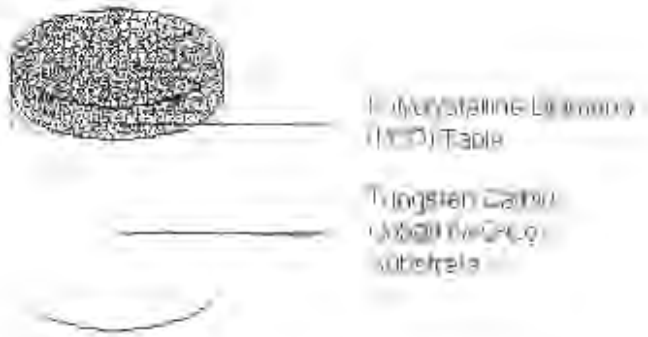

Figure 2-2: Diagram of a PDC cutter [17]

2.2.2 Material Properties of PDC Cutters

A PDC cutter is a composite structure consisting of two distinct materials. It is comprised of a thin layer of sintered PCD bonded to a WC-Co substrate as described in section 2.2.1. The properties of PCD with a cobalt catalyst compared to those of WC-Co are shown in Table 2-1 [20].

WC-Co is commonly referred to as a cermet due to the fact that it consists of small grains of a ceramic material in a binding metallic matrix. This combination of the hard, brittle ceramic grains in the soft, tough metallic matrix gives the material its high wear resistance while maintaining an acceptable level of toughness for industrial applications. WC-Co was discovered more than a hundred years ago and since then much research has been done in an attempt to manipulate and improve its already high wear resistant properties [21].

One such attempt has been to make use of a protective PCD table. PCD is formed by sintering together diamond powder under a combination of high temperatures and pressures in the presence of a suitable catalyst. This randomly orientated diamond-to-diamond bonding overcomes the low fracture toughness disadvantages of single crystal diamond while still maintaining the high strength and wear properties [22].

	PCD	WC-Co
Density (kg m^{-3})	4100	15000
Youngs Modulus (GPa)	800	600
Compressive Strength (GPa)	7.4	5
Fracture Toughness (MPa $m^{0.5}$)	9	11
Thermal Expansion (10^{-6} K^{-1})	4	5.4
Knoop Hardness (GPa)	50	50

Table 2-1: PCD and WC-Co material properties [20].

2.2.3 Operational Loading Conditions Of PDC Cutters

During rock-cutting operations PDC cutters experience the following fundamental loads and are shown in Figure 2-3:

- Cutting forces.
- Normal forces.

The cutting forces that are experienced by the PDC cutter are due to the cutting resistance of the rock and are in the cutting direction while the normal forces are due to the applied weight on the cutter and are perpendicular to the cutting direction. Given a constant rotational / cutting speed and feed rate these forces may be varied by altering the negative rake angle [23].

The negative rake angle is defined as the angle at which the PDC cutter operates relative to the cutting surface and affects the wear resistance and depth of cut. The common wisdom in PDC cutter design is that increasing the negative rake angle helps to increase the wear resistance [19].

This is due to the fact that on a given drill bit for a given weight-on-bit, the cutter automatically adjusts its depth of cut so that the sum of the normal forces balances the applied weight-on-bit. Thus increasing the PDC cutter negative rake angle results in a shallower cut and therefore less damage to the cutter. Figure 2-3 shows the approximate constant angle of the resultant applied force acting on a PDC cutter during rock-cutting operations [16].

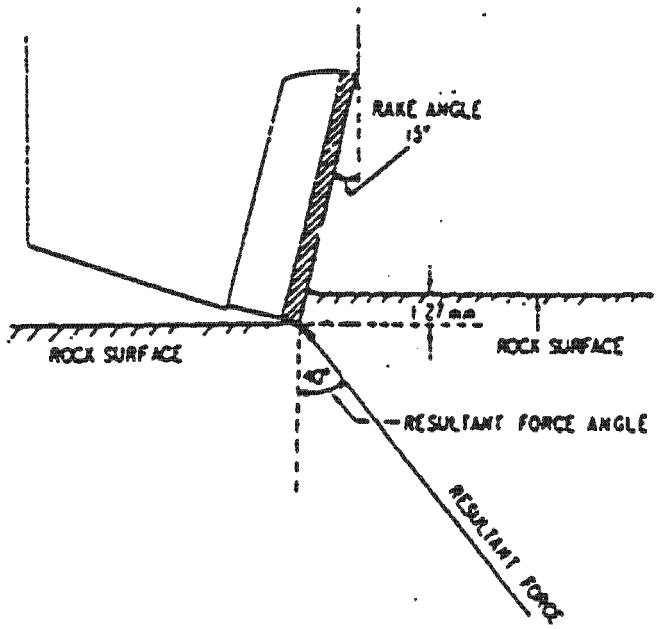

Figure 2-3: Resultant force during rock-cutting operation [16].

2.2.4 Failure Mechanisms Of PDC Cutters

The wear and failure of diamonds and PDC cutters has long been the subject of concern and research attention. Lin *et al.* [16] performed detailed studies of cutter damaged in both laboratory rock-cutting tests and field operation and identified four main mechanisms of PDC cutter failure.

i. Smooth-wear which occurs when individual diamond grains are removed by a combination of high mechanical and thermal loads.
ii. Micro-chipping of the PCD table caused mainly by the action of the PDC cutters cutting forces.
iii. Gross fracturing or spalling (Section 2.2.4.1) caused by the application of excessive normal force to the PDC cutter.
iv. Delamination (Section 2.2.4.2) as a result of both impact loading in the PDC cutter normal direction and thermal stress build-up at the interface between the diamond layer and carbide substrate.

Hibbs *et al.* [24] performed lathe cutting of rock in the laboratory with a single PDC cutter and identified a number of failure modes. These modes were similar to failure modes (i) and (ii) above. Sneddon *et al.* [25] classified the failure mechanisms of the diamond tables of PDC cutters into mechanical and thermal effects, similar to failures mode (iii) and (iv) reported by Lin *et al.* [16].

Some investigations have stressed the effects of thermal overload on PDC cutter life. Glowka *et al.* [26] distinguished between microscopic and macroscopic failures. Microscopic failures were attributed either to impact shock and fatigue or thermal shock and an important contribution was made by observing that PDC cutter wear accelerates when the temperature is allowed to rise above 350 °C. Macroscopic failures they reported were caused by impact shock and fatigue.

Other investigations have focussed on the mechanical overloading of PDC cutters. Dunn *et al.* [23] found the fracture stress on a PDC cutter was reduced under cyclic loading but concluded that the mechanical fatigue effect is not expected to be important in an idealised rock-drilling system due to the supposed steady state strength of the cutters.

However, considering the proposed failure mechanisms it is believed that gross fracture (iii) and delamination (iv) are largely responsible for PDC cutter failure and are particularly harmful. This is due to the fact that they tend to remove large areas of diamond layer and leave the WC-Co substrate unprotected which then rapidly wears.

2.2.4.1 Gross Fracturing (Spalling)

Gross fracturing is believed to be caused by the application of excessive normal forces to the cutter and unlike either smooth wear or micro-chipping, gross fracturing usually takes place over a short period of time. This damage usually occurs when the rock formation changes and the cutter runs into a hard band [27].

One obvious difference between this type of cutter damage and micro-chipping is that with gross fracturing the crack nucleates on the curved surface of the PCD table on the cutter and propagates towards the centre, removing a more or less circular chip whose fracture plane is mostly normal to the cutting direction [16].

Since this type of failure is observed on some cutters that have done very little cutting, the cause of this damage can be attributed solely to mechanical overload. Figure 2-4 shows that from the orientation of the crack it seems likely that this type of damage is caused mainly by the application of excessive normal forces.

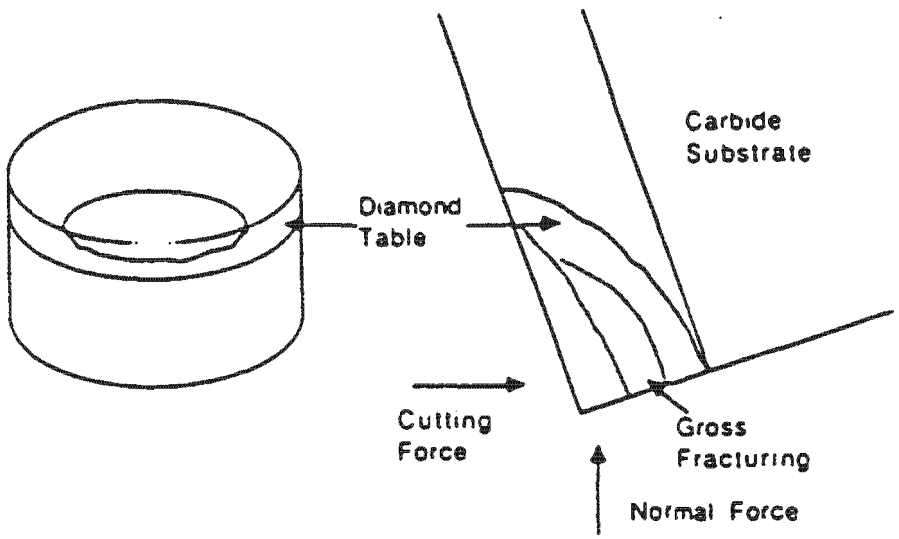

Figure 2-4: Proposed model for the process of gross fracturing [16].

2.2.4.2 Delamination

Delamination is believed to be the result of both impact loading in the cutter normal-force direction and thermal stress build-up at the interface between the PCD layer and WC-Co substrate due to the mismatch in the thermal expansion coefficients at elevated temperatures. Glowka *et al.* [26] stated that when the temperature rises, as it does during the drilling process, high tensile stresses are induced in the diamond table.

Lin *et al.* [16] however believe that an overall increase in temperature of the cutter would be expected to reduce the residual stresses. This is due to the fact that PDC cutters are manufactured by sintering diamond powder onto a WC-Co substrate as described in section 2.2.1. As the temperature decreases after sintering, a residual compressive stress is set up in the diamond layer and a tensile stress in the carbide substrate. This residual stress increases as the temperature falls.

Therefore when the temperature rises, as it does during the drilling process, residual stresses are actually reduced in the diamond table. The delamination is therefore mainly caused by impact loading in the cutter normal-force direction, although this process may be enhanced by the residual thermal stress [16].

3 EXPERIMENTAL APPARATUS AND PROCEDURES

The SHPB apparatus was used to test the PDC cutters under impact conditions in order to identify the spalling mechanism and the effects of stress wave shape on the degree of spalling. This chapter describes the SHPB apparatus used, calibration, testing, identification as well as data analysis procedures.

3.1 The SHPB Apparatus

A photograph of the SHPB apparatus used to test the PDC cutters is shown in Figure 3-1 and consists of the following:

- Compressed gas gun.
- Pressure bars and mountings.
- Electronics and instrumentation.
- Data acquisition and recording system.

Figure 3-1: Photograph of the split Hopkinson pressure bar apparatus.

3.1.1 Compressed Gas Gun and Striker Bars

The compressed gas gun, which is shown in Figure 3-2, is used to fire the striker bars in order to produce a controlled compressive stress wave in the incident pressure bar. The gun is approximately 1.5 m long and is mounted on the same I-beam arrangement as the pressure bars. There are two 1.5 m barrels available with a 12.5 mm and 20 mm bore diameter. Both the pressure chambers and the barrels of the compressed gas gun are designed to sustain a maximum working pressure of approximately 120 bar and striker impact velocities of up to 150 $m.s^{-1}$.

However, in the SHPB system a much lower pressure is required to launch the striker bars at velocities of approximately 25 $m.s^{-1}$, restricted by the elastic limit of the pressure bars and the limitations of the strain gauge cement. The pressure in the chambers is controlled through inlet and outlet valves and monitored through pressure gauges.

The compressed gas gun is equipped with striker bars of 10 mm, 12 mm and 20 mm diameters, with lengths of between 100 mm and 300 mm. The 20 mm diameter striker bars were used with lengths of 150 mm, 200 mm, 250 mm and 300 mm. They are manufactured from the same high strength silver steel material as the pressure bars and are rounded at one impact end, with a suitable curvature, to avoid the difficulty of achieving perfectly plane impact between the end faces of the striker and incident pressure bar.

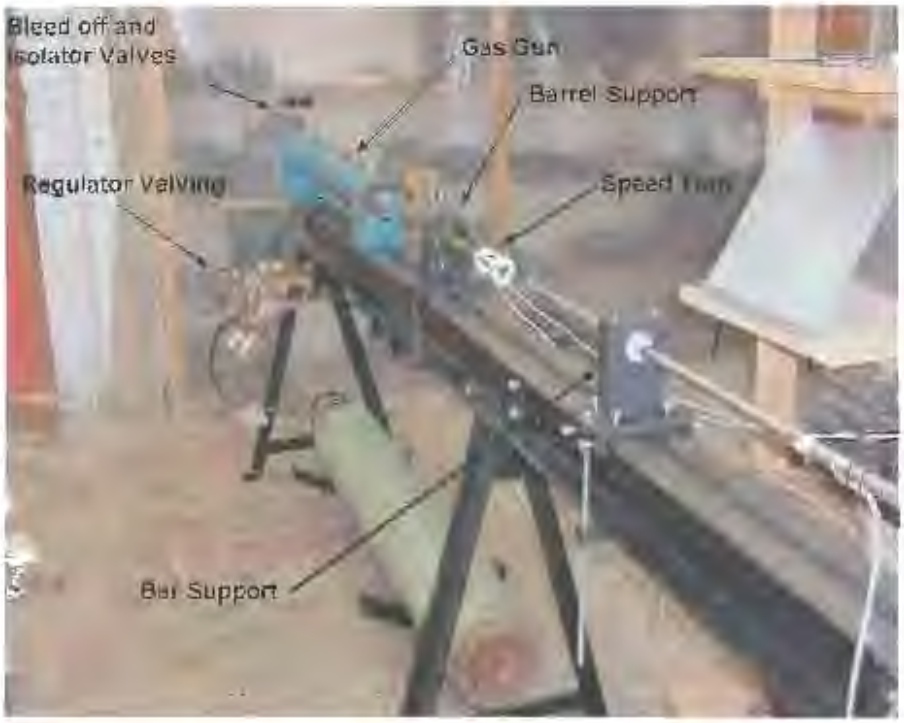

Figure 3-2: Photograph of the compressed gas gun.

3.1.2 Pressure Bars And Mountings

The pressure bars are made of high strength silver steel and have a length of approximately 2 m and a diameter of 25 mm. Teflon rings and adjustable mountings support each of the two bars and are mounted on the same I-beam arrangement as the compressed gas gun.

The pressure bars can be aligned by means of adjusting screws on the mountings as the exact alignment of the pressure bars along the centre line of the compressed gas gun barrel is of extreme importance. A photograph of the pressure bars and mountings are shown in Figure 3-3.

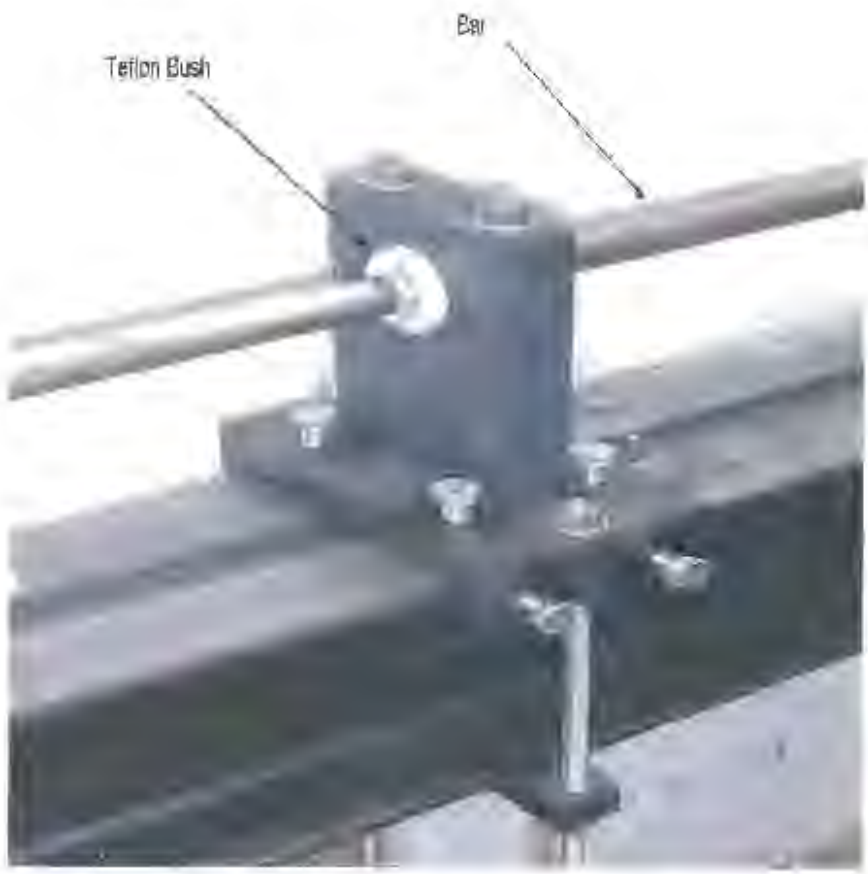

Figure 3-3: Photograph of the pressure bar and mounting.

3.1.3 Electronics And Instrumentation

The dynamic strain in the pressure bars is measured with the aid of electrical resistance strain gauges. Pairs of strain gauges are mounted diametrically opposite to each other on each of the two pressure bars at a known distance from the specimen. Each set of strain gauges is connected together with two dummy strain gauges in a full bridge arrangement, which is only sensitive to longitudinal strain components. The strain gauges used are temperature compensated, *Kyowa* type KFG-2-120-C1-11 with a gauge length of 2 mm, 120.2 Ω gauge resistance and a gauge factor of 2.11. These were bonded to the pressure bars using *Kyowa* CC-33A Cyno-Acrylate strain gauge cement.

The full bridge is connected to a *Burr-Brown* INA110 fast settling instrumentation amplifier of which two are used for the strain measurement on the two pressure bars. The full bridge and amplifiers are powered by two *Agilent Technologies* E3630A triple output variable DC power supplies. A photograph of an amplifier is shown in Figure 3-4.

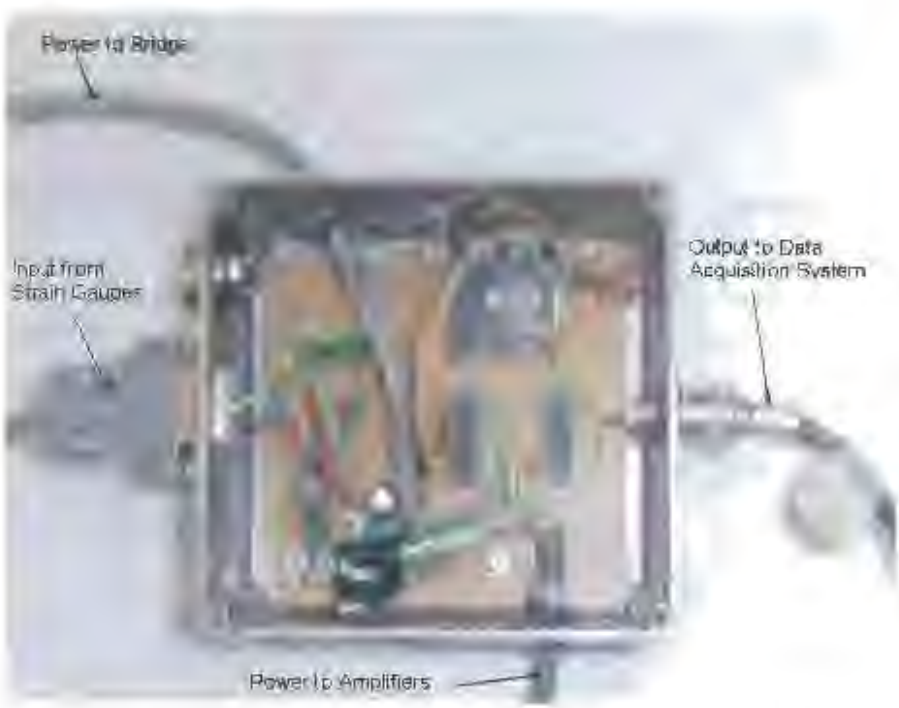

Figure 3-4: Photograph of the instrumentation signal amplifier.

3.1.4 Data Acquisition System

The strain measurements are recorded using a personal computer equipped with an *Adlink Technology Inc.* PCI-9812, 20 MHz simultaneous 4 channel analog input card. The output of the amplifiers were connected to two of the channels of the input card and stored as a text document.

The text document was then imported into the data processing program where the stress wave was characterised as described in section 3.5.2. The data processing program consisted of a *Microsoft Excel 2000* spreadsheet that analysed the data using a link to *Matlab 6.0*. This approach combines the use of the powerful functions available in *Matlab* with the ease of the *Excel* spreadsheet environment.

3.2 Calibration Of The SHPB Apparatus

In order to be confident in the meaningful interpretation of the data obtained from the SHPB apparatus it is necessary to calibrate the system. This was achieved by calibrating the following associated equipment:

- Data acquisition card.
- Speed trap.
- Amplifiers.
- Pressure bars.

Marais [28] performed the calibration of the data acquisition card, speed trap and amplifiers during the construction of the SHPB, and it was therefore only necessary to calibrate the 25 mm pressure bars that were purchased specifically for this project.

3.2.1 Calibration Of The Pressure Bars

In order to calibrate the pressure bars it is necessary to obtain the material constants experimentally. These constants are in turn used to determine the dynamic calibration factor of the pressure bars. The dynamic calibration factor is required in order to convert the measured voltage readings from the data acquisition system to the appropriate associated stress levels within the data processing program.

3.2.1.1 Determining The Material Properties

The material properties that are required for determining the dynamic calibration factor for the pressure bars are the Young's modulus and Poisson's ratio. These values were determined using a calibration method that assumes that the stress at the free end of the pressure bar is zero. This is achieved by shifting the incident and reflected waves to the free end of the pressure bar using the data processing program as described in section 3.5.2. The sum of these waves should then be equal to zero if the Young's modulus and Poisson's ratio are correct.

For the series of calibration experiments each pressure bar was struck using the 300 mm striker and the data recorded. This data was then processed using the data processing program. The Young's modulus and Poisson's ratio were then adjusted until the resultant stress trace was almost zero and the material properties were then assumed correct. A sample graph of the stress at the free end of a pressure bar is shown in Figure 3-5.

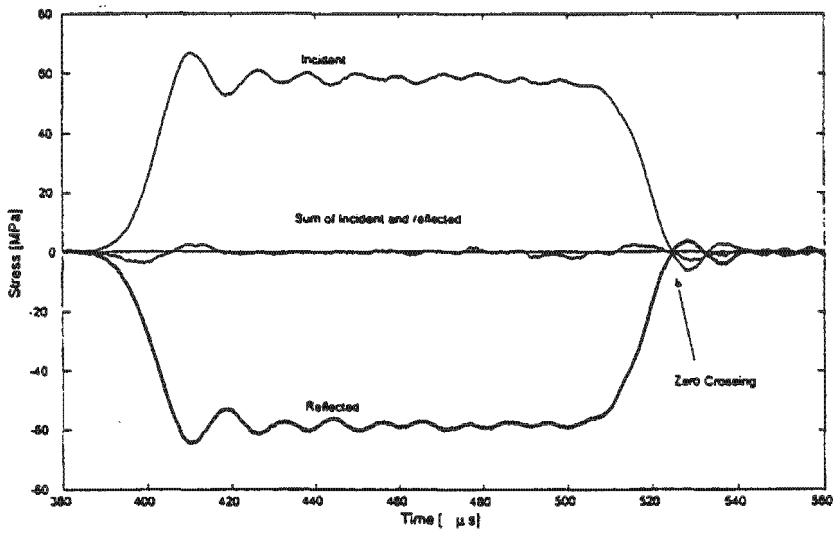

Figure 3-5: Graph of the stress at the free end of the pressure bar.

3.2.1.2 Determining The Dynamic Calibration Factor

The calibration of the pressure bars was performed using the impulse / momentum and energy of the striker bar and a travelling wave. The impulse / momentum of the wave was obtained by integrating the measured wave in the following way:

$$I = \int_0^t F.dt \tag{27}$$

Using the definitions $\sigma = E.\varepsilon$ and $F = A.\sigma$ the equation becomes:

$$I = \int_0^t A.E.\varepsilon.dt = A.E.\int_0^t \varepsilon.dt \tag{28}$$

The energy of the wave was obtained by integrating the measured strain-time wave in the following way:

$$Energy = \int_0^t p.v.dt \tag{29}$$

Using the definitions $\sigma = E.\varepsilon$ and $v = \frac{\sigma}{\rho.c_o}$ (Equation 11) the equation becomes:

$$Energy = \int_0^t A.E.\varepsilon.\frac{E.\varepsilon}{\rho.c_0}.dt = \frac{A.E^2}{\rho.c_0}.\int_0^t \varepsilon^2.dt \tag{30}$$

From the energy and momentum of the wave the theoretical impact velocity of the striker bar can be calculated. The change in momentum of the striker bar is equal to that of the pressure bar and is given by:

$$\Delta I = m.(v_I - v_F) \tag{31}$$

And the change in energy of the striker bar is equal to that of the pressure bar and is given by:

$$\Delta Energy = m.(v_I^2 - v_F^2) \tag{32}$$

Therefore by substitution of equations (31) and (32) yields:

$$v_I = \frac{\Delta Energy}{\Delta I} + \frac{\Delta I}{2.m} \tag{33}$$

The theoretical calibration factor is then adjusted within the data processing program until the calculated velocity of the striker bar matches the measured value. The calibration process was repeated and after several iterations the values converge and the calibration factor is obtained.

3.3 Identification Of The Failure Mechanism

A detailed study of relevant literature and the operating conditions of PDC cutters resulted in a number of possible failure mechanisms being postulated. The PDC cutters were then loaded under the various conditions in order to identify the mechanism / mechanisms responsible for the spalling phenomenon.

3.3.1 Compressive Stress Wave

In the compression testing set-up of the SHPB apparatus the specimen is positioned between the two pressure bars as illustrated in Figure 3-6. The specimen is then subjected to a compressive stress wave as described in section 3.4.

At the interface the incident wave is partially reflected and partially transmitted through the specimen into the transmitter pressure bar. In the case of the PDC cutters the incident compression wave is mostly transmitted through the specimen into the transmitter pressure bar, resulting in an overall compressive load on the specimen.

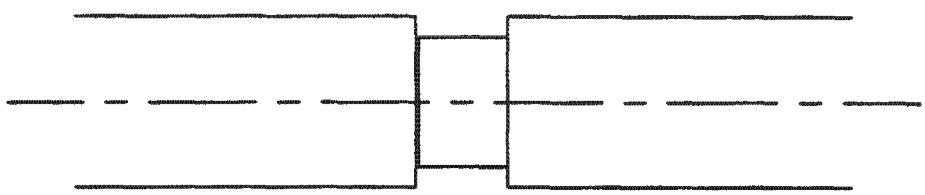

Figure 3-6: Loading arrangement of the pressure bars and PDC cutter for compression testing.

3.3.2 Tensile Stress Wave

Figure 3-7 shows the loading arrangement for the pressure bar and PDC cutter during the tensile testing set-up of the SHPB apparatus. The PDC cutter is then subjected to a compressive stress wave as described in section 3.4.

At the interface the compressive incident wave is mostly transmitted into the specimen and as it reaches the free end of the PDC cutter it is reflected as a tensile stress wave, which results in an overall tensile load on the PDC cutter.

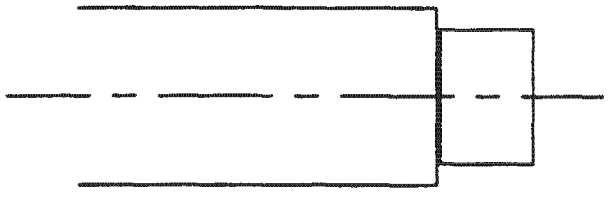

Figure 3-7: Loading arrangement of the pressure bar and PDC cutter for tensile testing.

3.3.3 Contact Stresses

Contact stresses take place when a body having a curved surface is pressed against another, which results in a point or line contact changing to an area contact. The shear stresses involved reach a maximum value slightly below the surface and are responsible for the surface failure of contacting elements [30].

The set-up for contact stress testing is similar to that for compressive testing, except that the single specimen is replaced by a pair of PDC cutters and a steel ball bearing sandwiched between the two pressure bars as illustrated in Figure 3-8.

The PDC cutter arrangement is then subjected to a compressive stress wave as described in section 3.4. This subjects the arrangement to a compressive load and due to the inclusion of the curved surface, large contact stresses are created at the interfaces between the PDC cutters and the ball bearing.

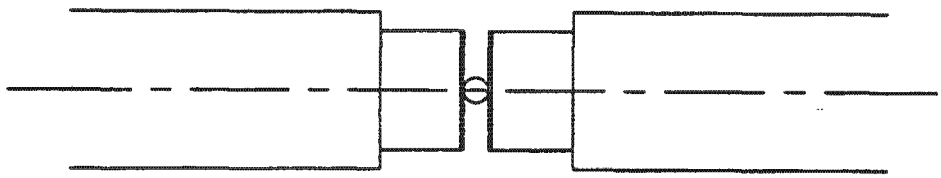

Figure 3-8: Loading arrangement of the pressure bars and PDC cutter for contact stress testing.

3.3.4 Resultant Force

As described in section 2.2.3 the PDC cutters experience both cutting and normal forces during rock-cutting operations. According to Dunn *et al.* [23] the angle of the resultant of theses two forces acting on the PDC cutter is approximately constant at an angle of 40° to the plane of the diamond table and is clearly shown in Figure 2-3 (Section 2.2.3).

The testing procedure for the resultant force involves the use of an angular insert to position the PDC cutter in such a manner that the resultant force experienced is at an angle of 40°. The cutting edge of the PDC cutter is impacted against a PCD surface in order to protect the incident pressure bar and the arrangement is shown in Figure 3-9. A compressive stress wave is then applied as described in section 3.4.

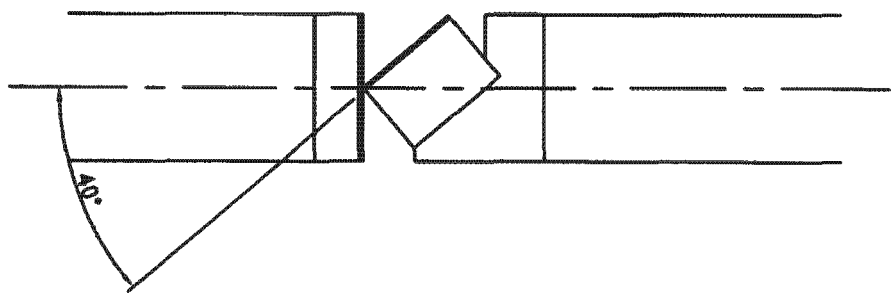

Figure 3-9: Loading arrangement of the pressure bars and PDC cutter for resultant force testing.

3.3.5 Normal Force

The normal forces experienced by the PDC cutters during rock-cutting operations are due to the applied weight on the cutters as mentioned in section 2.2.3 and may be varied by changing the negative rake angle.

For this series of experiments a negative rake angle of 15° was chosen as described in section 3.4.5. The PDC cutter is positioned against a protective PCD surface using an angular insert in such a manner as to ensure that a force at an angle of -15° to the PCD table is experienced. Figure 3-10 shows the PDC cutter arrangement that is used to subject the specimens to a normal force (A photograph is shown in Figure 3-12). The arrangement is then loaded by a compressive stress wave as described in section 3.4.

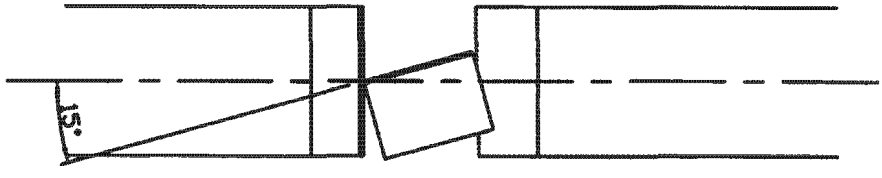

Figure 3-10: Loading arrangement of the pressure bars and PDC cutter for normal force testing.

3.4 Testing Procedures And Data Analysis Using The SHPB Apparatus

In order to use the SHPB apparatus to test the PDC cutters the following testing procedures need to be carefully adhered to before and during each experimental session.

3.4.1 Installation Of The Pressure Bars

Valid results using the SHPB apparatus may only be obtained if the pressure bars are correctly installed. To achieve this the pressure bars are mounted on the common I-beam by means of the Teflon rings and adjustable mountings. Using a spirit level the mountings are adjusted so that the pressure bars are level and coplanar, with the compressed gas gun and each other.

Once this has been achieved fine adjustments are made to ensure that the striker bar / incident pressure bar and the incident / transmitter pressure bar interfaces are accurately aligned. The mountings are then secured and the bars once again checked to ensure that no movement has taken place.

3.4.2 Charging Of The Gas Gun

The compressed gas gun is used to propel the striker bar in order to produce a controlled compressive wave in the incident pressure bar. This was achieved by pressurising the primary cylinder to 6 bar and the trigger cylinder to approximately 10 bar. The trigger cylinder pressure is not critical although the pressure must always be greater than that of the primary cylinder. As a general rule the pressure was set to approximately 150 % of that of the primary cylinder. The pressure of the primary cylinder is however critical and was carefully monitored.

The striker bars were loaded to the required depths with the aid of a plunger, in order to achieve the desired impact velocities. Once testing was complete the compressed gas gun was depressurised and all valves closed.

3.4.3 Set-Up Of The Instrumentation

Following the installation of the pressure bars and the charging of the gas gun the instrumentation required must be set up. This requires firstly that the strain gauge leads be plugged into the amplifiers and the power supplies set to the required voltage levels. The power for the amplifiers was set to ±7 V and the bridge voltage to ±5 V.

The ±7 V power input for the amplifiers is not critical since as the maximum input voltage is ±18 V but in order to protect the data capture card the voltage was reduced. The bridge voltage setting is however critical as it dictates the gain of the amplifiers. The ±5 V setting allowed for a full-scale stress level of ±120 MPa in the pressure bars. This bridge voltage was chosen as it allowed a maximum voltage into the card at the predicted allowable stress in the pressure bar.

3.4.4 Set-Up Of The Data Capture Card

In order to capture data using the SHPB apparatus and the data capture card, it was necessary to run the data capture program first. Once this program had been initiated the user interface was displayed. This interface is shown in Figure 3-11 along with a trace of typical sample data.

The amplifiers were then zeroed by setting the data capture program to a continuous scan mode and adjusting the bridge resistor in such a way as to move the input signal near the zero mark. It was not necessary to set the level to exactly zero as the data processing program tests for this and sets the level to zero. Once the amplifiers had been zeroed the continuous scan mode was switched off and the system was ready to be set for single shot data capturing. In order to do this the following parameters were set:

- The trigger mode was set to middle trigger.
- The trigger channel was set to channel 0.
- The trigger polarity was set to positive.
- The trigger level was set to 0.6 V.
- The post trigger count was set to 13 000.
- The number of data points was set to 15 000.
- The number of channels was set to 2.
- The clock setting was set to internal.
- The sample frequency was set to 10 MHz.

Figure 3-11: User interface of the data processing program.

3.4.5 Mounting Of The Specimen

The mounting of the PDC cutter specimens is dependent on the loading condition that is being investigated as described in section 3.3. Therefore the mounting orientation may require the use of a specific loading arrangement and careful note should be taken of which experiment is being performed.

The PDC cutters were loaded during the series of experiments to characterise the spalling behaviour under impact conditions as described in section 3.3.5. This involved the use of an angular insert in order to ensure that the specimen is mounted at a negative rake angle of 15°. The cutting edge of the PDC cutter was impacted against a PCD surface in order to protect the pressure bar against damage. A photograph of the angular insert and PDC cutter is shown in Figure 3-12 (Schematically shown in Figure 3-10).

Figure 3-12: Photograph of the angular insert and PDC cutter

3.4.6 Performing The Experiment

Once the apparatus has been correctly installed and set up it is possible to perform the experiments and capture the data. This is achieved by completing the following procedures:

- Reset the measuring equipment.
- Press the start button on the data capture program.
- Lift the safety catch and fire the compressed gas gun.
- Enter the experimental parameters into the data-capturing program.
- Enter a location / file name and save the data.
- Label and store specimen.

It is now possible to test another PDC cutter by mounting a specimen (Section 3.4.3) and repeating the procedures detailed above.

3.5 *Analysis Of The Specimen and Data*

Once the experimentation had been completed the specimens and data is processed and analysed. This involved the evaluation of the degree of spalling, the characterisation of the stress waves and a statistical analysis of the data.

3.5.1 Evaluating The Degree Of Spalling

During the experimentation it was found that the shape and area of the PCD chips that were removed under the impact conditions showed a large variance. It was therefore decided to use three methods to evaluate the degree of spalling of the PDC cutters.

The first method was an area loss evaluation and involved the measurement of the projected damage area. This was achieved by importing a scanned *Bitmap (bmp)* image file of the PDC cutter into *AutoCAD 2000*. A scanned image of the spalled PDC cutter is shown in Figure 3-13. Once the image file had been imported the damage area was traced and using a package function the enclosed area was measured and recorded.

Figure 3-13: Scanned image of a spalled specimen

The measurement of the projected damage area is a one-dimensional evaluation and does not take into account any other dimensional characteristics of the PDC cutter damage. For this reason a second volume loss evaluation method was used and involved the measurement of the change in mass of the PDC cutters using the *Sartorious* digital balance in the *Centre of Materials Engineering* at the *University of Cape Town*. The specimens were weighed before and after testing and the mass loss converted to a volume loss using the theoretical published density of PCD and the values recorded.

$$Volume = {Mass}/{Density}$$

This volume loss measurement therefore allowed the calculation of the average crack depth by using the ratio of the obtained damage volume to that of the projected damage area. A schematic side view of a spalled PDC cutter is shown in Figure 3-14.

$$Depth = {Volume}/{Area}$$

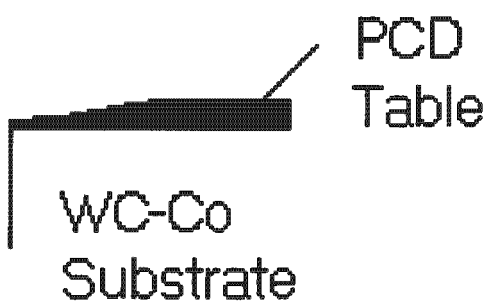

Figure 3-14: Schematic side view of a spalled PDC cutter.

3.5.2 Characterising The Stress Wave

As the strain signals were measured at some distance from the specimen it was necessary to shift the signal to the pressure bar / specimen interface. The shifting procedure is complicated by the fact that the higher frequency components of a longitudinal stress wave propagate slower than the lower frequency components in the bar, and is known as dispersion. A dispersion correction program was therefore used to shift the wave to the interface where the characterisation of the loading conditions could then be performed.

The measured strain signal of the transmission pressure bar was used in order to characterise the stress wave. This signal was used in order to eliminate the effect of any external factors, as only the forces experienced by the PDC cutter could be transmitted and measured.

The characterisation of the stress wave involved the measurement of the peak amplitude, period and impulse. The peak amplitude and period of the stress wave were obtained from the various strain-time plots program while the impulse / momentum value was obtained by suitable integration of the force-time plot (Equation 27).

$$I = \int_0^t F.dt$$

The average force was then calculated by dividing the measured impulse / momentum by the period as described in experimental method texts [31] and demonstrated in Figure 3-15.

$$F_{Avg} = I/Period \tag{34}$$

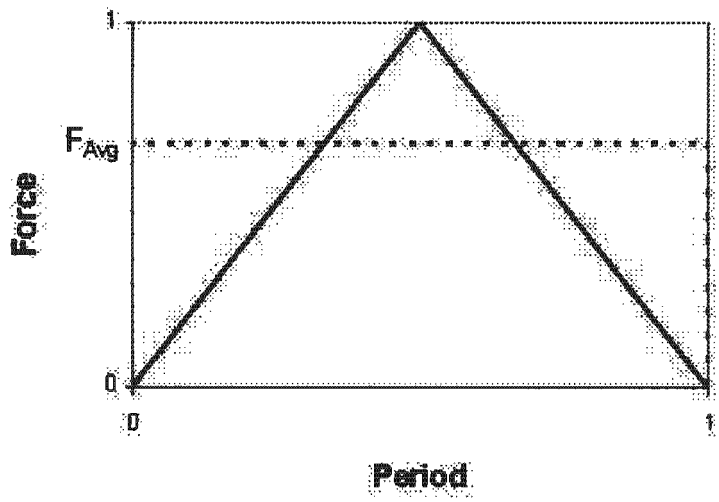

Figure 3-15: Graph of the relationship between force, average force and period.

3.5.3 Plotting The Processed Data

The processed data was examined and plotted as follows (Presented in chapter 4), in order to show all relevant trends and relationships:

- Peak Force vs. Damage Volume
- Peak Force vs. Projected Damage Area
- Peak Force vs. Average Crack Depth
- Average Force vs. Damage Volume
- Average Force vs. Projected Damage Area
- Average Force vs. Average Crack Depth
- Damage Volume vs. Impulse
- Projected Damage Area vs. Impulse
- Average Crack Depth vs. Impulse
- Projected Damage Area vs. Damage Volume
- Log (Projected Damage Area) vs. Log (Damage Volume)

3.5.4 Statistical Analysis Of The Data

Statistics offers a quantitative method for an objective analysis of the presented data. When two or more sets of data are present there are a number of possibilities that may exist:

- A better correlation results if individual lines are drawn with a pooled slope.
- There is a significant offset in the vertical direction (Y intercept).

The statistical method used was to determine the sum of squares of deviations from the best straight line through all the data, the best straight line through the individual sets with a pooled estimate of the slope, and the best straight line through the individual sets, each with its own slope. The comparison of each of the sums of squares at its degrees of freedom with the minimum sum of squares from each line separately provides a variance ratio that can be tested using the *F* test.

If the decrease in the sum of squares of deviation when using several lines with individual slopes compared with using a pooled slope for all the lines is not significantly larger than might be expected for the number of degrees of freedom available, then for the data involved there is no basis for using different slopes for different sets of data (Significance of slope < Critical significance value using a 99 % confidence level then a pooled slope may be used).

The significance of the balance of sum of squares with one degree of freedom is a measure of the difference between the slope of the means and the slope of the data within sets and is therefore an indication of the displacement in the *Y* direction of the correlations (Significance of intercept < Critical significance value using a 99 % confidence level then a pooled intercept may be used). A detailed discussion of the entire procedure is given in Volks [32].

4 EXPERIMENTAL RESULTS AND DATA ANALYSIS

The PDC cutters were all tested under the same conditions using the SHPB as described in section 3.4. In the following chapter the results and observations that were obtained are presented. These are discussed in chapter 5 and detailed results, graphs and the statistical analyses are available in the appendices.

4.1 Results Of The Failure Mechanism Identification

In order to isolate and identify the mechanism responsible for the spalling of PDC cutters required them to be tested under the various loading conditions as described in section 3.3. Even under extreme loading during the series of experiments conducted to reproduce a failure due to a compression wave (Section 3.3.1), reflected tensile wave (Section 3.3.2) and contact stresses (Section 3.3.3) the cutters showed no signs of failure.

The testing procedures of the PDC cutters where a resultant force (Section 3.3.4) was applied managed to cause failure. The fracture planes were however more or less perpendicular to that of the PCD table.

The failure investigation due to the normal force (Section 3.3.5) resulted in a reproducible failure due to spalling.

4.3 *Effect Of The Peak Force On PDC Cutter Damage*

The effect of the peak force on the damage volume, projected damage area and average crack depth for the various striker bar lengths are shown in Figure 4-1 through Figure 4-3

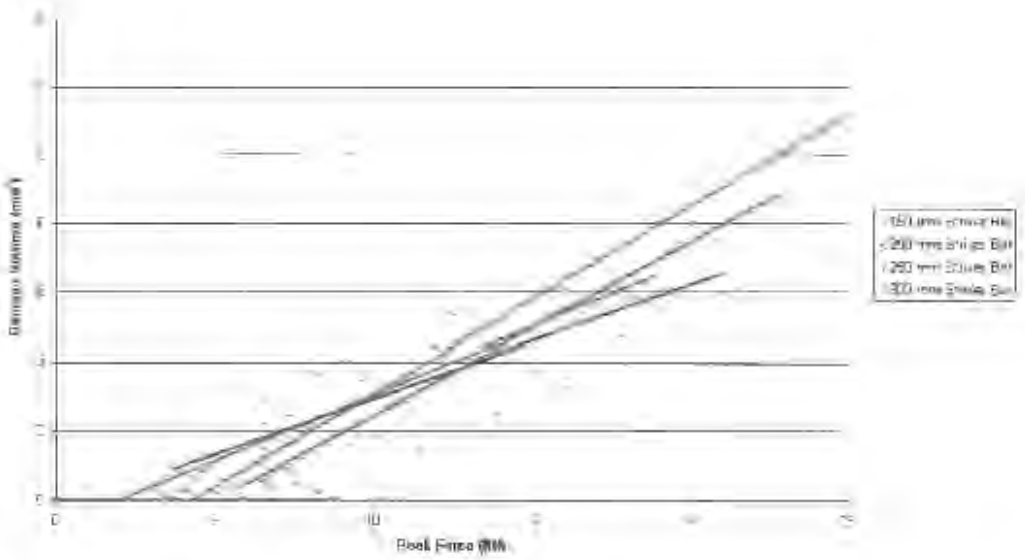

Figure 4-1: Graph of the relationship between the damage volume and peak force for the various striker bar lengths.

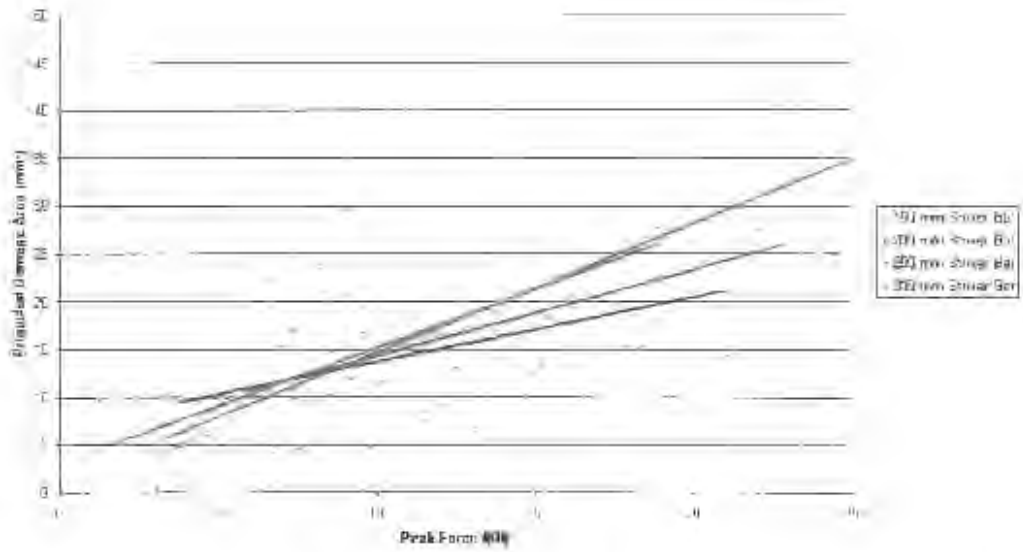

Figure 4-2: Graph of the relationship between the projected damage area and peak force for the various striker bar lengths.

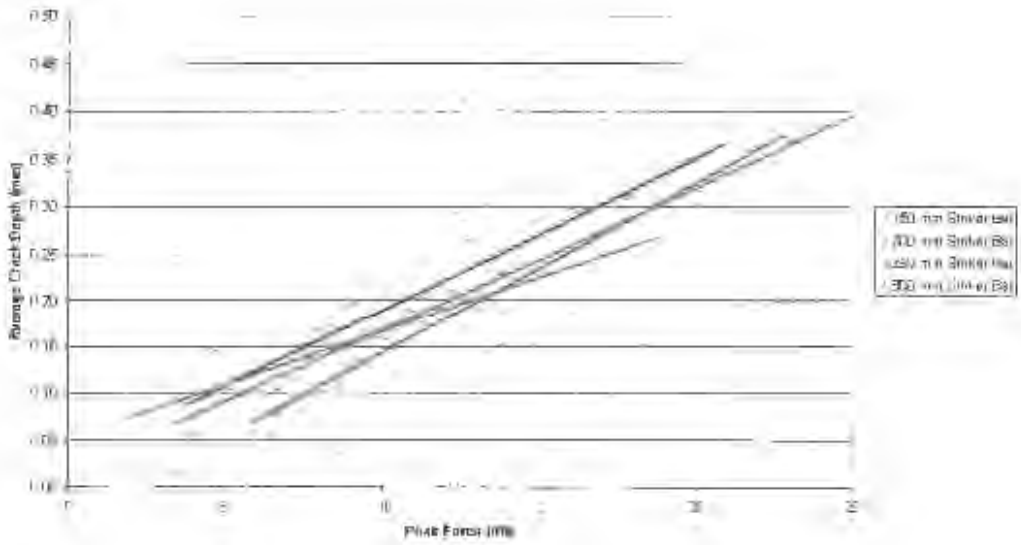

Figure 4-3: Graph of the relationship between the average crack depth and peak force for the various striker bar lengths.

Table 4-1 shows a summary of the statistical analysis of the significance of slope and intercept for the graphs of the effect of the applied peak force on PDC cutter damage for the various striker bar lengths shown in Figure 4-1 through Figure 4-3. The statistical analysis of the pooled data is summarised in Table 4-2 and the graphs shown in Figure 4-4 through Figure 4-6 with a 75% confidence limit.

	Significance Of Slope	Critical Significance Value	Significance Of Intercept	Critical Significance Value
Damage Volume vs. Peak Force	1.32	2.71	0.65	3.95
Projected Damage Area vs. Peak Force	0.82	2.71	0.27	3.95
Average Crack Depth vs. Peak Force	1.10	2.71	0.71	3.95

Table 4-1: Summary of the statistical analysis for the relationships between PDC cutter damage and peak force

	Pooled Slope	Pooled Intercept	Correlation Coefficient
Damage Volume vs. Peak Force	0.43	-1.37	0.72
Projected Damage Area vs. Peak Force	1.00	4.21	0.84
Average Crack Depth vs. Peak Force	0.015	0.019	0.77

Table 4-2: Summary of the statistical analysis of the pooled data for the relationships between the PDC cutter damage and the peak force

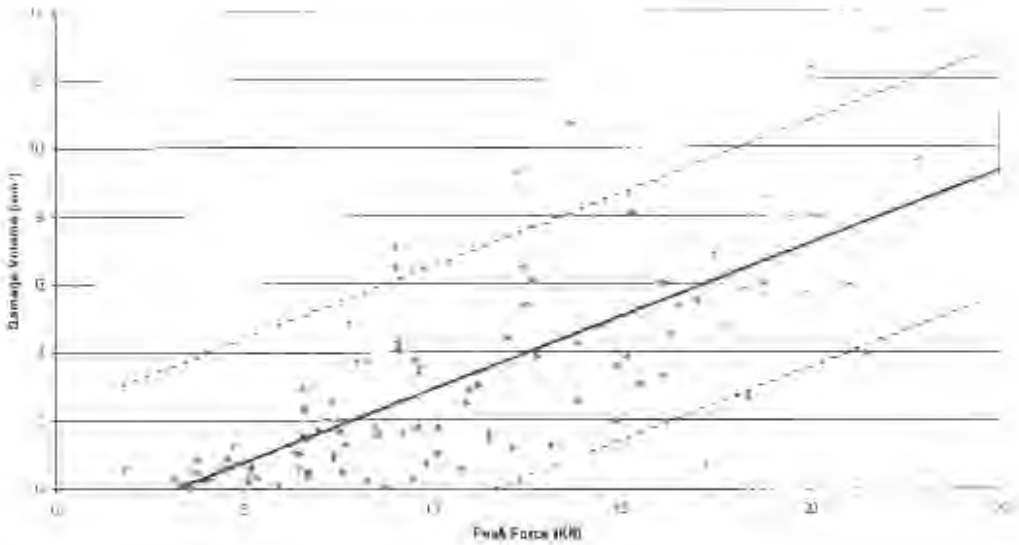

Figure 4-4: Graph of the relationship between the damage volume and peak force.

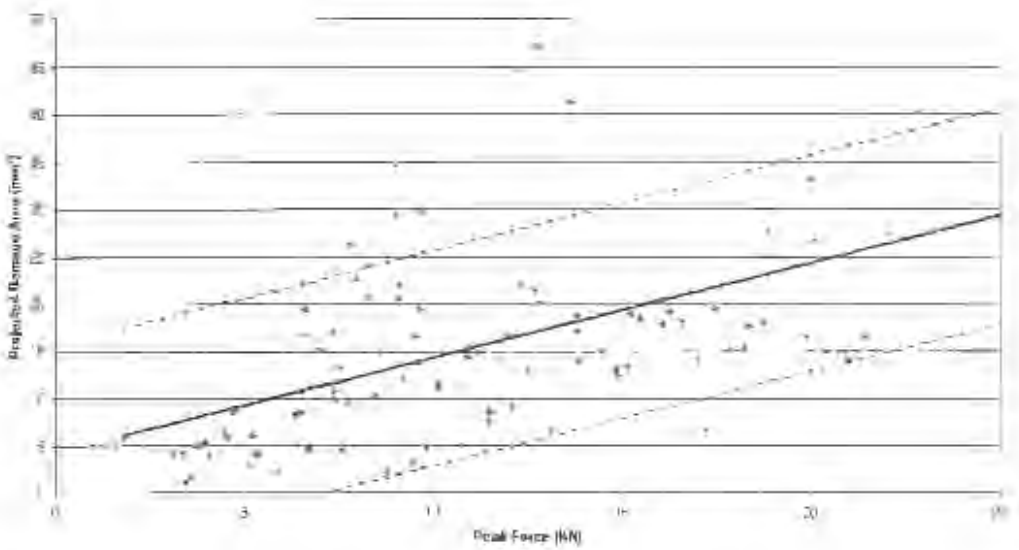

Figure 4-5: Graph of the relationship between the projected damage area and peak force.

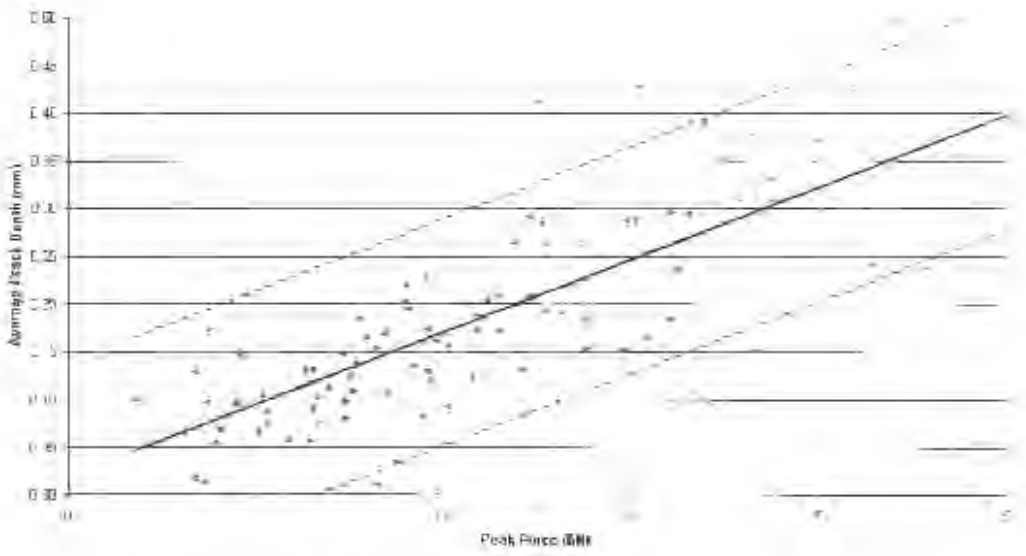

Figure 4-6: Graph of the relationship between the average crack depth and peak force

4.3 *Effect Of The Average Force On PDC Cutter Damage*

Figure 4-7 through Figure 4-9 show the relationship between the average force and damage volume, projected damage area and the average crack depth for the various striker bar lengths.

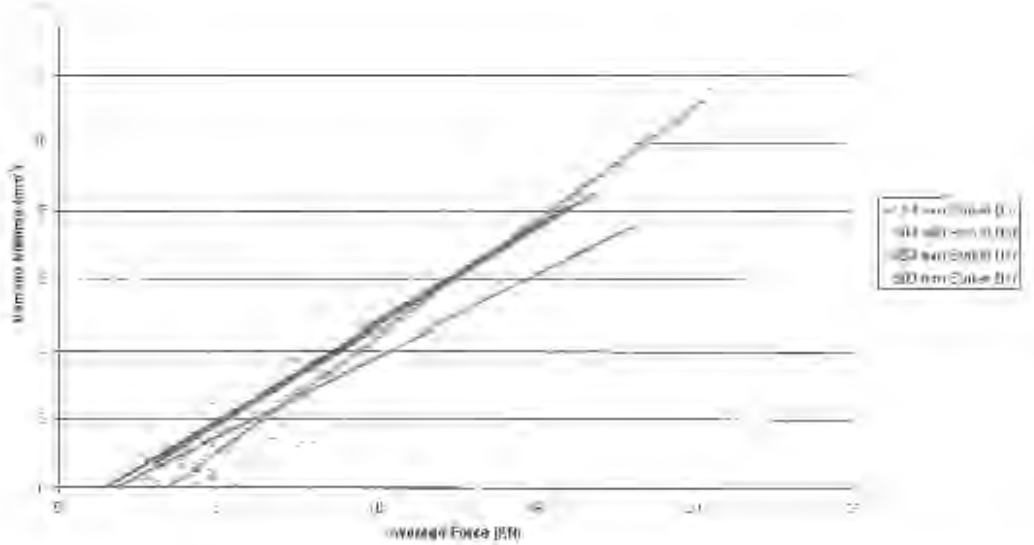

Figure 4-7: Graph of the relationship between the damage volume and average force for the various striker bar lengths

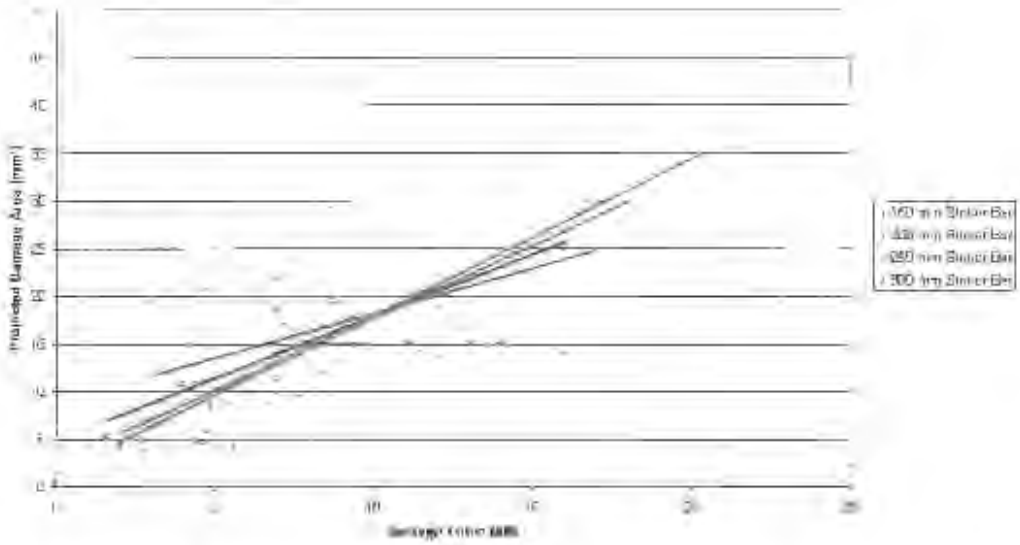

Figure 4-8: Graph of the relationship between the projected damage area and average force for the various striker bar lengths.

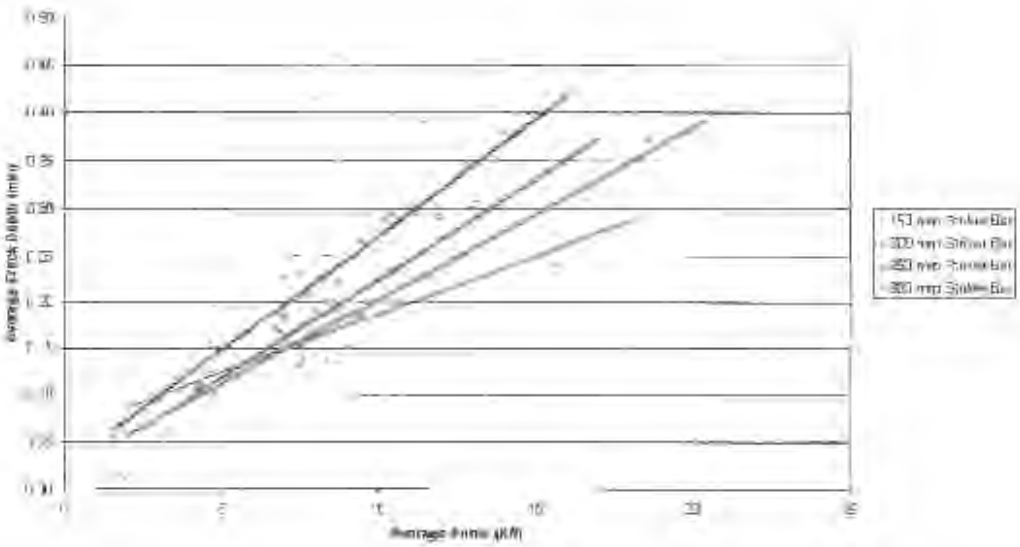

Figure 4-9: Graph of the relationship between the average crack depth and average force for the various striker bar lengths.

A summary of the statistical analysis of the significance of slope and intercept for the graphs of the effect of the applied average force on PDC cutter damage for the various striker bar lengths is presented in Table 4-3. The statistical analysis of the pooled data is summarised in Table 4-4 and the graphs shown in Figure 4-10 through Figure 4-12 with a 75% confidence limit.

	Significance Of Slope	Critical Significance Value	Significance Of Intercept	Critical Significance Value
Damage Volume vs. Average Force	9.63	2.71	0.00	3.95
Projected Damage Area vs. Average Force	0.56	2.71	0.11	3.95
Average Crack Depth vs. Average Force	2.26	2.71	2.64	3.95

Table 4-3: Summary of the statistical analysis for the relationships between PDC cutter damage and average force.

	Pooled Slope	Pooled Intercept	Correlation Coefficient
Damage Volume vs. Average Force	0.56	-1.23	0.74
Projected Damage Area vs. Average Force	1.37	-4.12	0.57
Average Crack Depth vs. Average Force	0.018	0.056	0.73

Table 4-4: Summary of the statistical analysis of the pooled data for the relationships between the PDC cutter damage and average force.

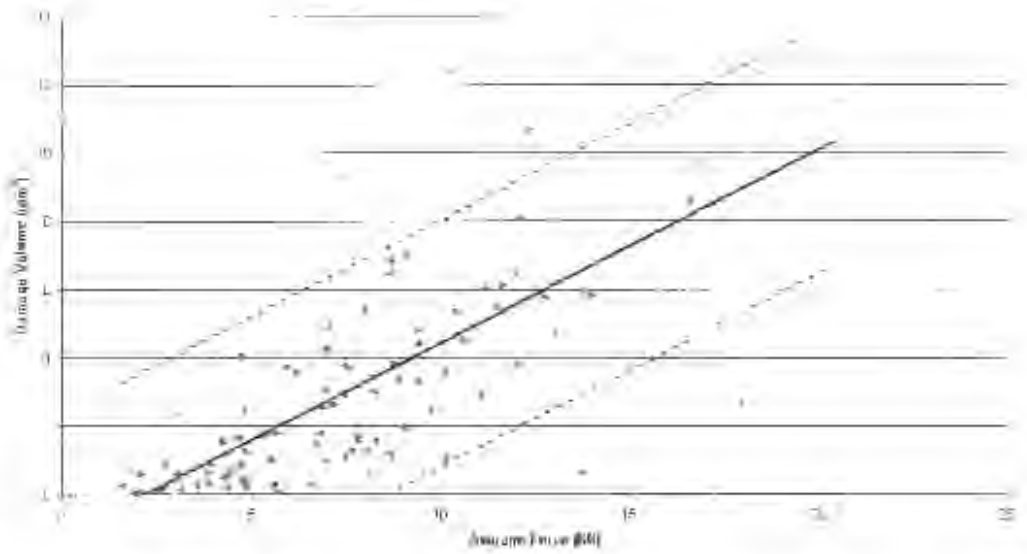

Figure 4-10: Graph of the relationship between the damage volume and average force.

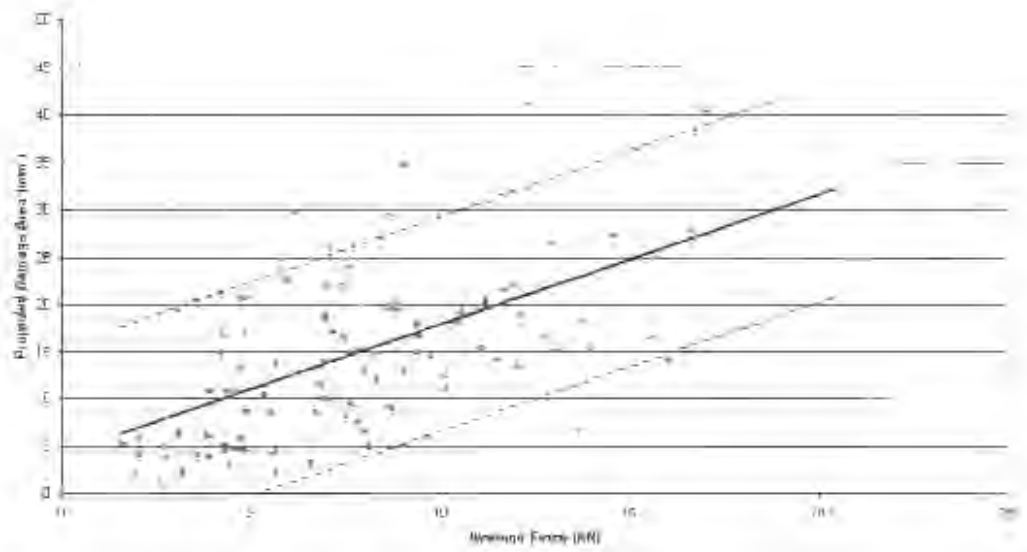

Figure 4-11: Graph of the relationship between the projected damage area and average force.

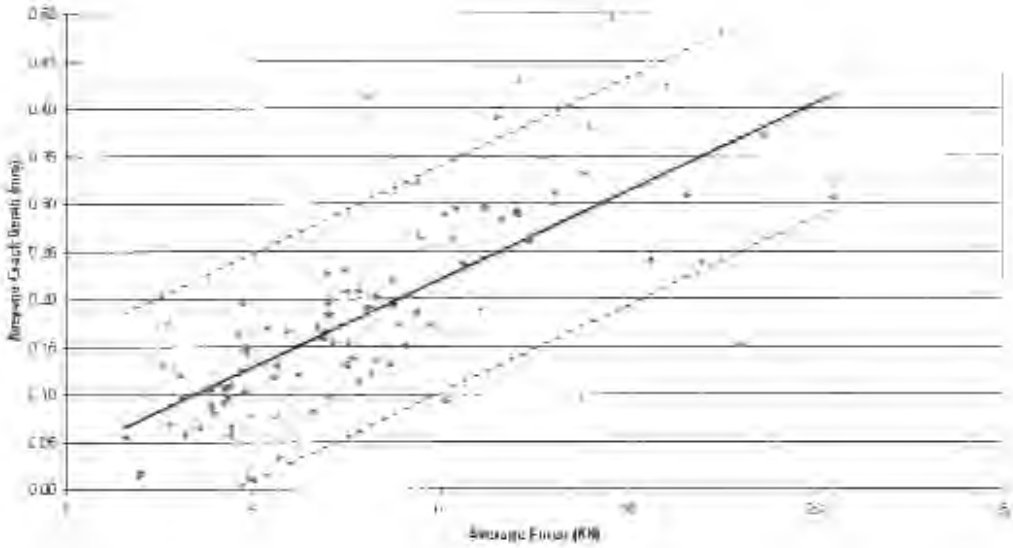

Figure 4-12: Graph of the relationship between the average crack depth and average force.

4.4 *Effect Of Impulse On PDC Cutter Damage*

The effect of the applied impulse on damage volume, projected damage area and the average crack depth for the various striker bar lengths are presented in Figure 4-13 through Figure 4-15.

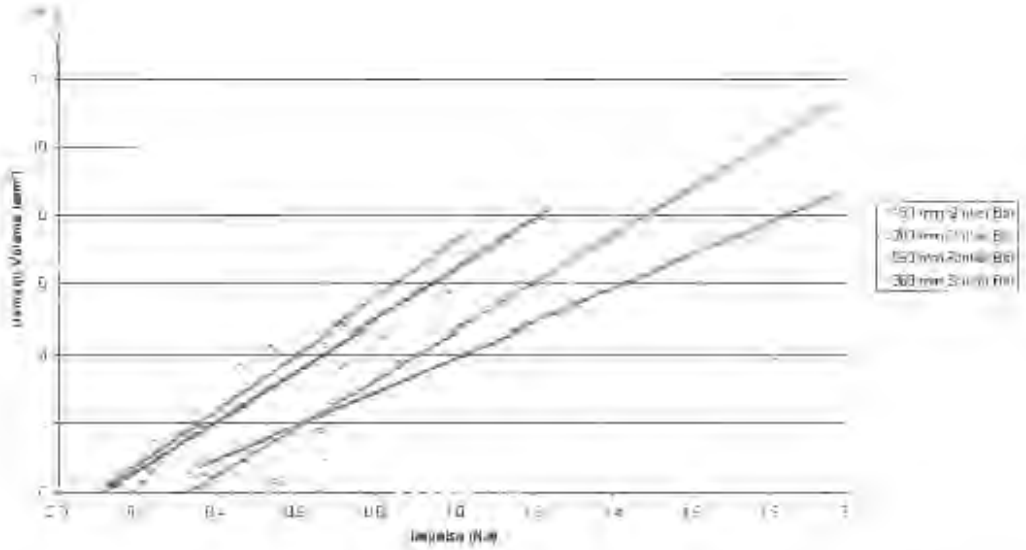

Figure 4-13: Graph of the relationship between the damage volume and applied impulse for the various striker bar lengths.

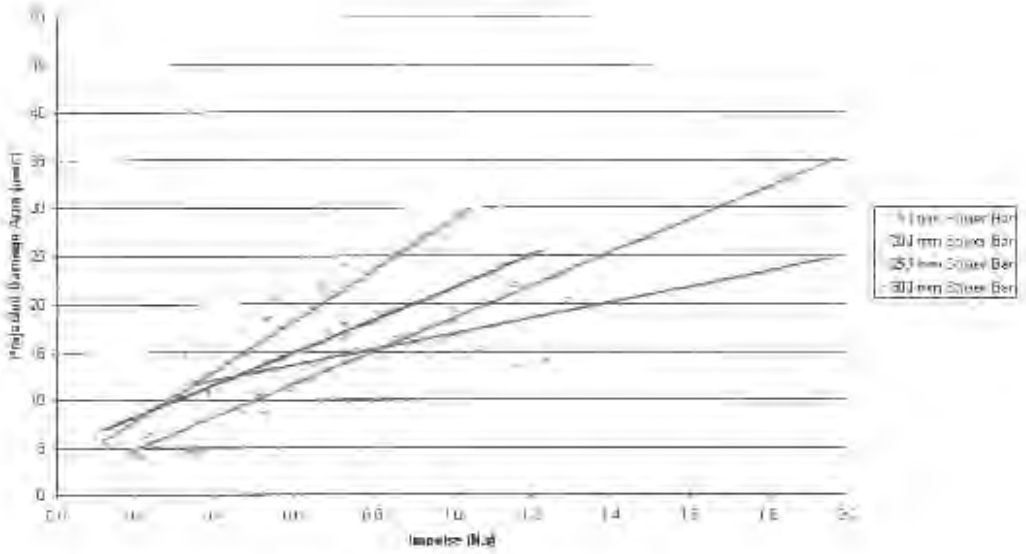

Figure 4-14: Graph of the relationship between the projected damage area and applied impulse for the various striker bar lengths.

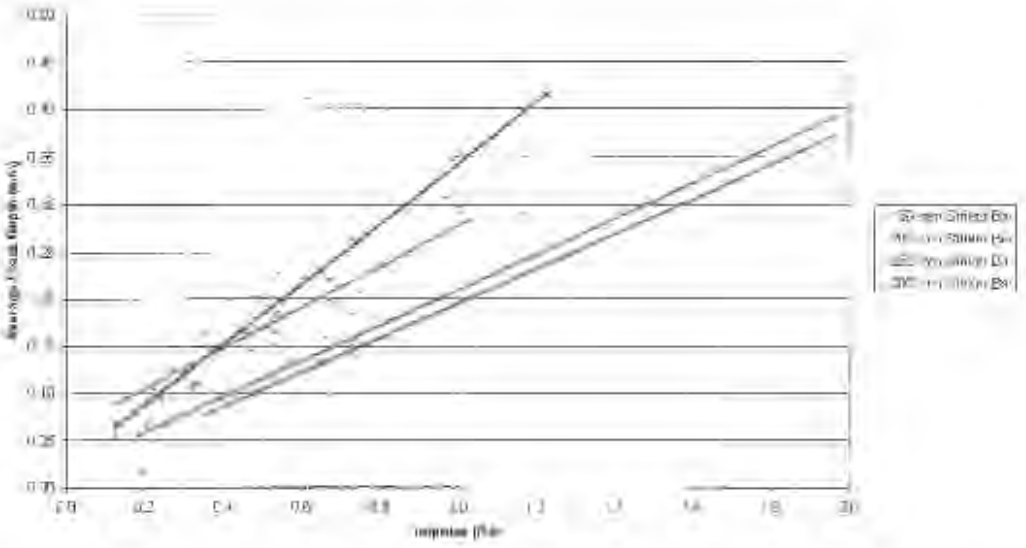

Figure 4-15: Graph of the relationship between the average crack depth and applied impulse for the various striker bar lengths.

Table 4-5 shows a summary of the statistical analysis of the significance of slope and intercept for the graphs of the effect of the applied impulse on the PDC cutter damage for the various striker bar lengths shown in Figure 4-13 through Figure 4-15.

	Significance Of Slope	Critical Significance Value	Significance Of Intercept	Critical Significance Value
Damage Volume vs. Impulse	1.31	2.71	14.69	3.95
Projected Damage Area vs. Impulse	2.15	2.71	4.62	3.95
Average Crack Depth vs. Impulse	2.18	2.71	21.03	3.95

Table 4-5: Summary of the statistical analysis for the relationships between the PDC cutter damage and applied impulse.

4.5 *Relationship Between Projected Damage Area And Damage Volume*

Figure 4-16 and Figure 4-17 show the relationship between the projected damage area and damage volume for the various striker bar lengths.

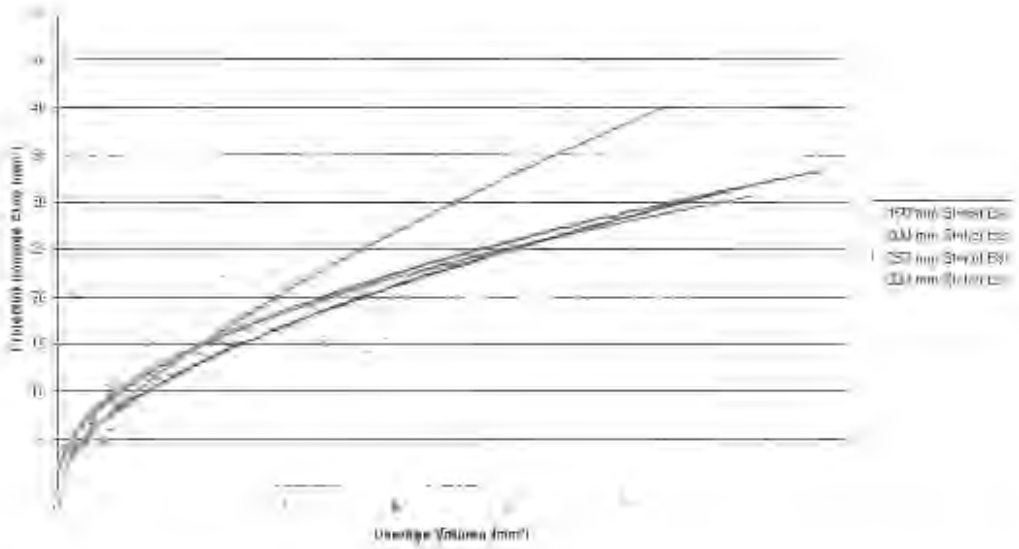

Figure 4-16: Graph of the relationship between the projected damage area and damage volume for the various striker bar lengths.

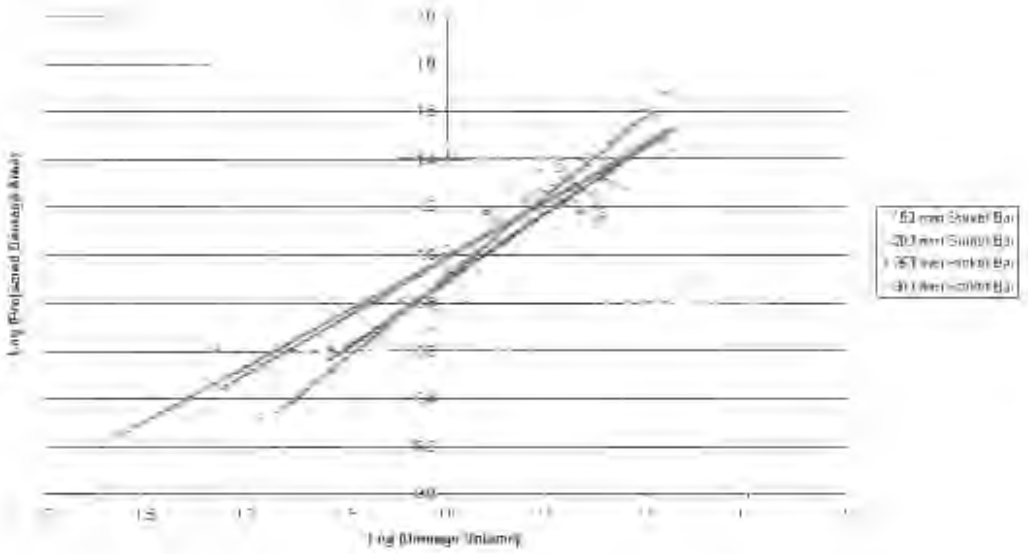

Figure 4-17: Graph of the relationship between the log of projected damage area and the log of damage volume for the various striker bar lengths.

A summary of the statistical analysis of the significance of slope and intercept for the graph of the log of the projected damage area and the log of the damage volume for the various striker bar lengths is presented in Table 4-6. The statistical analysis of the pooled data is summarised in Table 4-7 and the graphs shown in Figure 4-18 and Figure 4-19 with a 75% confidence limit.

	Significance Of Slope	Critical Significance Value	Significance Of Intercept	Critical Significance Value
Log (Projected Damage Area) vs. Log (Damage Volume)	1.88	2.71	1.51	3.95

Table 4-6: Summary of the statistical analysis for the relationship between the log of the projected damage area and the log of the damage volume.

	Pooled Slope	Pooled Intercept	Correlation Coefficient
Log (Projected Damage Area) vs. Log (Damage Volume)	0.53	0.94	0.91

Table 4-7: Summary of the statistical analysis of the pooled data for the relationship between the log of projected damage area and the log of damage volume.

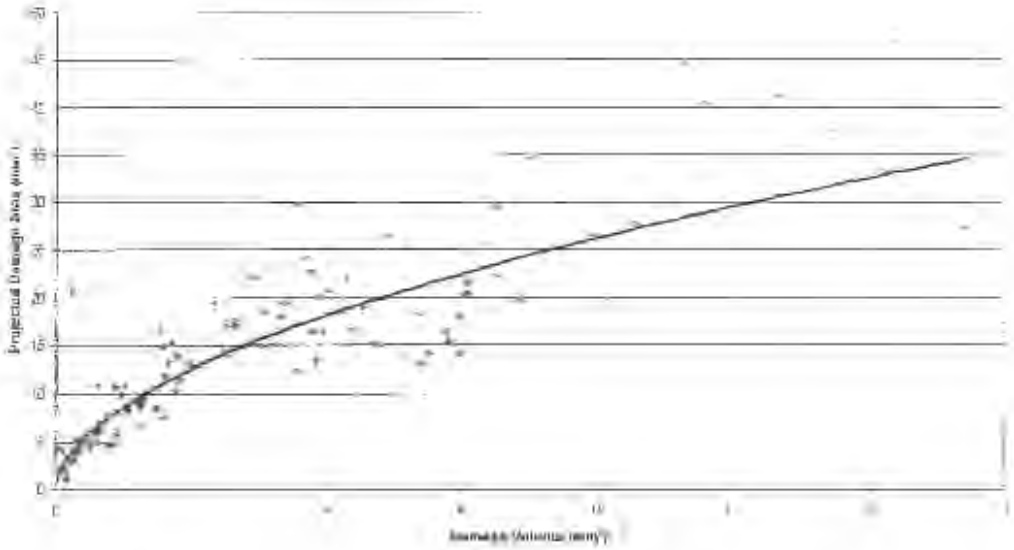

Figure 4-18: Graph of the relationship between the projected damage area and damage volume

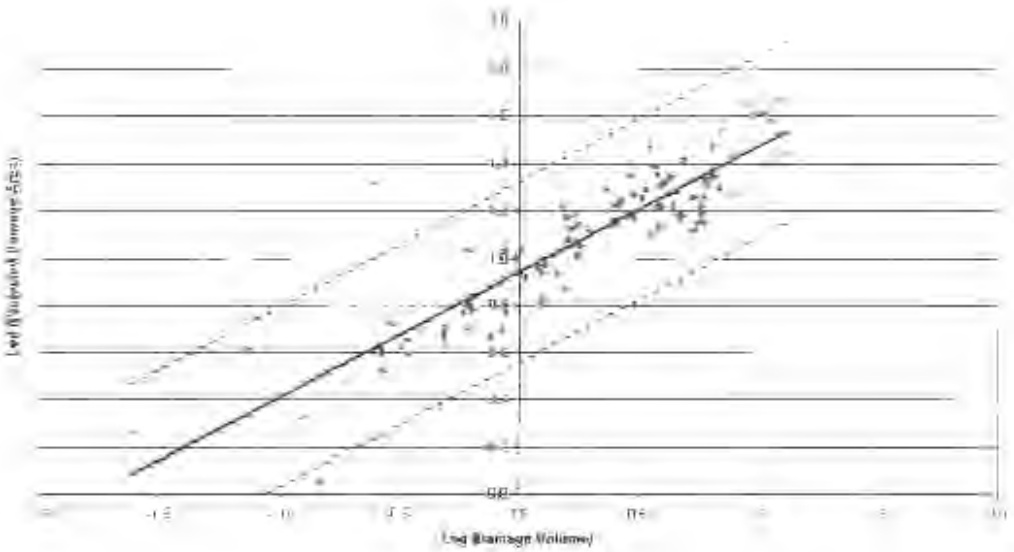

Figure 4-19: Graph of the relationship between the log of projected damage area and the log of damage volume.

5 *DISCUSSION OF RESULTS AND FINDINGS*

In order to be able to identify the spalling mechanisms of PDC cutters and compare the effect of stress wave shape on the degree of spalling using the SHPB apparatus it was vital that all experimental procedures and parameters were consistent throughout testing. This resulted in experimental data that could be compared and allowed the evaluation of the impact characteristics of the PDC cutters. This has been an introductory investigation and further investigations are necessary to evaluate the effect of the following on PDC cutter spalling:

- Negative rake angle
- PCD table thickness
- Impact surface
- PDC cutter type

In order to isolate and identify the mechanism responsible for the spalling of the PDC cutters required them to be tested under extreme loading conditions for compression waves, reflected tensile waves, contact stresses, resultant forces and normal forces.

All data obtained during the impact testing of the PDC cutters was of projected damage area and mass losses, which were converted to volume losses and average crack depth measurements. The loading conditions were characterised as the peak force, average force and impulse experienced by the PDC cutters which were then plotted as a function of each other as well as of the damage measurements. In the following chapter the results and findings are discussed.

5.1 Results Of The Failure Mechanism Identification

The PDC cutters were loaded under the various conditions in order to identify the mechanism / mechanisms responsible for the spalling phenomenon. The cutters showed no signs of spalling even under extreme loading during the series of experiments conducted to reproduce a failure due to a compression waves, reflected tensile waves and contact stresses as described in section 3.3.1 through 3.3.3.

The testing procedures for the PDC cutters where a resultant force (Section 3.3.4) was applied managed to cause failure, although it was not due to spalling. It resembled rather a micro-chipping / chipping failure, as the fracture planes were more or less perpendicular to that of the PCD table and not in-plane as with the spalling phenomenon.

The failure investigation due to the normal force (Section 3.3.5) resulted in a reproducible failure due to spalling of the PDC cutters. Although the degree varied throughout the series of experiments, the failures were consistent with those of spalling. It is therefore believed that the spalling phenomenon of PDC cutters is due to the application of an excessive normal force, which agrees well with the results obtained in similar investigations [16, 23, 24, 25, 26] as described in section 2.2.4.

5.2 *Effect Of The Peak Force On PDC Cutter Damage*

Figure 4-1 through Figure 4-6 show the relationship between the peak force and the average crack depth, projected damage area and damage volume. From these graphs it is evident that the PDC cutter damage is directly proportional to the applied peak force and linear trend lines were used to describe the impact behaviour.

The effect of the various striker bar lengths is shown in Figure 4-1 through Figure 4-3 and there do not appear to be any obvious trends. From the summary of the statistical analysis in Table 4-1 it is evident that the slopes and intercepts are not significantly different using a 99 % confidence level as described in section 3.5.4. The data may therefore be pooled and described using a single linear trend line. The graphs are shown in Figure 4-4 through Figure 4-6 with a 75% confidence limit

Table 4-1 also presents the correlation coefficients of the pooled data, which shows that the average crack depth and damage volume plots offer a better correlation. This suggests that the projected damage area is not necessarily the most accurate method of measuring the PDC cutter damage, but a further investigation will be required into the significance of these values. The correlation coefficients of the pooled data also show that the scatter for this investigation is relatively large and similar observations have been noted in all published data. This is believed to be due to the failure process that involves a brittle fracture of the PCD table of the PDC cutters.

The observations above suggest that the failure of PDC cutters is dependent on the amplitude and independent of the period of the applied stress wave. This in itself has serious repercussions on the traditional testing methods of PDC cutters and will be discussed further in section 5.4.

5.3 *Effect Of The Average Force On PDC Cutter Damage*

The relationship between the average applied force and the average crack depth, projected damage area and damage volume are presented in Figure 4-7 through Figure 4-12. These graphs indicate a linear relationship and that as PDC cutter damage increases so there is a corresponding increase in the average applied force.

Figure 4-7 through Figure 4-9 show the effect of the various striker bar lengths and it appears that there is no obvious relationship between the striker bar lengths, applied average force and PDC cutter damage. From the summary of the statistical analysis in Table 4-3 it is evident that neither the slopes nor intercepts are significantly different using a 99 % confidence level, and the data may therefore be combined and described using a common slope and intercept. The graphs are shown in Figure 4-10 through Figure 4-12 with a 75% confidence limit

The correlation coefficients of the combined data are also presented in Table 4-3 and indicate that the average crack depth and damage volume plots offer a better correlation than that of the projected damage area. A further investigation will however be required into the significance of these values and into which method is the most accurate for measuring PDC cutter damage. The correlation coefficients also show that the data scatter for this investigation is relatively large, which is expected because of the failure process that involves the brittle fracture of the PCD table.

These observations are similar to those of the peak applied force and also suggest that the failure of PDC cutters is dependent on amplitude and independent of the period of the applied stress wave (Discussed further in section 5.4).

5.4 *Effect Of Impulse On PDC Cutter Damage*

Figure 4-13 through Figure 4-15 show the relationship between the applied impulse and the average crack depth, projected damage area and damage volume for the various striker bar lengths. From these graphs it is evident that the PDC cutter damage is directly proportional to the applied impulse and linear trend lines were used to describe the impact behaviour.

It appears that there is a definite influence of the striker bar lengths on PDC cutter damage and from the summary of the statistical analysis in Table 4-5, it is evident that the slopes are not significantly different using a 99 % confidence level. The intercepts are however significantly different and the pooled data intercepts may not be used.

The graphs show that there is a distinct vertical displacement in the linear trend lines and that for any given value of PDC cutter damage, an increased applied impulse is required for the decreasing striker bar lengths. This believed to be due to the fact that the applied impulse is a function of the force and period of the measured stress wave. Therefore a decreasing striker bar length requires an increased applied force in order to achieve the same impulse value.

This is an important observation as it implies that the failure of PDC cutters is not a dependant on the applied impulse but rather on the magnitude of the force experienced. This in itself has serious repercussions on traditional drop testing experimental methods and suggests that they cannot be used to describe the impact behaviour of PDC cutters.

This is due to the fact that drop testing techniques make use of the transfer of impact energy to the PDC cutters by means of the common principles of the potential and kinetic energy. These principles do not take into account either the amplitude or period of the applied stress wave, which would account for the lack of correlation.

Each and every drop tester is unique and thus the characteristics of the impulse that the PDC cutters are subjected to will vary. The SHPB apparatus therefore offers an experimental technique that allows the characterisation of the applied stress wave in terms of amplitude and period and will ensure that experimental data is comparable.

5.5 *Relationship Between Projected Damage Area And Damage Volume*

The effect of the projected damage area on the damage volume for the various striker bar lengths as well as the pooled data are presented in Figure 4-16 through Figure 4-19. These graphs indicate a general trend that as the damage volume increases so the projected damage area increases.

Figure 4-16 and Figure 4-17 shows the effects of the various striker bar lengths and it appears that there is no distinct relationship between the striker bar lengths, projected damage area and damage volume. From the summary of the analysis in Table 4-6 it is evident that the slopes and intercepts are not significantly different using a 99 % confidence level as described in section 3.5.4. The data may therefore be combined and described using a common slope and intercept.

Graphs of the combined data are shown in Figure 4-18 and Figure 4-19 with a 75% confidence limit. The graphs show that initially the projected damage area rises steeply compared to the damage volume, but as PDC cutter damage increases so the rate of change of damage volume increases.

This suggests that the crack shape changes as the PDC cutter damage increases. These observations display an interesting behavioural characteristic that is outside the scope of the current report, but warrants further investigation.

The correlation coefficient of the combined data is presented in Table 4-7 and shows that the data scatter for the relationship between the projected damage area and damage volume is relatively small.

6 CONCLUSIONS

Under the experimental conditions detailed in this report and from the results that were obtained, the following conclusions could be made:

- The SHPB apparatus offers an experimental technique that allows the characterisation of the applied stress wave in terms of amplitude and period.
- The spalling of PDC cutters can be achieved using the SHPB apparatus.
- The phenomenon spalling in PDC cutters is due to the application of excessive normal forces.
- Peak force, average force and applied impulse are directly proportional to PDC cutter damage when subjected to the experimental loading conditions.
- Under the experimental impact loading the failure of PDC cutters is dependent on the amplitude and independent of the period of the applied stress wave.
- Drop testing and other energy techniques cannot be used to describe the impact behaviour of PDC cutters.

7 FUTURE WORK

The following suggestions are made to assist and improve on this experimental project in the future:

- The effect of the negative rake angle, PCD table thickness, impact surface and PDC cutter type should be investigated.

- The relationship between the projected damage area and damage volume should be further investigated.

- An investigation into the method that offers the best correlation of measuring PDC cutter damage should be conducted.

- The use of a high-speed camera should be considered in conjunction with the SHPB apparatus.

This study was an introductory investigation and it is hoped that this will stimulate further investigation in this field.

8 REFERENCES

1. B. Hopkinson, *A method of measuring the pressure produced in the detonation of high explosives or by the impact of bullets*, Phil. Trans. R. Lond., Vol. A213, pp. 437-456, 1914.

2. G.T. Gray, *Classic split-Hopkinson pressure bar technique*, to be published in ASM, Vol. 8, 1999.

3. R.M. Davies, *A simple modification of the Hopkinson pressure bar*, Proc. 7th Int. Cong. On Appl. Mech., Vol. 1, pp. 404, 1948.

4. H. Kolsky, *An investigation of the mechanical properties of materials at very high rates of loading*, Proc. Phys. Soc. Lond. Vol. B62, pp. 676-700, 1949.

5. M. Daimaruya and H. Kobayashi, *Measurements of impact tensile strength of concrete and mortar using reflected tensile stress waves*, J. Phys. IV France 10, pp. 173-178, 2000.

6. J. Duffy, J.D. Campbell and R.H. Hawley, *On the use of a torsional split Hopkinson bar to study rate effects in 1100-0 aluminium*, Trans. ASME: J. Appl. Mech., Vol. 38, pp. 83-91, 1971.

7. J.L. Lewis and W. Goldsmith, *A biaxial split Hopkinson bar for simultaneous torsion and compression*, Rev. Sci. Instrum., Vol. 44, pp. 811-813, 1973.

8. D.E. Lambert and C.A. Ross, *Strain rate effects on dynamic fracture and strength*, Int. J. Impact Eng., Vol. 24, pp. 985-989, 2000.

9. A.M. Bragov and A.K. Lomunov, *Methodological aspects of studying dynamic material properties using the Kolsky method*, Int. J. Impact Eng., Vol. 16, pp. 321-330, 1995.

10. T.J. Cloete and G. Nurick, *A data procedure for the direct impact Hopkinson bar that accounts for stress wave reflections in the striker bar*, Departmental report, University of Cape Town, 2001.

11. S. Nemat-Nasser, J.B. Isaacs and J.E. Starrett, *Hopkinson techniques for dynamic recovery experiments*, Proc. R. Soc. Lond., Vol. 435, pp. 371-391, 1991.

12. H. Zhao and G. Gary, *On the use of SHPB techniques to determine the dynamic behaviour of materials in the range of small strains*, Int. J. Solid Struc., Vol. 33, pp. 3363-3375, 1996.

13. F.E. Hauser, *Techniques for measuring stress-strain relations at high strain rates*, Exp. Mech., Vol. 6, pp. 395-402, 1966.

14. M.M. Al-Mousawi, S.R. Reid and W.F. Deans, *The use of the split Hopkinson pressure bar techniques in high strain rate materials testing*, J. Mech. Eng. Sci., Vol. 221, pp. 273-292, 1997.

15. W. Johnson, *Impact strength of materials*, Edward Arnold, 1972.

16. T. Lin, M. Hood, G.A. Cooper and X. Li, *Wear and failure mechanisms of polycrystalline diamond compact bits*, Wear, Vol. 156, pp. 133-150, 1992.

17. L.E. Hibbs Jr. and R.H. Wentworth Jr., *Borazon and diamond compact tools*, High Temp. High Press., Vol. 6, pp. 409-413, 1974.

18. D. Miess and G. Rai, *Fracture toughness and thermal resistance of polycrystalline diamond compacts*, Mater. Sci. And Eng., Vol. A209, pp. 270-276, 1996.

19. M. Davies, *An investigation into the procedures and results of drop testing used to establish the cause of failure of PDC drilling cutters*, B.Sc. Thesis, University Of Cape Town, 1997.

20. J. Wilks and E. Wilks, *Properties of diamond*, Butterworth-Heinemann Ltd., 1991.

21. H. Pastor, *Historical review of developments of tungsten carbide and its composites since its discovery by Henri Moissan in 1896*, 1961.

22. A Lamer, *Mechanical properties of polycrystalline diamonds*, Mater. Sci. And Technol., Vol. 4, pp. 949-955, 1988.

23. K.J. Dunn and M. Lee, *The fracture and fatigue of sintered diamond compact*, J. Mater. Sci., Vol. 14, pp. 882-890, 1979.

24. L.E. Hibbs, Jr. and M. Lee, *Some aspects of the wear of polycrystalline diamond tools in rock removal processes*, Wear, Vol. 46, pp. 141-147, 1978.

25. M.V. Sneddon and D.R. Hall, *Polycrystalline diamond: manufacture, wear mechanisms and the implications for bit design*, J. Petrol. Technol., Vol. 40(12), pp. 1593-1601, 1988.

26. D.A. Glowka and C.M. Stone, *Effects of thermal and mechanical loading on PDC bit life*, Soc. Petrol. Eng. Drill. Eng., Vol. 1(3), pp. 201-214, 1986.

27. F.J. Brett, T.M. Warren and S.M. Behr, *Bit whirl – a new theory of PDC bit failure*, Soc. Petrol. Eng. Drill. Eng., Vol. 5(4), pp. 275-281, 1990.

28. S. Marais, *Split-Hopkinson pressure bar*, M.Sc. Thesis, University of Cape Town, 2001.

29. F. Galvez, J. Rodriguez and V. Sanchez Galvez, *A wave propagation technique to measure the dynamic tensile strength of brittle materials*, J. Phys. IV France 10, pp. 203-208, 2000.

30. J.E. Shigley, *Mechanical engineering design*, McGraw-Hill, 1st Metric Edition, 1986.

31. J.P. Holman, *Experimental Methods for Engineers*, McGraw-Hill Inc., 6th Edition, 1994.

32. W. Volk, *Applied statistics for engineers*, Robert E. Krieger, 1980.

33. N. Jones, *Structural Impact*, Cambridge University Press, 1989.

APPENDIX – EXPERIMENTAL RESULTS AND DATA ANALYSES

Results Of PDC Cutter Testing

Specimen	Series	Striker Bar (mm)	Peak Force (KN)	Average Force (KN)	Damage Area (mm^2)	Damage Volume (mm^3)
P-13-1-01	1	200	4.4726	3.0822	6.4007	0.6098
P-13-1-02	1	300	9.0912	4.7101	20.7023	4.0488
P-13-1-03	1	150	6.3228	7.4862	8.2607	1.0732
P-13-1-05	1	200	7.5851	4.3551	4.4814	0.4878
P-13-1-06	1	300	6.5928	3.0191	19.4065	2.3171
P-13-1-07	1	150	7.7735	7.0314	26.3888	4.8780
P-13-1-08	1	250	10.1338	6.8523	11.4163	1.8049
P-13-1-09	1	200	11.4809	6.6984	8.4867	1.4634
P-13-1-10	1	300	14.8946	10.1169	12.4478	3.5854
P-13-2-01	1	150	13.6575	12.3604	41.2089	10.7073
P-13-2-02	1	250	12.3261	11.9839	22.1825	6.4878
P-13-2-03	1	200	14.4827	9.3545	14.8954	4.7805
P-13-2-04	1	300	18.2390	13.9692	15.3089	5.8049
P-13-2-05	1	150	18.8267	16.6000	27.7644	8.5610
P-13-2-06	1	250	19.9882	18.5812	33.1697	12.3171
P-13-2-07	1	200	12.5008	7.9706	13.0864	5.3902
P-13-2-08	1	300	20.0583	12.9730	26.5481	7.9756
P-16-1-01	1	150	5.1957	3.8410	6.0377	0.6341
P-16-1-02	1	250	5.3345	5.6030	4.2262	0.3171
P-16-1-03	1	200	3.7599	2.6967	4.9023	0.8537
P-16-1-04	1	300	8.7397	5.6657	2.1532	0.0732
P-16-1-05	1	150	9.6199	8.8540	19.4248	3.3659
P-16-1-06	1	250	10.9520	11.0663	15.3427	2.9024
P-16-1-07	1	200	15.4501	6.8899	18.4578	3.0488
P-16-1-08	1	300	9.6697	6.1623	29.6654	3.5610
P-16-1-09	1	150	18.3434	17.9866	17.5662	2.6585
P-16-2-01	1	200	13.8358	6.9111	13.8899	2.5366
P-16-2-02	1	300	16.0629	11.1582	20.4842	6.0488
P-16-2-03	1	150	10.1239	10.1373	10.9668	1.0244
P-16-2-04	1	250	7.7058	7.6280	9.3861	1.2927

P-16-2-05	1	200	13.81	6.95	18.72	4.24	0.54
P-16-2-09	1	200	19.85	12.78	16.50	5.76	0.99
P-16-2-10	1	300	22.00	14.55	27.31	13.46	1.69
P-16-2-11	1	150	18.75	13.80	18.11	5.98	0.80
P-16-2-12	1	250	25.37	20.43	37.72	11.51	1.97
P-13-1-01	2	150	6.55	4.22	16.70	1.51	0.24
P-13-1-02	2	250	3.38	2.01	4.13	0.07	0.19
P-13-1-03	2	200	4.56	4.70	5.88	0.88	0.36
P-13-1-04	2	300	6.47	4.38	10.80	0.61	0.51
P-13-1-05	2	150	5.33	3.88	3.91	0.34	0.22
P-13-1-06	2	250	16.57	10.39	18.14	5.34	1.00
P-13-1-07	2	200	16.99	11.47	14.12	5.51	0.89
P-13-1-09	2	150	8.44	5.35	10.37	1.76	0.31
P-13-1-10	2	250	6.47	5.50	8.58	1.00	0.53
P-13-2-01	2	200	7.94	5.90	22.63	3.76	0.46
P-13-2-02	2	300	17.21	13.73	6.77	0.63	1.59
P-13-2-03	2	150	11.20	8.28	14.87	3.02	0.48
P-13-2-05	2	200	11.95	9.42	16.63	4.39	0.73
P-13-2-07	2	150	3.43	2.58	1.13	0.15	0.15
P-16-1-01	2	200	9.20	8.31	11.99	1.61	0.64
P-16-1-02	2	300	9.47	6.58	3.27	0.27	0.76
P-16-1-03	2	150	1.81	2.05	5.82	0.59	0.12
P-16-1-04	2	250	7.36	3.93	10.80	0.88	0.38
P-16-1-06	2	300	12.11	8.67	9.13	1.20	1.00
P-16-1-07	2	150	7.53	4.65	13.25	1.66	0.27
P-16-1-08	2	250	6.95	7.82	15.22	1.71	0.75
P-16-1-09	2	200	16.24	10.56	19.11	4.54	0.82
P-16-1-10	2	300	13.11	8.05	6.65	1.27	0.93
P-16-2-01	2	150	10.89	9.73	14.37	2.49	0.56
P-16-2-02	2	250	13.80	7.12	17.08	2.63	0.69
P-16-2-04	2	300	21.45	15.60	16.44	3.95	1.81
P-16-2-05	2	150	12.67	11.62	21.54	6.10	0.67
P-16-2-07	2	200	6.66	4.75	4.76	0.49	0.37
P-16-2-08	2	300	17.48	8.69	19.60	6.85	1.01
P-16-2-11	2	200	9.01	8.66	29.46	6.49	0.67
P-16-2-12	2	300	22.81	16.97	40.36	9.61	1.97

P-13-1-01	3	200	3.94	1.59	5.31	0.29	0.12
P-13-1-03	3	150	3.69	4.30	5.08	0.49	0.25
P-13-1-04	3	250	11.47	7.81	7.47	1.56	0.75
P-13-1-05	3	200	8.55	4.21	14.88	1.59	0.32
P-13-1-06	3	300	12.28	7.50	44.60	9.29	0.87
P-13-1-07	3	150	10.78	8.13	5.00	0.61	0.47
P-13-1-08	3	250	15.15	12.06	13.37	3.85	1.16
P-13-1-09	3	200	9.81	4.56	4.68	0.76	0.35
P-13-1-10	3	300	15.27	12.09	18.90	8.10	1.40
P-13-2-02	3	250	9.10	6.98	21.99	4.29	0.67
P-13-2-03	3	200	16.09	9.36	17.91	3.32	0.72
P-13-2-05	3	150	8.99	9.07	34.69	7.05	0.53
P-13-2-06	3	250	3.59	1.91	1.82	0.02	0.18
P-13-2-07	3	200	6.53	7.46	22.25	2.93	0.58
P-13-2-08	3	300	8.27	4.85	20.81	0.24	0.56
P-16-1-01	3	150	3.09	3.57	4.09	0.27	0.21
P-16-1-03	3	200	4.06	2.76	3.91	0.27	0.21
P-16-1-04	3	300	9.59	5.63	13.83	1.78	0.65
P-16-1-05	3	150	5.12	4.38	2.90	0.19	0.25
P-16-1-07	3	200	17.87	13.05	15.20	4.71	1.01
P-16-1-08	3	300	6.70	4.85	4.48	0.34	0.56
P-16-1-09	3	150	14.82	9.04	12.99	1.98	0.52
P-16-1-10	3	250	7.39	6.94	9.93	0.98	0.67
P-16-2-01	3	200	20.97	16.01	14.09	5.98	1.24
P-16-2-02	3	300	9.53	7.45	16.48	3.78	0.86
P-16-2-04	3	250	4.72	4.83	8.68	1.24	0.47
P-16-2-05	3	200	12.72	10.30	47.09	12.39	0.80
P-16-2-06	3	300	5.87	3.15	2.13	0.12	0.37
P-16-2-07	3	150	12.75	8.76	20.10	3.88	0.51
P-16-2-08	3	250	7.34	4.81	16.94	2.51	0.46
P-16-2-12	3	250	8.24	7.52	24.10	3.71	0.73

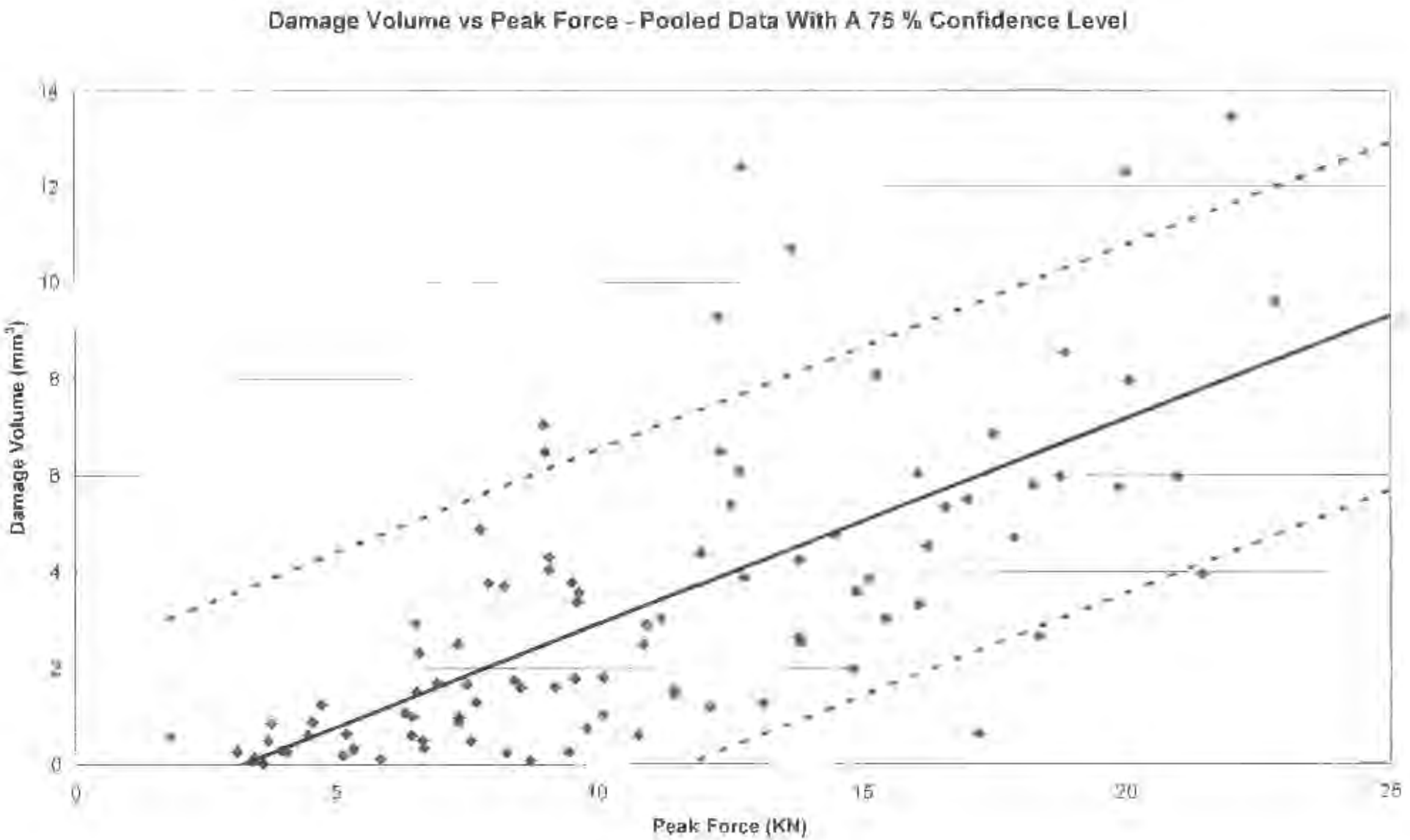
Damage Volume vs Peak Force - Pooled Data With A 75 % Confidence Level
Damage Volume (mm³)
Peak Force (KN)
0
5
10
15
20
25
0
2
4
6
8
10
12
14

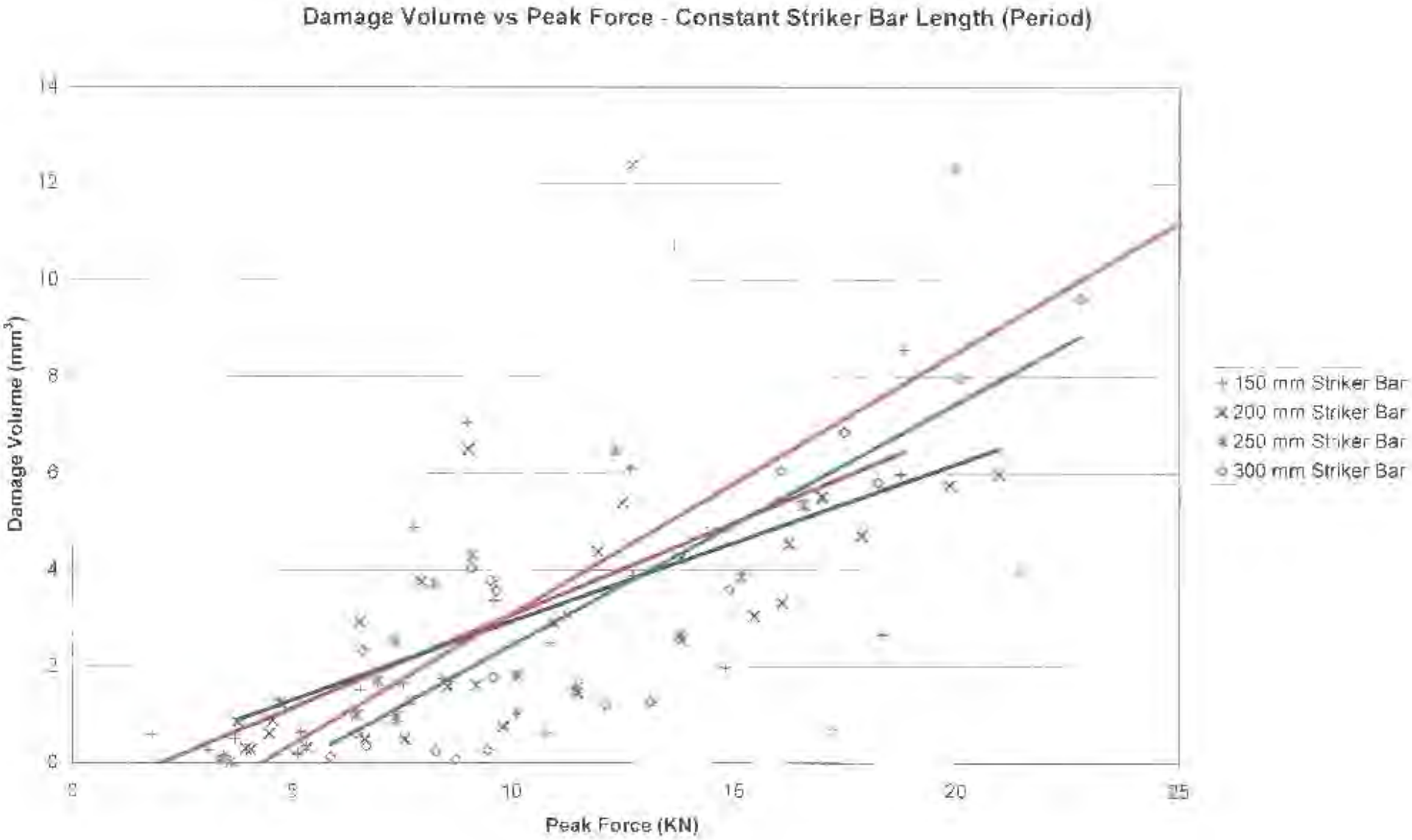
Damage Volume vs Peak Force - Constant Striker Bar Length (Period)
Damage Volume (mm³)
Peak Force (KN)
0
4
8
10
15
20
150 mm Striker Bar
200 mm Striker Bar
250 mm Striker Bar
300 mm Striker Bar

Statistical Analysis Of Damage Volume vs Peak Force - Constant Striker Bar Length

Original Data:

Striker Bar Length	150 mm	200 mm	250 mm	300 mm
N	28	27	21	24
Σx	235.70	300.32	213.23	312.96
Σx^2	2798.85	4017.37	2781.50	4741.17
Σy	70.95	89.05	66.44	94.93
Σy^2	398.50	486.60	448.22	690.85
Σxy	890.06	1210.96	1067.33	1567.84

Sums Of Squares:

	$\Sigma' x^2$	$\Sigma' y^2$	$\Sigma' xy$	$\Sigma' x^2$	$\Sigma' y^2$	Slope
Total	2704.81	949.80	1156.77	404.71	355.00	0.40
Means	176.70	16.02	52.71	16.72	0.30	0.30
Difference	2528.11	933.78	1104.06	482.16	451.03	0.44
1	576.61	197.57	221.17	84.63	112.24	0.39
2	678.90	192.80	220.47	71.01	120.99	0.34
3	614.39	228.02	332.42	178.80	48.16	0.64
4	660.21	315.39	330.00	184.95	150.64	0.50
Sum	2528.11	933.78	1104.06	501.45	432.34	

Analysis Of Variance

Source Of Variance	Sum Of Squares	Degrees Of Freedom	Mean Square
Means Of Correlation	0.30	7	0.19
Difference Between Means			
Slope And Pooled Slope:	3.17	1	3.17
Between Slopes:	19.24	1	0.43
Error	432.34	83	5.08
Total	459.09	85	

	Significance Value	Critical Significance Value
Significance Of Slopes	1.32	2.71
Significance Of Intercepts	0.85	3.95

Summary:

Pooled Slope:	0.43
Pooled Intercept:	-1.37
Correlation Coefficient:	0.72

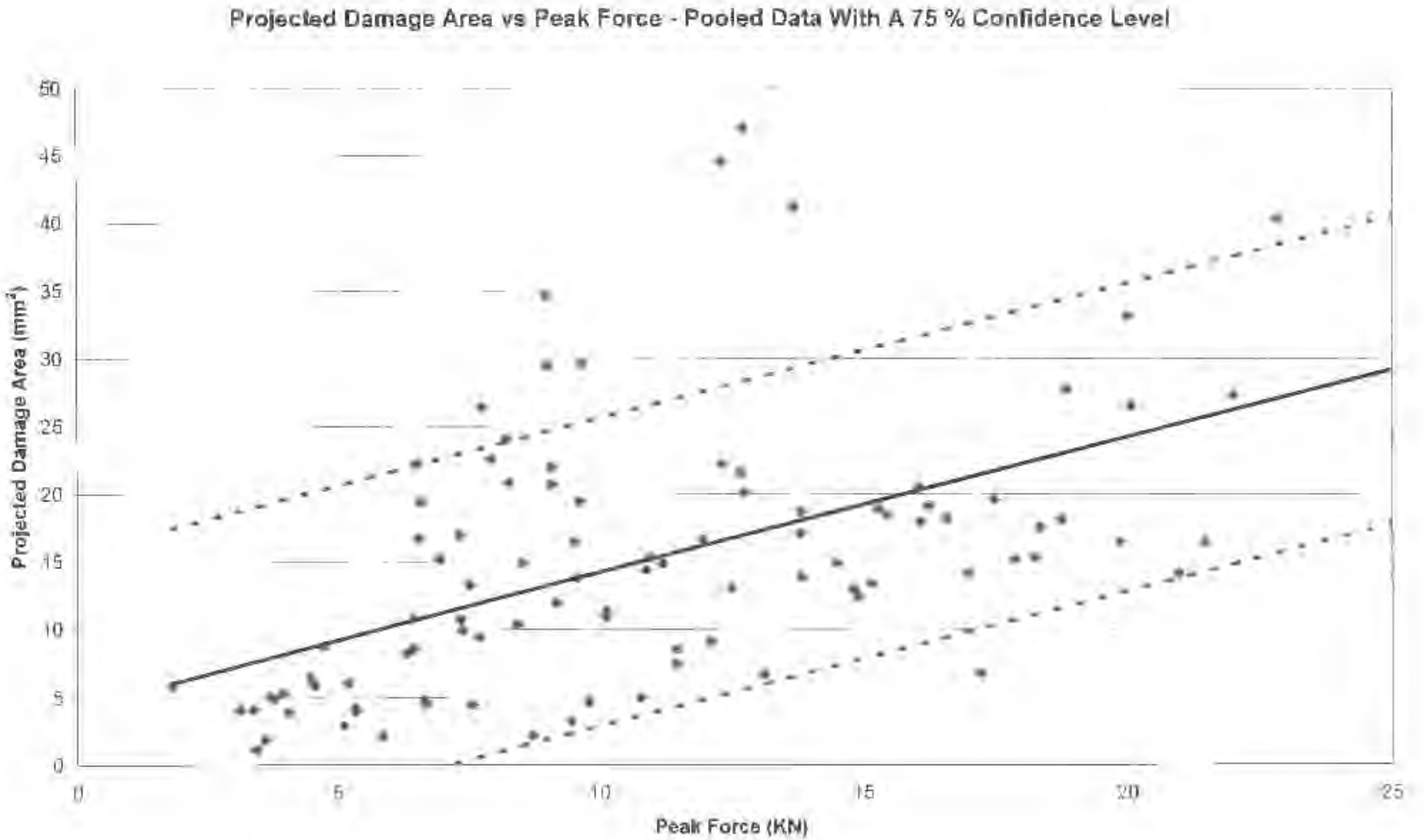
Projected Damage Area vs Peak Force - Pooled Data With A 75 % Confidence Level
Projected Damage Area (mm²)
50
45
40
35
30
25
20
15
10
5
0
0
5
10
15
20
25
Peak Force (KN)

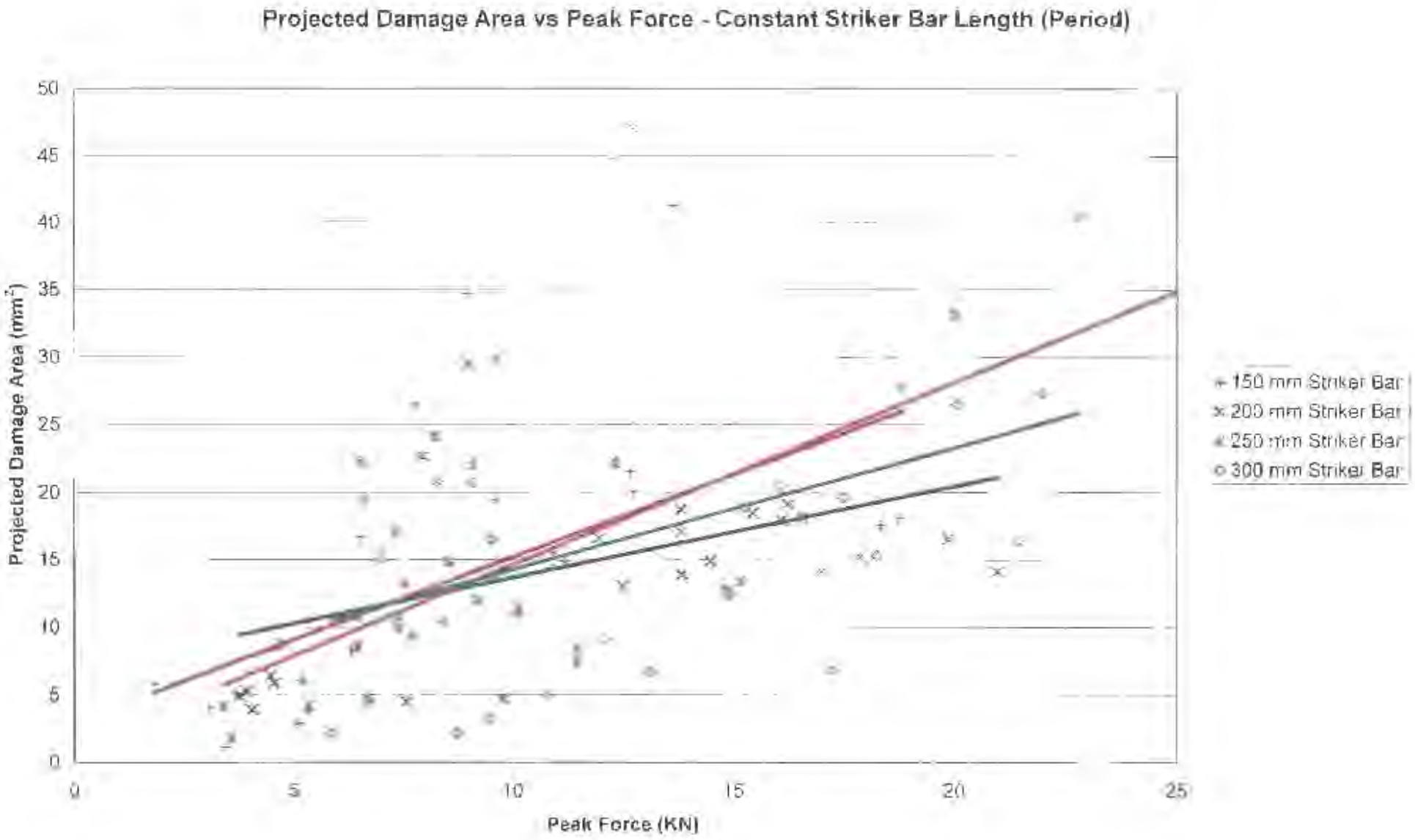
Projected Damage Area vs Peak Force - Constant Striker Bar Length (Period)
Projected Damage Area (mm²)
Peak Force (KN)
0
5
10
15
20
25
30
35
40
45
50
150 mm Striker Bar
200 mm Striker Bar
250 mm Striker Bar
300 mm Striker Bar

Statistical Analysis Of Projected Damage Area vs Peak Force - Constant Striker Bar Length

Original Data:

Striker Bar Length	150 mm	200 mm	250 mm	300 mm
N	25	27	21	24
Σx	235.70	300.32	213.33	342.96
Σx^2	2798.85	4017.87	2781.44	4741.17
Σy	362.54	389.75	317.69	608.26
Σy^2	7760.47	7878.40	6309.56	9799.80
Σxy	4122.60	4793.72	3994.98	5920.07

Sums Of Squares:

	$\Sigma' x^2$	$\Sigma' y^2$	$\Sigma' xy$	$\Sigma' c^2$	$\Sigma' y^2$	Slope
Total	2704.81	9403.49	2708.18	2711.56	6691.94	1.00
Means	176.70	109.35	119.77	81.19	28.17	0.68
Difference	2528.11	9294.14	2588.41	2630.15	6644.00	1.07
1	579.61	2602.96	704.56	860.80	1042.07	1.21
2	676.90	2252.84	456.74	810.89	1941.95	0.60
3	514.39	1653.41	828.74	1117.87	535.54	1.34
4	860.21	2854.93	598.37	538.70	2318.23	0.90
Sum	2528.11	9294.14	2588.41	2628.37	6465.78	

Analysis Of Variance

Source Of Variance	Sum Of Squares	Degrees Of Freedom	Mean Square
Means Of Correlation:	28.17	2	14.08
Difference Between Means			
Slope And Pooled Slope	19.73	1	19.73
Between Slopes:	178.22	3	59.41
Error:	6485.74	89	72.63
Total	6691.94	95	

	Significance Value	Critical Significance Value
Significance Of Slopes:	0.82	2.71
Significance Of Intercepts:	0.27	3.95

Summary:

Pooled Slope:	1.00
Pooled Intercept:	4.21
Correlation Coefficient:	0.54

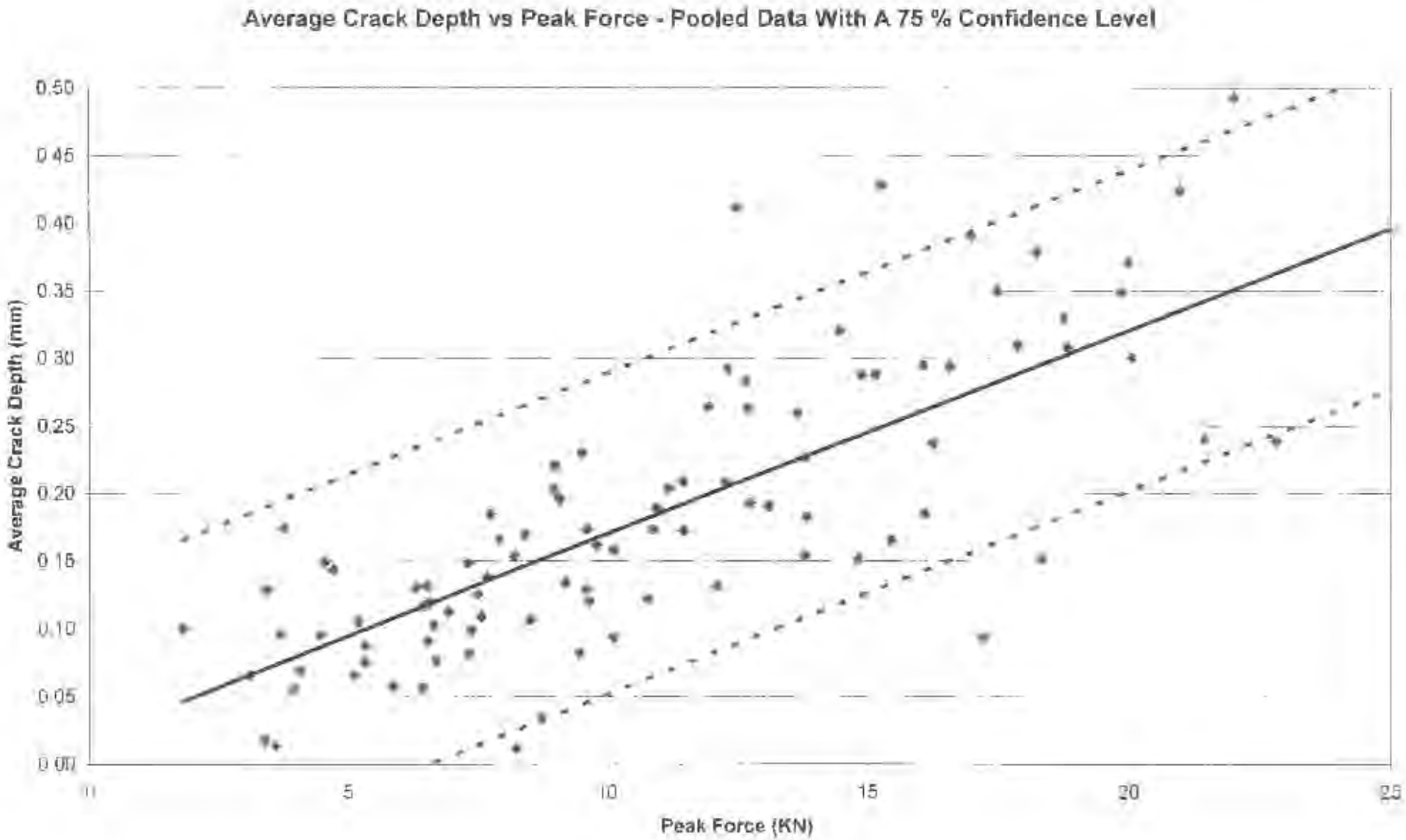
Average Crack Depth vs Peak Force - Pooled Data With A 75 % Confidence Level
Average Crack Depth (mm)
0.50
0.45
0.40
0.35
0.30
0.25
0.20
0.15
0.10
0.05
0.00
0
5
10
15
20
25
Peak Force (KN)

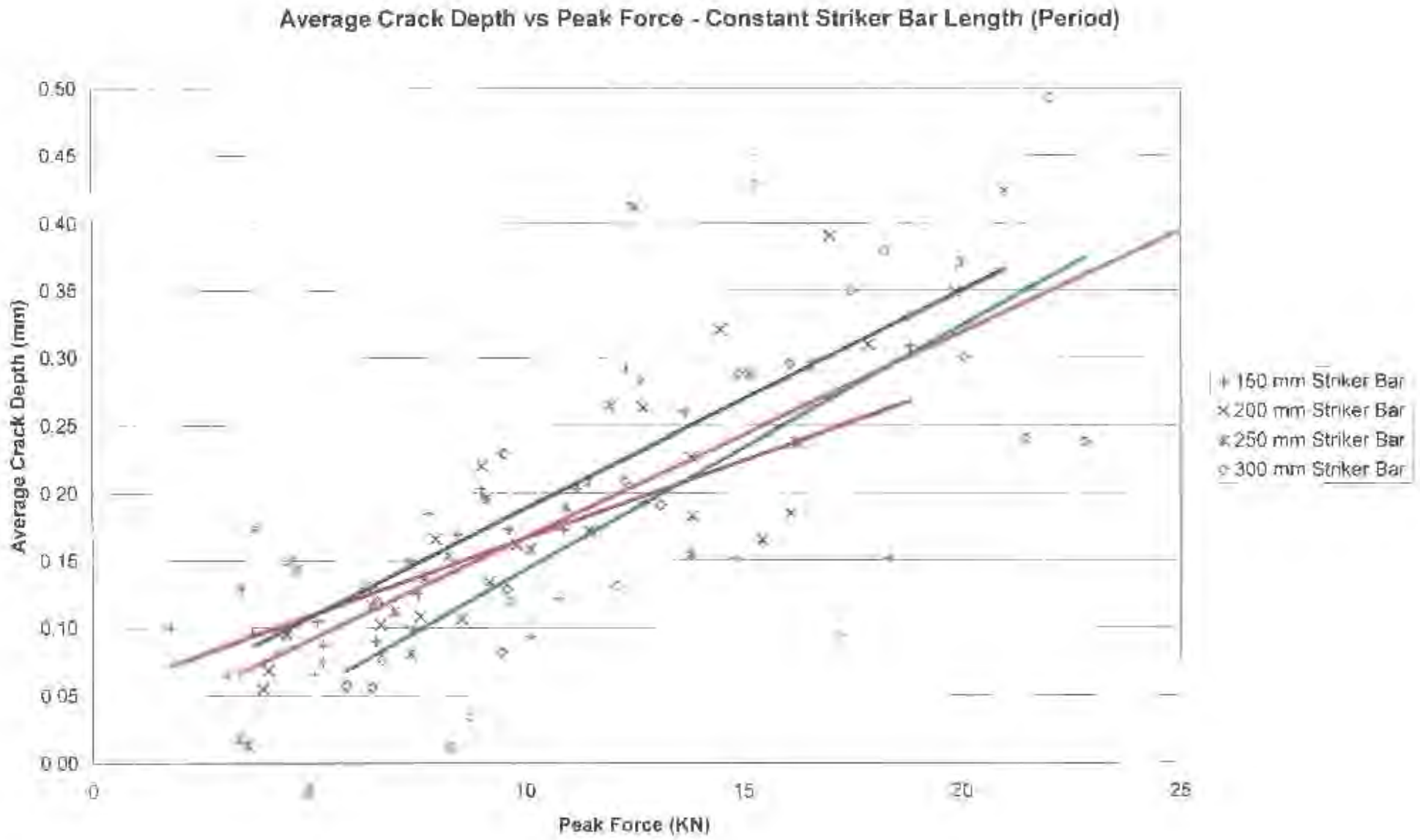
Average Crack Depth vs Peak Force - Constant Striker Bar Length (Period)
Average Crack Depth (mm)
0.50
0.45
0.40
0.35
0.30
0.25
0.20
0.15
0.10
0.05
0.00
0
5
10
15
20
25
Peak Force (KN)
150 mm Striker Bar
200 mm Striker Bar
250 mm Striker Bar
300 mm Striker Bar

Statistical Analysis Of Average Crack Depth vs Peak Force - Constant Striker Bar Length

Original Data:

Strikel Bar Length	150 mm	200 mm	250 mm	300 mm
N	25	27	21	24
Σx	335.70	500.32	213.33	312.96
Σx^2	2798.86	4017.37	2761.44	4741.17
Σy	4.00	5.50	3.55	4.75
Σy^2	0.77	1.43	0.79	1.33
Σxy	34.29	72.96	45.45	73.65

Sums Of Squares:

	Σx^2	Σy^2	Σxy	Σe^2	Σy^2	Slope
Total	2704.81	1.03	40.40	0.62	0.81	0.04
Means	176.70	0.04	1.96	0.02	0.02	0.01
Difference	2528.11	0.99	38.84	0.60	0.79	0.03
1	676.01	0.13	6.62	0.08	0.05	0.01
2	670.90	0.28	10.94	0.16	0.11	0.02
3	514.39	0.18	8.33	0.14	0.04	0.02
4	660.21	0.39	11.94	0.22	0.17	0.02
Sum	2528.11	0.99	38.84	0.61	0.38	

Analysis Of Variance:

Source Of Variance	Sum Of Squares	Degrees Of Freedom	Mean Square
Means Of Correlation:	0.02	2	0.01
Difference Between Means			
Slope And Pooled Slope:	0.00	1	0.00
Between Slopes:	0.01	1	0.00
Error:	0.38	89	0.00
Total	0.41	93	

	Significance Value	Critical Significance Value
Significance Of Slopes	1.10	2.71
Significance Of Intercepts	0.71	3.95

Summary:

Pooled Slope:	0.015
Pooled Intercept:	0.019
Correlation Coefficient:	0.77

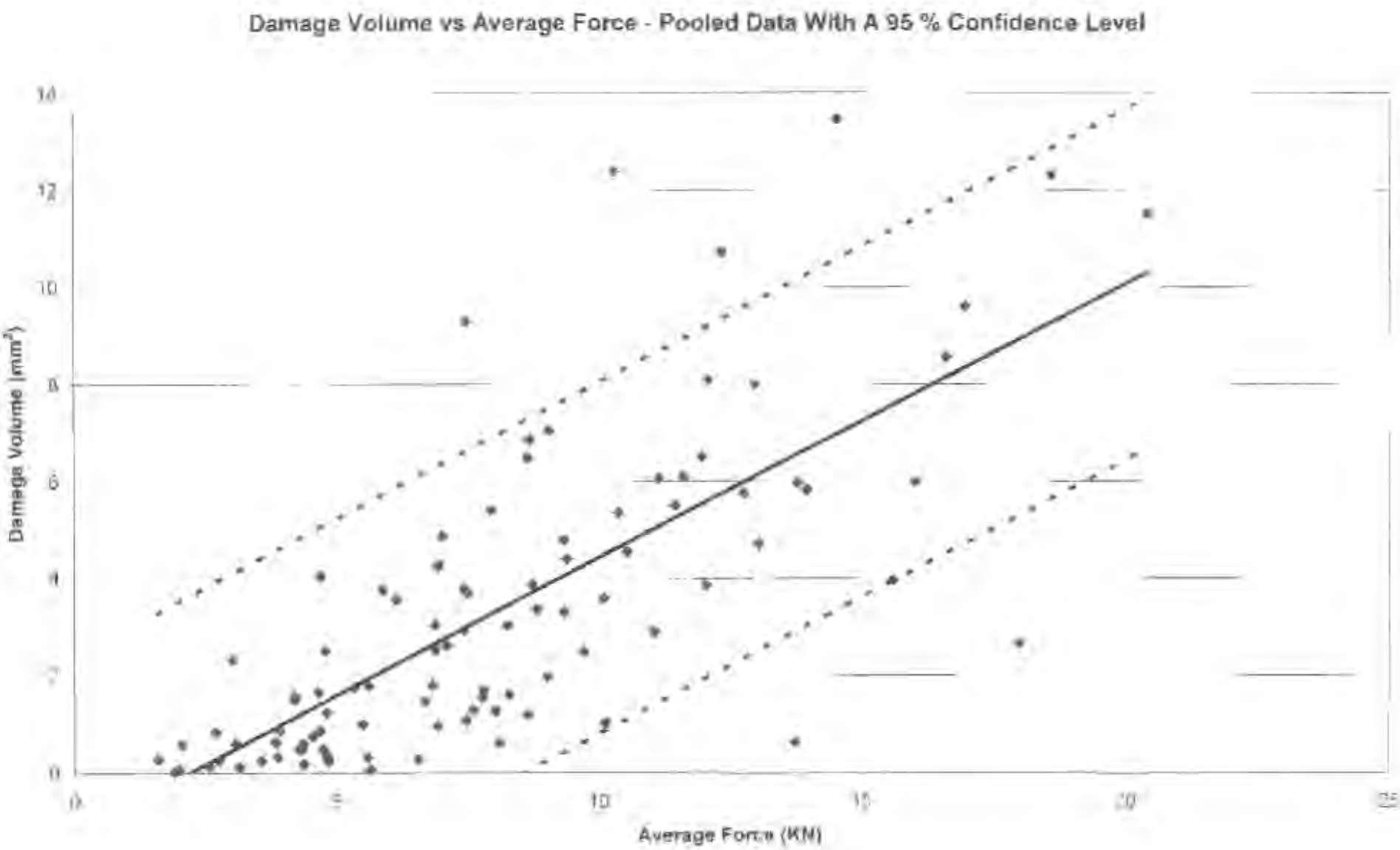
Damage Volume vs Average Force - Pooled Data With A 95 % Confidence Level
Damage Volume (mm³)
Average Force (KN)
0
10
14

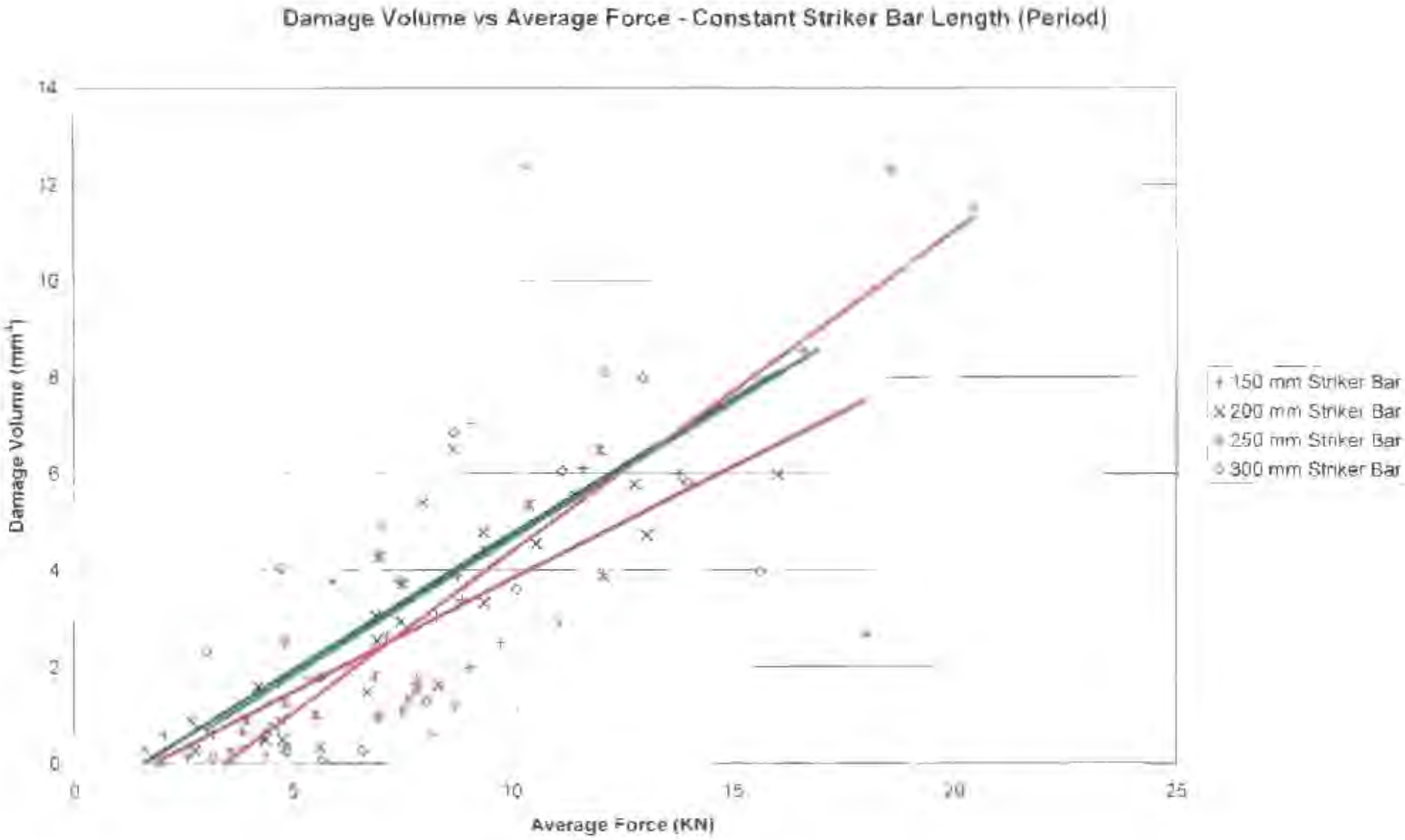
Damage Volume vs Average Force - Constant Striker Bar Length (Period)
Damage Volume (mm³)
Average Force (KN)
0
2
4
6
8
10
12
14
0
5
10
15
20
25
150 mm Striker Bar
200 mm Striker Bar
250 mm Striker Bar
300 mm Striker Bar

Statistical Analysis Of Damage Volume vs Average Force - Constant Striker Bar Length

Original Data:

Striker Bar Length	150 mm	200 mm	250 mm	300 mm
N	25	27	21	24
Σx	197.89	300.76	171.76	219.51
Σx^2	1992.81	1818.89	1044.47	2247.55
Σy	70.95	89.05	66.44	94.93
Σy^2	398.90	486.50	438.22	690.85
Σxy	760.71	845.01	635.88	1059.55

Sums Of Squares:

	$\Sigma'x^2$	$\Sigma'y^2$	$\Sigma'xy$	$\Sigma'e^2$	$\Sigma'y^2$	Slope
Total	1619.76	949.80	914.79	518.69	433.30	0.56
Means	23.54	16.02	12.65	6.80	9.22	0.54
Difference	1596.22	933.78	902.10	509.82	423.97	0.57
1	429.80	197.57	199.71	92.84	104.73	0.46
2	325.88	192.80	182.89	102.64	90.16	0.56
3	439.57	228.02	292.56	194.71	33.31	0.67
4	401.17	315.39	226.94	128.38	187.01	0.57
Sum	1596.22	933.78	902.10	518.57	415.21	

Analysis Of Variance:

Source Of Variance	Sum Of Squares	Degrees Of Freedom	Mean Square
Means Of Correlation:	433	1	433
Difference Between Means:			
Slope And Pooled Slope:	0.82	1	0.82
Between Slopes	3.76	2	1.88
Error:	116.31	93	1.25
Total	433.28	95	

	Significance Value	Critical Significance Value
Significance Of Slopes:	0.62	3.71
Significance Of Intercepts:	0.00	3.95

Summary:

Pooled Slope:	0.50
Pooled Intercept:	-1.23
Correlation Coefficient:	0.74

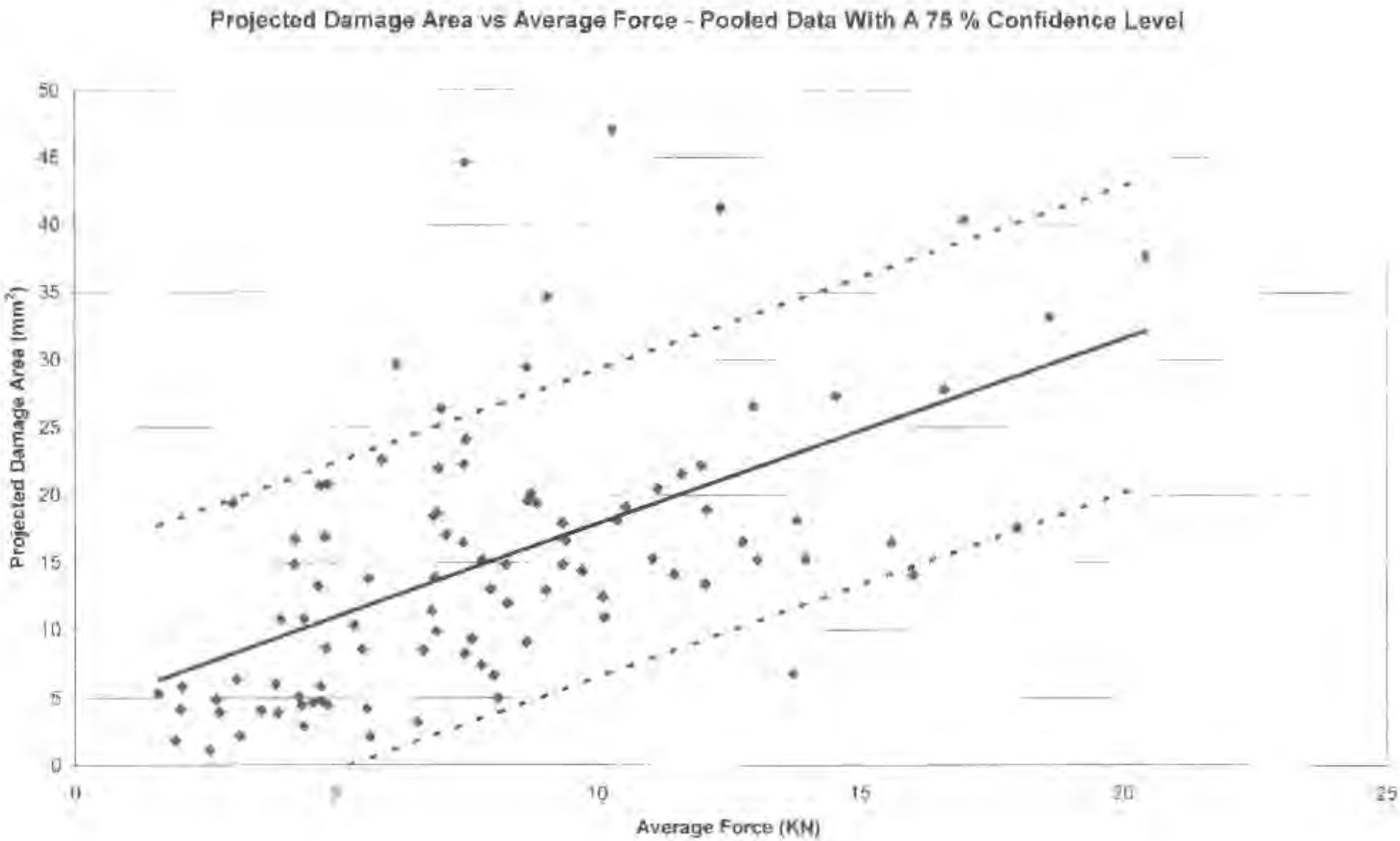
Projected Damage Area vs Average Force - Pooled Data With A 75 % Confidence Level
Projected Damage Area (mm²)
Average Force (KN)
0
5
10
15
20
25
30
35
40
45
50

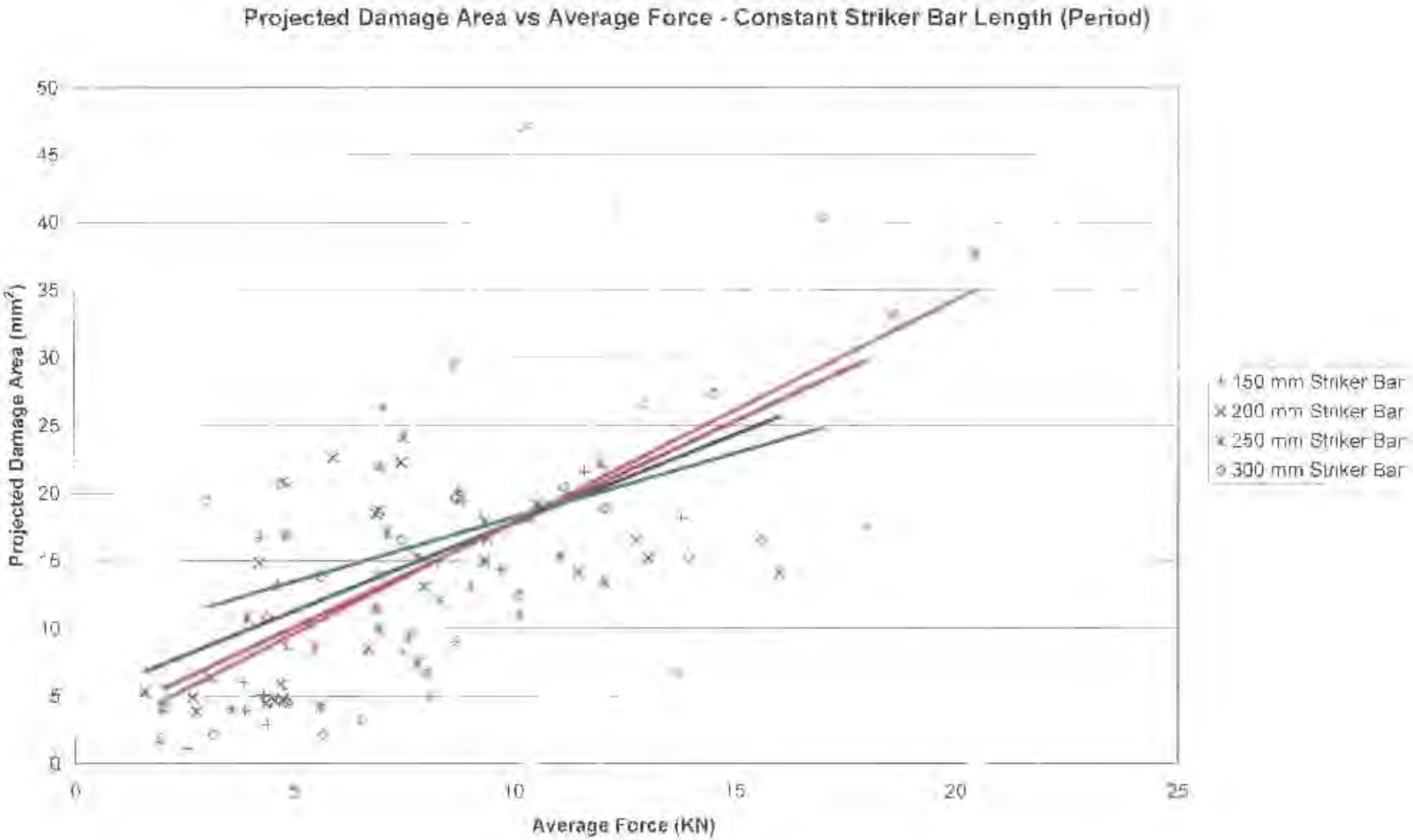
Projected Damage Area vs Average Force - Constant Striker Bar Length (Period)
Projected Damage Area (mm²)
Average Force (KN)
0
5
10
15
20
25
30
35
40
45
50
150 mm Striker Bar
200 mm Striker Bar
250 mm Striker Bar
300 mm Striker Bar

Statistical Analysis Of Projected Damage Area vs Average Force - Constant Striker Bar Length

Original Data:

Striker Bar Length	150 mm	200 mm	250 mm	300 mm
N	25	27	21	24
Σx	197.69	200.76	171.76	210.51
Σx^2	1992.81	1818.58	1844.47	2247.55
Σy	362.54	389.73	311.69	408.26
Σy^2	7760.47	7878.40	6309.55	9799.80
Σxy	3518.26	3321.97	3272.94	3959.99

Sums Of Squares:

	$\Sigma' x^2$	$\Sigma' y^2$	$\Sigma' xy$	$\Sigma' c^2$	$\Sigma' y^2$	Slope
Total	1619.76	9403.49	2223.85	3053.25	6350.24	1.37
Means	23.54	109.35	45.56	88.18	21.17	1.94
Difference	1596.22	9294.14	2178.30	2972.63	6321.51	1.36
1	429.60	2502.96	651.46	987.89	1515.07	1.52
2	325.88	2252.84	424.16	552.09	1700.75	1.30
3	439.57	1683.41	723.58	1191.10	492.31	1.65
4	401.17	2854.93	379.10	358.23	2496.70	0.94
Sum	1596.22	9294.14	2178.30	3089.31	6204.83	

Analysis Of Variance:

Source Of Variance	Sum Of Squares	Degrees Of Freedom	Mean Square
Means Of Correlation:	21.17	2	10.59
Difference Between Means Slope And Pooled Slope:	7.56	1	7.56
Between Slopes:	116.68	3	38.89
Error:	6204.83	89	69.72
Total	6350.24	95	

	Significance Value	Critical Significance Value
Significance Of Slopes:	0.56	**2.71**
Significance Of Intercepts:	0.11	**3.95**

Summary:

Pooled Slope:	1.37
Pooled Intercept:	4.13
Correlation Coefficient:	0.57

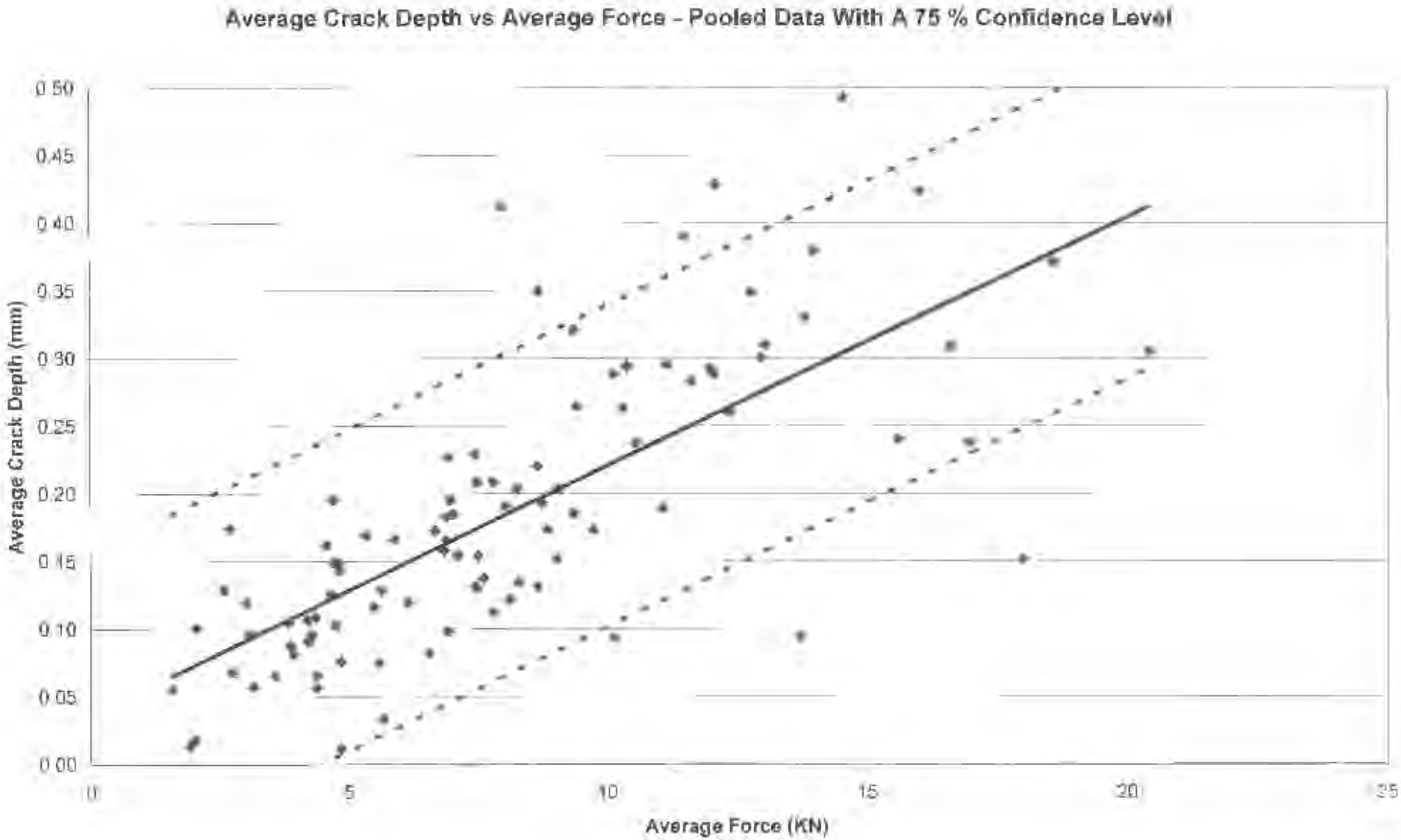
Average Crack Depth vs Average Force - Pooled Data With A 75 % Confidence Level
Average Crack Depth (mm)
0.50
0.45
0.40
0.35
0.30
0.25
0.20
0.15
0.10
0.05
0.00
0
5
10
15
20
25
Average Force (KN)

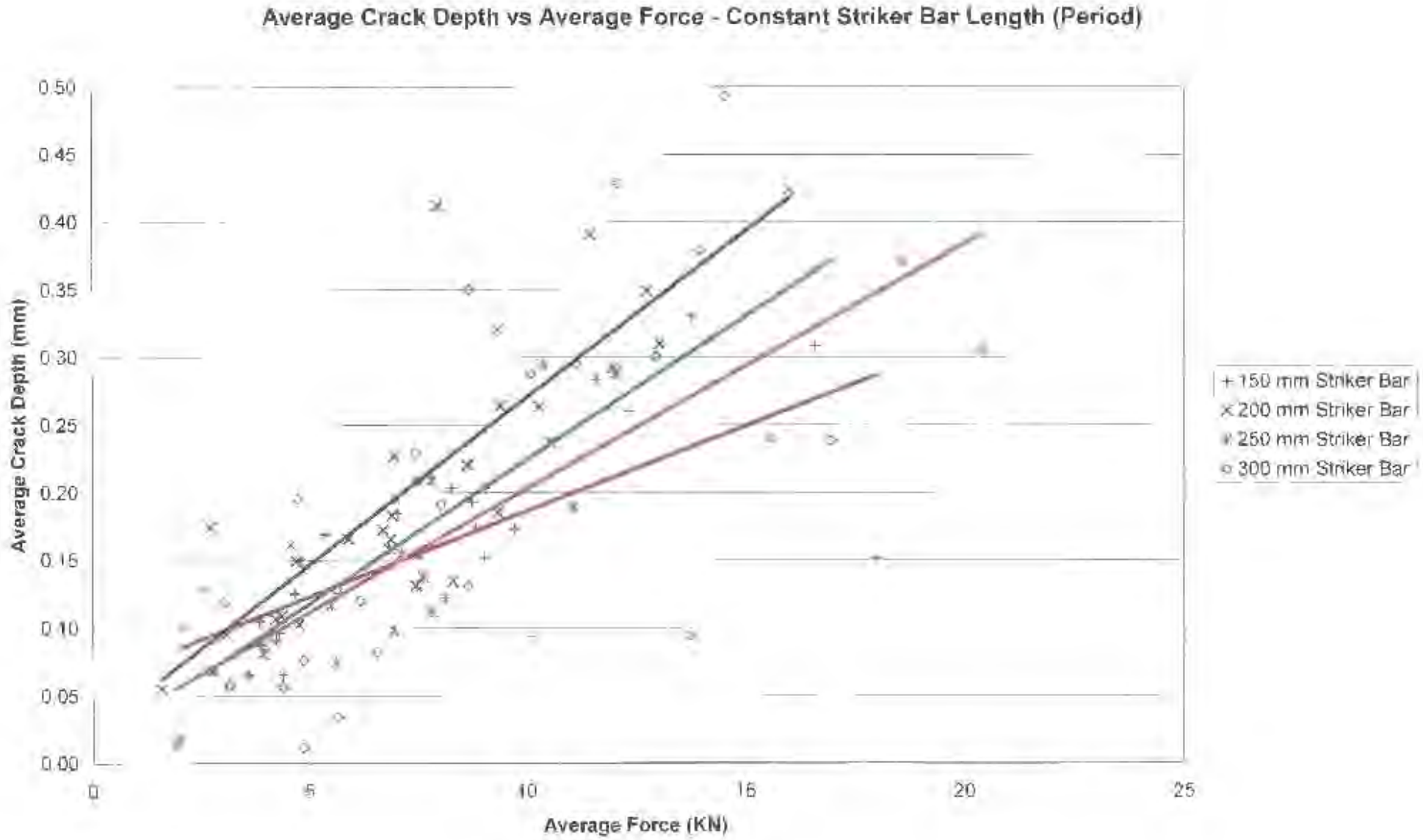
Average Crack Depth vs Average Force - Constant Striker Bar Length (Period)
Average Crack Depth (mm)
0.50
0.45
0.40
0.35
0.30
0.25
0.20
0.15
0.10
0.05
0.00
0
5
10
15
20
25
Average Force (KN)
+ 150 mm Striker Bar
× 200 mm Striker Bar
250 mm Striker Bar
300 mm Striker Bar

Statistical Analysis Of Average Crack Depth vs Average Force - Constant Striker Bar Length

Original Data:

Striker Bar Length	150 mm	200 mm	250 mm	300 mm
N	25	27	21	24
Σx	197.69	200.76	171.76	210.51
Σx^2	1992.81	1818.58	1844.47	2247.55
Σy	4.00	5.58	3.55	4.75
Σy^2	0.77	1.43	0.79	1.33
Σxy	37.00	49.49	37.06	50.15

Sums Of Squares:

	$\Sigma' x^2$	$\Sigma' y^2$	$\Sigma' xy$	$\Sigma' c^2$	$\Sigma' y^2$	Slope
Total	1619.76	1.03	29.84	0.55	0.48	0.02
Means	23.54	0.04	-0.09	0.00	0.04	0.00
Difference	1596.22	0.99	29.92	0.56	0.43	0.02
1	429.60	0.13	5.41	0.07	0.06	0.01
2	325.88	0.28	8.03	0.20	0.08	0.02
3	439.57	0.18	7.98	0.14	0.04	0.02
4	401.17	0.39	8.51	0.18	0.21	0.02
Sum	1596.22	0.99	29.92	0.59	0.40	

Analysis Of Variance:

Source Of Variance	Sum Of Squares	Degrees Of Freedom	Mean Square
Means Of Correlation:	0.04	2	0.02
Difference Between Means Slope And Pooled Slope:	0.01	1	0.01
Between Slopes:	0.03	3	0.01
Error:	0.40	89	0.00
Total	0.48	95	

	Significance Value	Critical Significance Value
Significance Of Slopes:	2.26	**2.71**
Significance Of Intercepts:	2.64	**3.95**

Summary:

Pooled Slope:	0.018
Pooled Intercept:	0.036
Correlation Coefficient:	0.73

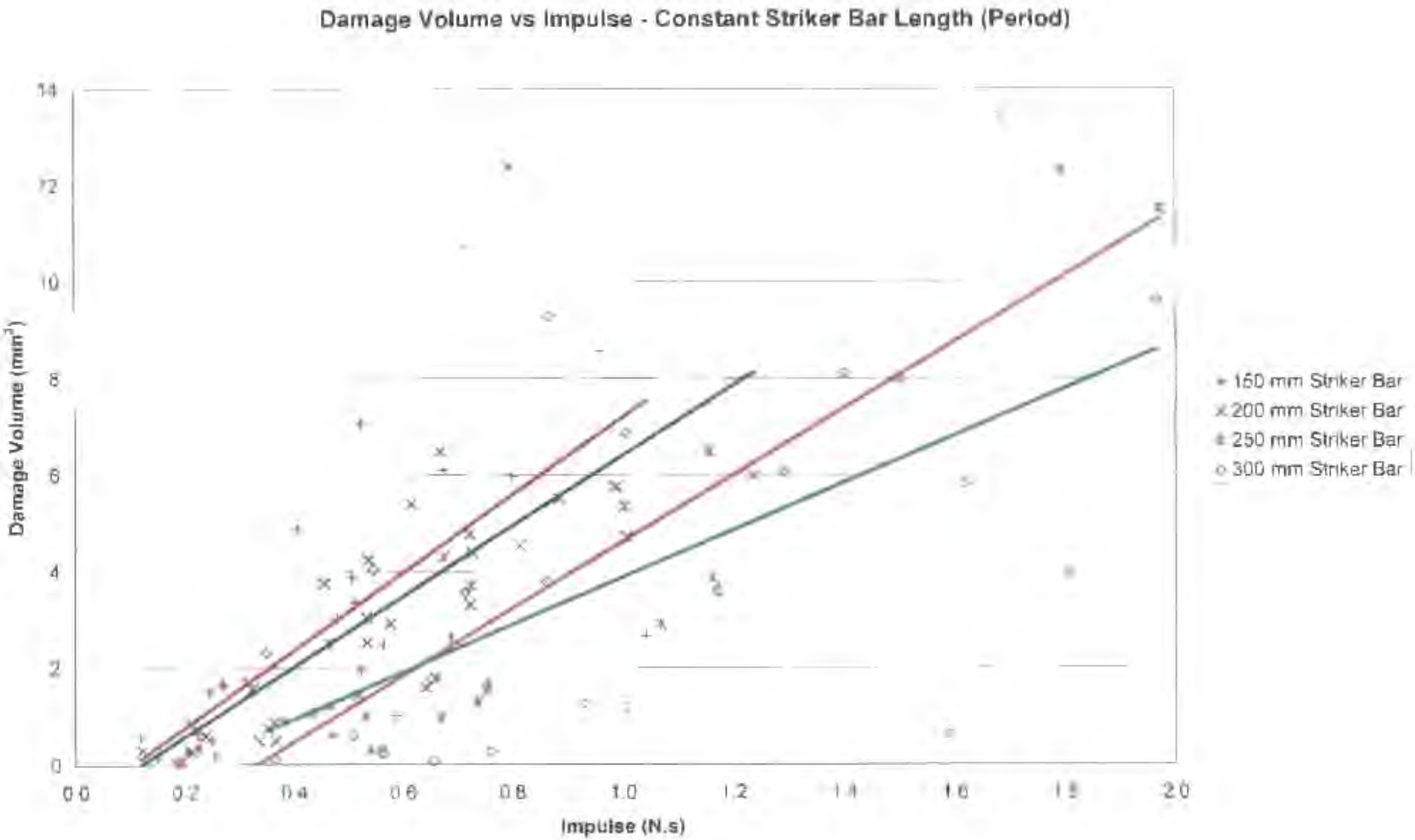
Damage Volume vs Impulse - Constant Striker Bar Length (Period)
Damage Volume (mm³)
Impulse (N.s)
0
2
4
6
8
10
12
14
0.0
0.2
0.4
0.6
0.8
1.0
1.2
1.4
1.6
1.8
2.0
150 mm Striker Bar
200 mm Striker Bar
250 mm Striker Bar
300 mm Striker Bar

Statistical Analysis Of Damage Volume vs Impulse - Constant Striker Bar Length

Original Data:

Striker Bar Length	150 mm	200 mm	250 mm	300 mm
N	25	27	21	24
Σx	11.45	15.50	16.58	24.39
Σx^2	6.69	10.85	17.19	30.16
Σy	70.95	89.05	66.44	94.93
Σy^2	398.90	486.50	438.22	690.85
Σxy	44.06	65.26	80.70	122.75

Sums Of Squares:

	$\Sigma' x^2$	$\Sigma' y^2$	$\Sigma' xy$	$\Sigma' c^2$	$\Sigma' y^2$	Slope
Total	17.32	949.80	87.74	444.42	505.38	5.06
Means	4.46	16.02	7.52	12.68	3.34	1.69
Difference	12.87	933.78	80.23	500.26	433.52	6.24
1	1.44	197.57	11.57	92.84	104.73	8.03
2	1.94	192.80	14.12	102.64	90.16	7.27
3	4.10	228.02	28.24	194.71	33.31	6.89
4	5.38	315.39	26.29	128.38	187.01	4.88
Sum	12.87	933.78	80.23	518.57	415.21	

Analysis Of Variance:

Source Of Variance	Sum Of Squares	Degrees Of Freedom	Mean Square
Means Of Correlation:	3.34	2	1.67
Difference Between Means Slope And Pooled Slope:	68.52	1	68.52
Between Slopes:	18.31	3	6.10
Error:	415.21	89	4.67
Total	505.38	95	

	Significance Value	Critical Significance Value
Significance Of Slopes:	1.31	**2.71**
Significance Of Intercepts:	14.69	**3.95**

Summary:

Pooled Slope:	5.06

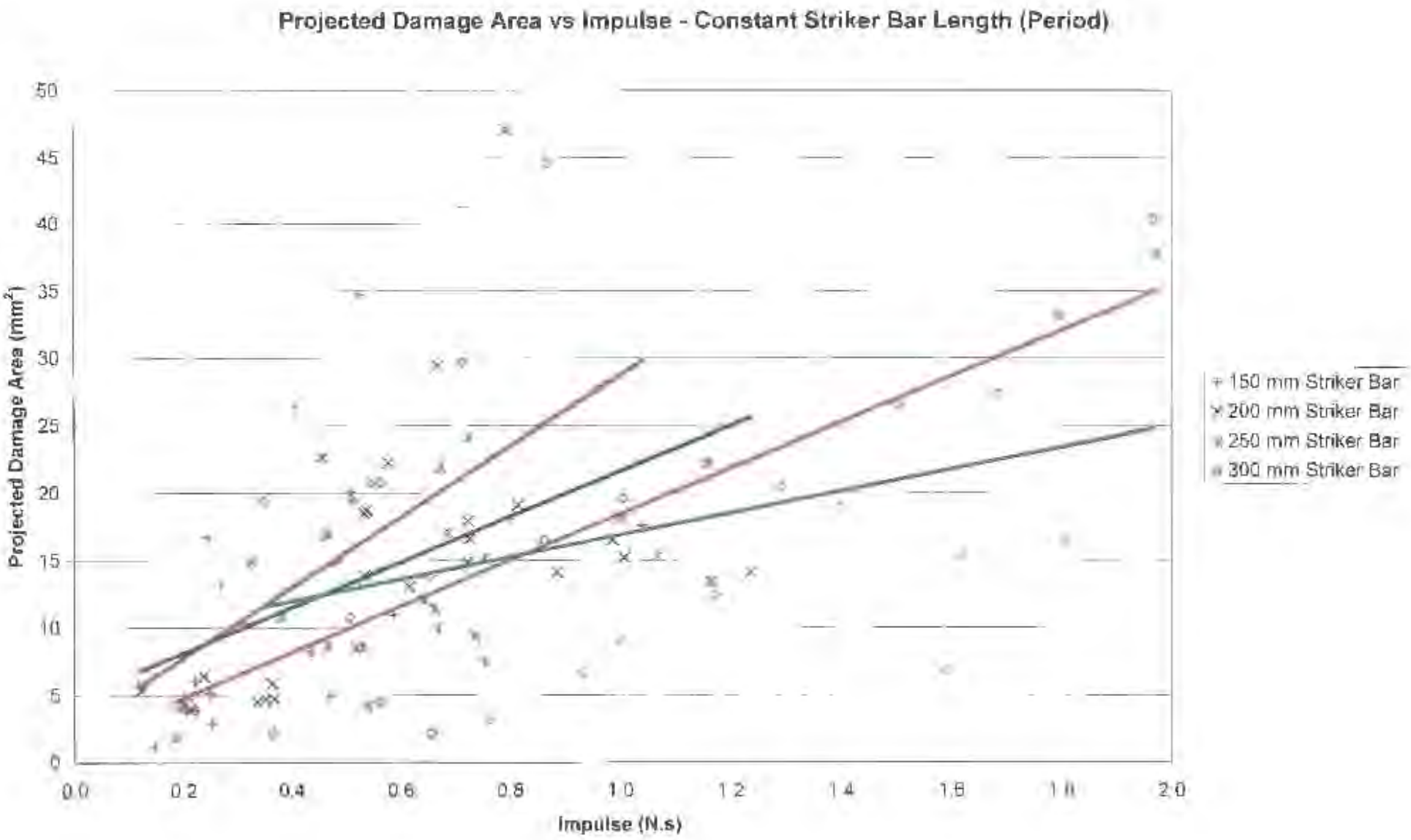
Projected Damage Area vs Impulse - Constant Striker Bar Length (Period)
Projected Damage Area (mm²)
Impulse (N.s)
0
5
10
15
20
25
30
35
40
45
50
0.0
0.2
0.4
0.6
0.8
1.0
1.2
1.4
1.6
1.8
2.0
150 mm Striker Bar
200 mm Striker Bar
250 mm Striker Bar
300 mm Striker Bar

Statistical Analysis Of Projected Damage Area vs Impulse - Constant Striker Bar Length

Original Data:

Striker Bar Length	150 mm	200 mm	250 mm	300 mm
N	25	27	21	24
Σx	11.45	15.50	16.58	24.39
Σx^2	6.69	10.85	17.19	30.16
Σy	362.54	389.73	311.69	408.26
Σy^2	7760.47	7878.40	6309.55	9799.80
Σxy	203.79	256.56	315.97	458.76

Sums Of Squares:

	$\Sigma' x^2$	$\Sigma' y^2$	$\Sigma' xy$	$\Sigma' c^2$	$\Sigma' y^2$	Slope
Total	17.32	9403.49	204.15	2405.92	6997.58	11.78
Means	4.46	109.35	19.89	88.74	20.61	4.46
Difference	12.87	9294.14	184.27	2639.04	6655.10	14.32
1	1.44	2502.96	37.73	987.89	1515.07	26.18
2	1.94	2252.84	32.76	552.09	1700.75	16.85
3	4.10	1683.41	69.85	1191.10	492.31	17.05
4	5.38	2854.93	43.92	358.23	2496.70	8.16
Sum	12.87	9294.14	184.27	3089.31	6204.83	

Analysis Of Variance:

Source Of Variance	Sum Of Squares	Degrees Of Freedom	Mean Square
Means Of Correlation:	20.61	2	10.31
Difference Between Means Slope And Pooled Slope:	321.86	1	321.86
Between Slopes:	450.27	3	150.09
Error:	6204.83	89	69.72
Total	6997.58	95	

	Significance Value	Critical Significance Value
Significance Of Slopes:	2.15	**2.71**
Significance Of Intercepts:	4.62	**3.95**

Summary:

Pooled Slope:	11.78

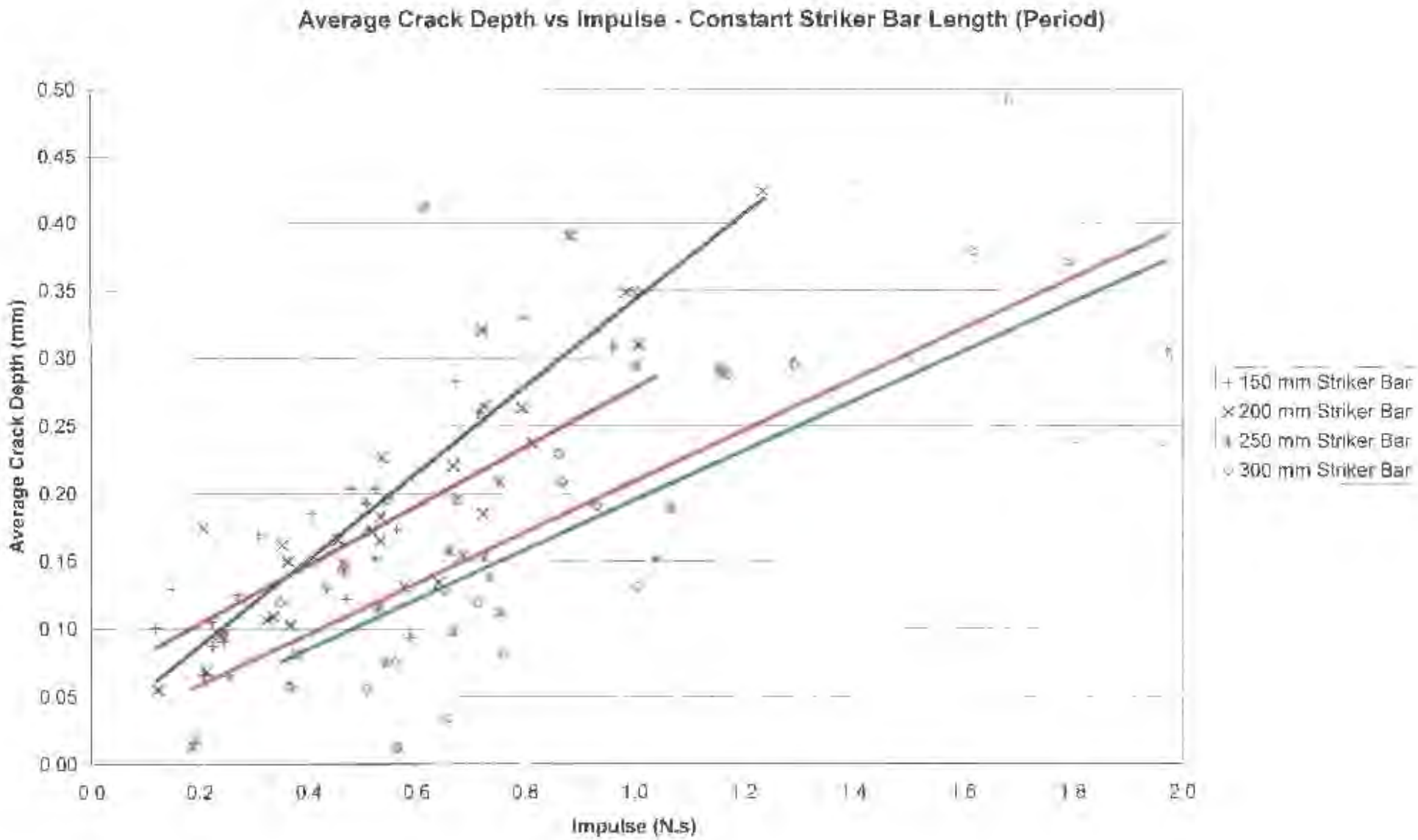
Average Crack Depth vs Impulse - Constant Striker Bar Length (Period)
Average Crack Depth (mm)
0.50
0.45
0.40
0.35
0.30
0.25
0.20
0.15
0.10
0.05
0.00
0.0
0.2
0.4
0.6
0.8
1.0
1.2
1.4
1.6
1.8
2.0
Impulse (N.s)
150 mm Striker Bar
200 mm Striker Bar
250 mm Striker Bar
300 mm Striker Bar

Statistical Analysis Of Average Crack Depth vs Impulse - Constant Striker Bar Length

Original Data:

Striker Bar Length	150 mm	200 mm	250 mm	300 mm
N	25	27	21	24
Σx	11.45	15.50	16.58	24.39
Σx^2	6.69	10.85	17.19	30.16
Σy	4.00	5.58	3.55	4.75
Σy^2	0.77	1.43	0.79	1.33
Σxy	2.14	3.82	3.58	5.81

Sums Of Squares:

	$\Sigma' x^2$	$\Sigma' y^2$	$\Sigma' xy$	$\Sigma' c^2$	$\Sigma' y^2$	Slope
Total	17.32	1.03	2.84	0.46	0.56	0.16
Means	4.46	0.04	0.15	0.00	0.03	0.03
Difference	12.87	0.99	2.69	0.56	0.43	0.21
1	1.44	0.13	0.31	0.07	0.06	0.22
2	1.94	0.28	0.62	0.20	0.08	0.32
3	4.10	0.18	0.77	0.14	0.04	0.19
4	5.38	0.39	0.99	0.18	0.21	0.18
Sum	12.87	0.99	2.69	0.59	0.40	

Analysis Of Variance:

Source Of Variance	Sum Of Squares	Degrees Of Freedom	Mean Square
Means Of Correlation:	0.03	2	0.02
Difference Between Means Slope And Pooled Slope:	0.10	1	0.10
Between Slopes:	0.03	3	0.01
Error:	0.40	89	0.00
Total	0.56	95	

	Significance Value	Critical Significance Value
Significance Of Slopes:	2.18	**2.71**
Significance Of Intercepts:	23.03	**3.95**

Summary:

Pooled Slope:	0.16

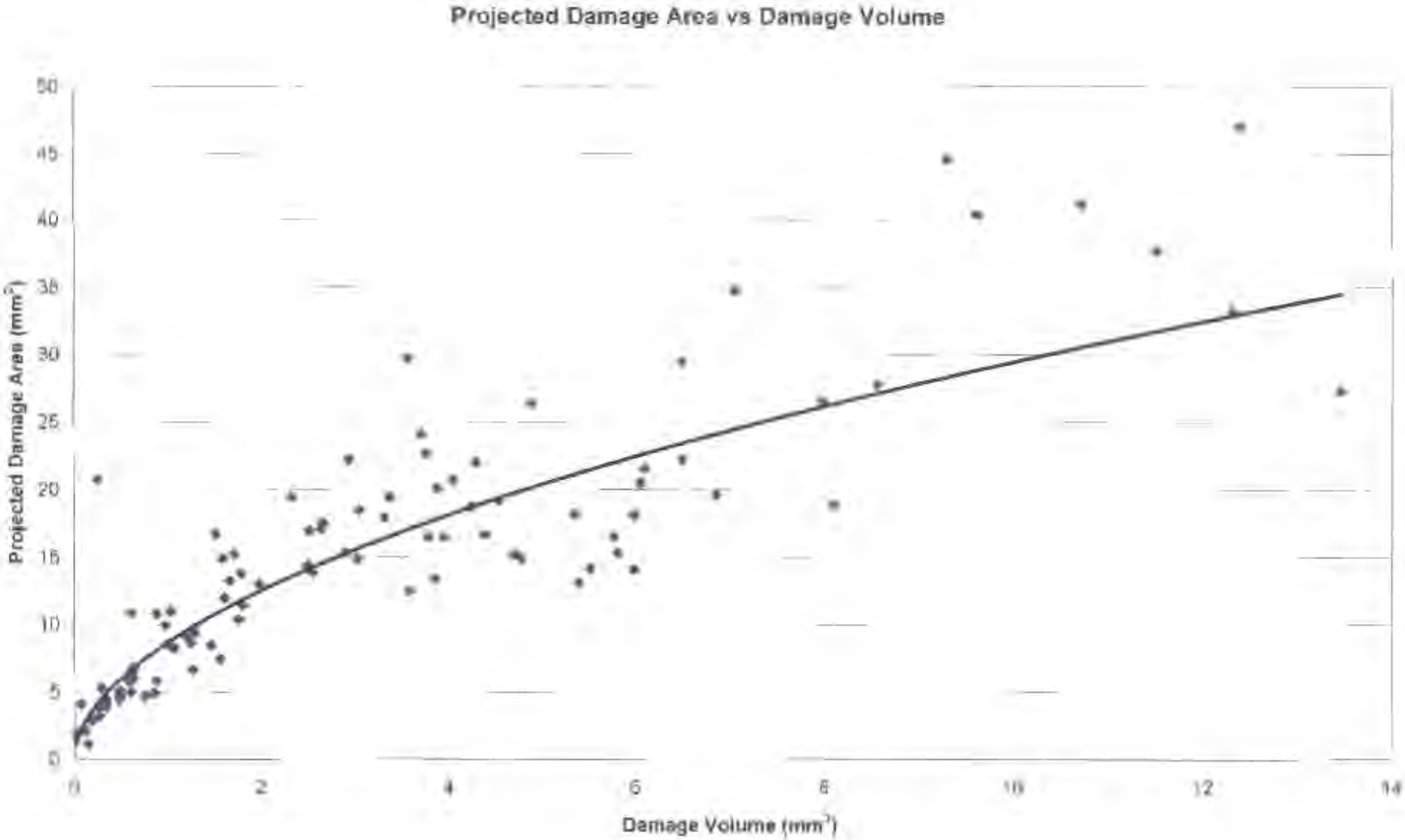
Projected Damage Area vs Damage Volume
Projected Damage Area (mm²)
Damage Volume (mm³)
0
5
10
15
20
25
30
35
40
45
50
0
2
4
6
8
10
12
14

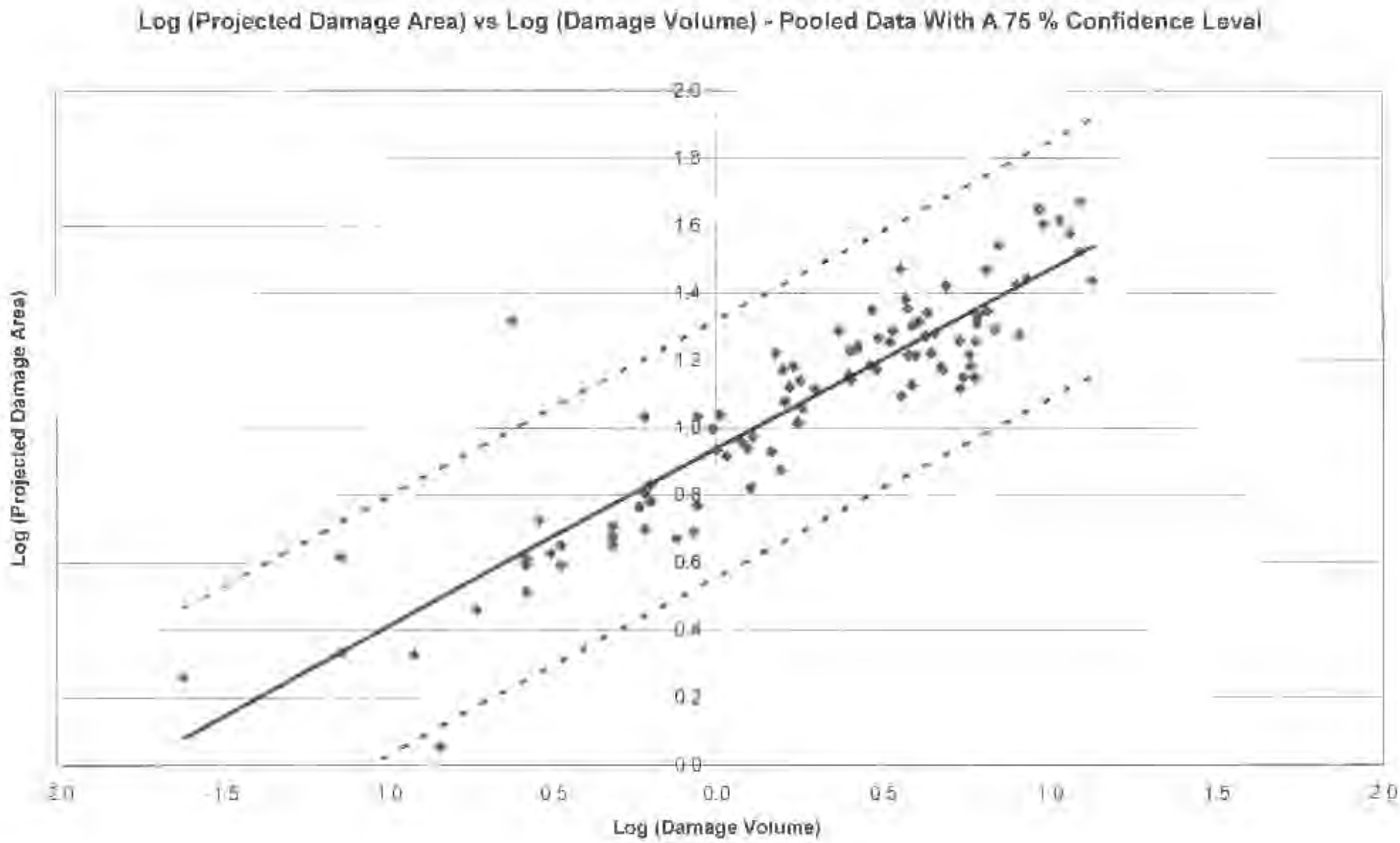
Log (Projected Damage Area) vs Log (Damage Volume) - Pooled Data With A 75 % Confidence Level
Log (Projected Damage Area)
2.0
1.8
1.6
1.4
1.2
1.0
0.8
0.6
0.4
0.2
0.0
-2.0
-1.5
-1.0
-0.5
0.0
0.5
1.0
1.5
2.0
Log (Damage Volume)

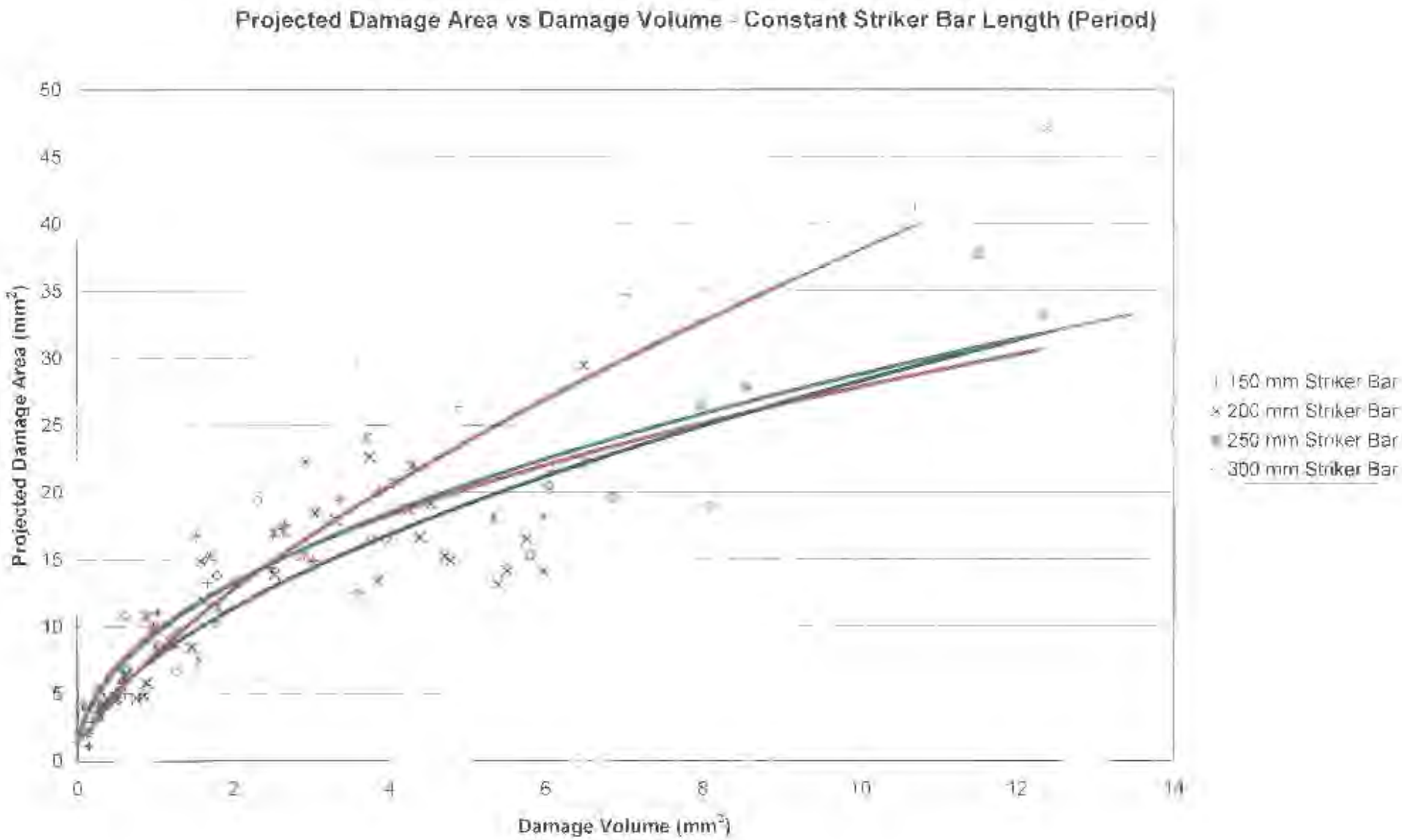
Projected Damage Area vs Damage Volume - Constant Striker Bar Length (Period)
Projected Damage Area (mm²)
Damage Volume (mm³)
0
5
10
15
20
25
30
35
40
45
50
0
2
4
6
8
10
12
14
150 mm Striker Bar
200 mm Striker Bar
250 mm Striker Bar
300 mm Striker Bar

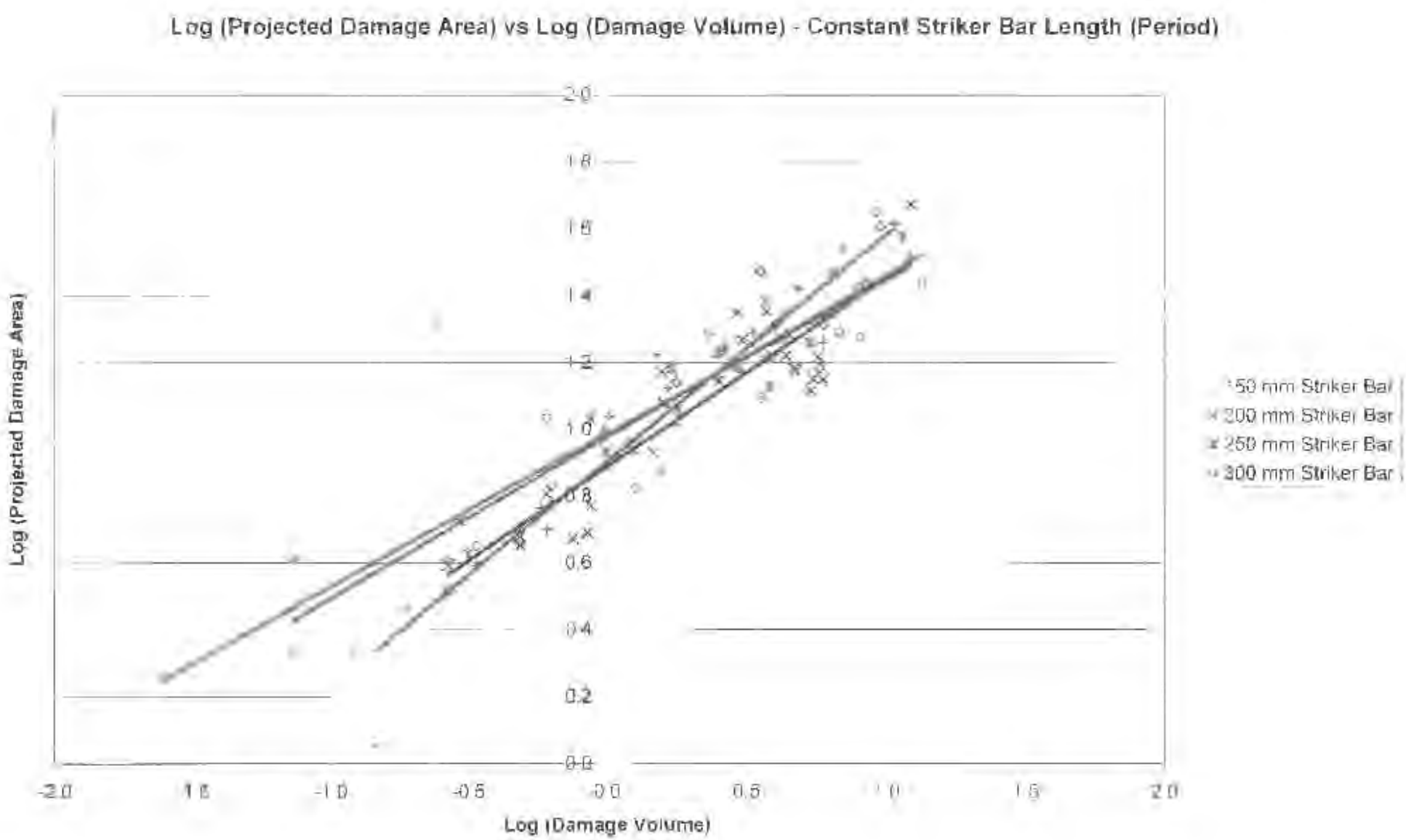
Log (Projected Damage Area) vs Log (Damage Volume) - Constant Striker Bar Length (Period)
Log (Projected Damage Area)
Log (Damage Volume)
2.0
1.8
1.6
1.4
1.2
1.0
0.8
0.6
0.4
0.2
0.0
-2.0
-1.5
-1.0
-0.5
0.0
0.5
1.0
1.5
2.0
150 mm Striker Bar
200 mm Striker Bar
250 mm Striker Bar
300 mm Striker Bar

Statistical Analysis Of Log (Projected Damage Area) vs Log (Volume Loss) - Constant Striker Bar Length

Original Data:

Striker Bar Length	150 mm	200 mm	250 mm	300 mm
N	25	27	21	24
Σx	4.91	9.03	4.34	6.84
Σx^2	7.76	8.47	9.44	11.72
Σy	25.88	29.03	22.69	26.72
Σy^2	30.14	33.31	26.49	32.83
Σxy	9.69	12.79	8.61	12.34

Sums Of Squares:

	$\Sigma' x^2$	$\Sigma' y^2$	$\Sigma' xy$	$\Sigma' c^2$	$\Sigma' y^2$	Slope
Total	30.90	10.58	16.42	8.72	1.86	0.53
Means	0.33	0.08	0.08	0.02	0.06	0.25
Difference	30.57	10.50	16.34	8.73	1.78	0.53
1	6.80	3.35	4.61	3.13	0.22	0.68
2	5.46	2.10	3.08	1.74	0.36	0.56
3	8.55	1.97	3.92	1.80	0.17	0.46
4	9.77	3.09	4.73	2.28	0.81	0.48
Sum	30.57	10.50	16.34	8.95	1.56	

Analysis Of Variance:

Source Of Variance	Sum Of Squares	Degrees Of Freedom	Mean Square
Means Of Correlation:	0.06	2	0.03
Difference Between Means Slope And Pooled Slope:	0.03	1	0.03
Between Slopes:	0.22	3	0.07
Error:	1.56	89	0.02
Total	1.86	95	

	Significance Value	Critical Significance Value
Significance Of Slopes:	1.58	**2.71**
Significance Of Intercepts:	1.51	**3.95**

Summary:

Pooled Slope:	0.53
Pooled Intercept:	0.94
Correllation Coefficient:	0.91

APPENDIX – SAMPLES OF UNPROCESSED EXPERIMENTAL DATA


Voltage vs Time - 150 mm Striker Bar
Voltage (V)
5
4
3
2
1
0
-1
-2
-3
-4
-5
0
0.0002
0.0004
0.0006
0.0008
0.001
Time (s)
Incident Bar
Transmitter Bar

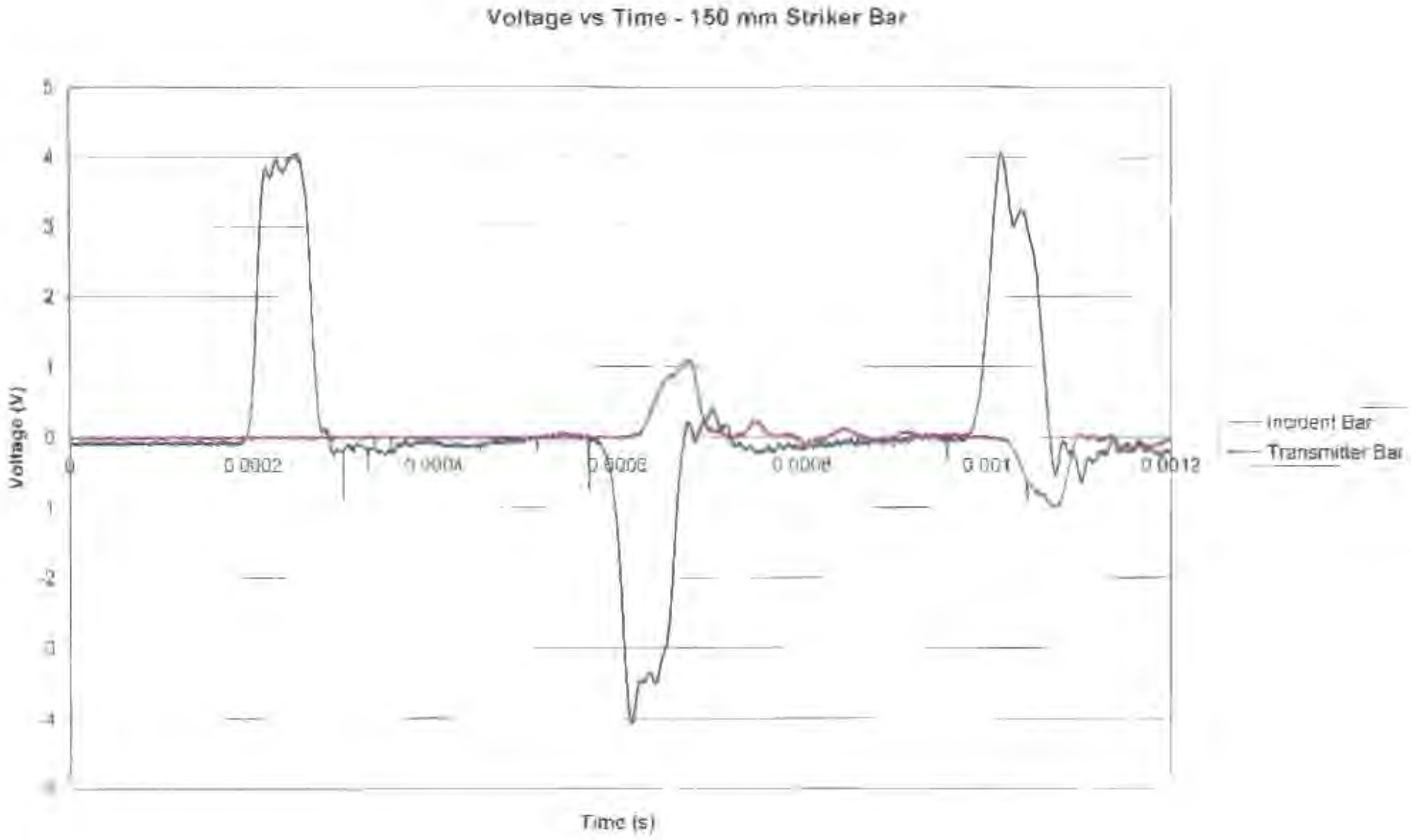
Voltage vs Time - 150 mm Striker Bar
Voltage (V)
5
4
3
2
1
0
-1
-2
-3
-4
0
0.0002
0.0004
0.0006
0.0008
0.001
0.0012
Time (s)
Incident Bar
Transmitter Bar

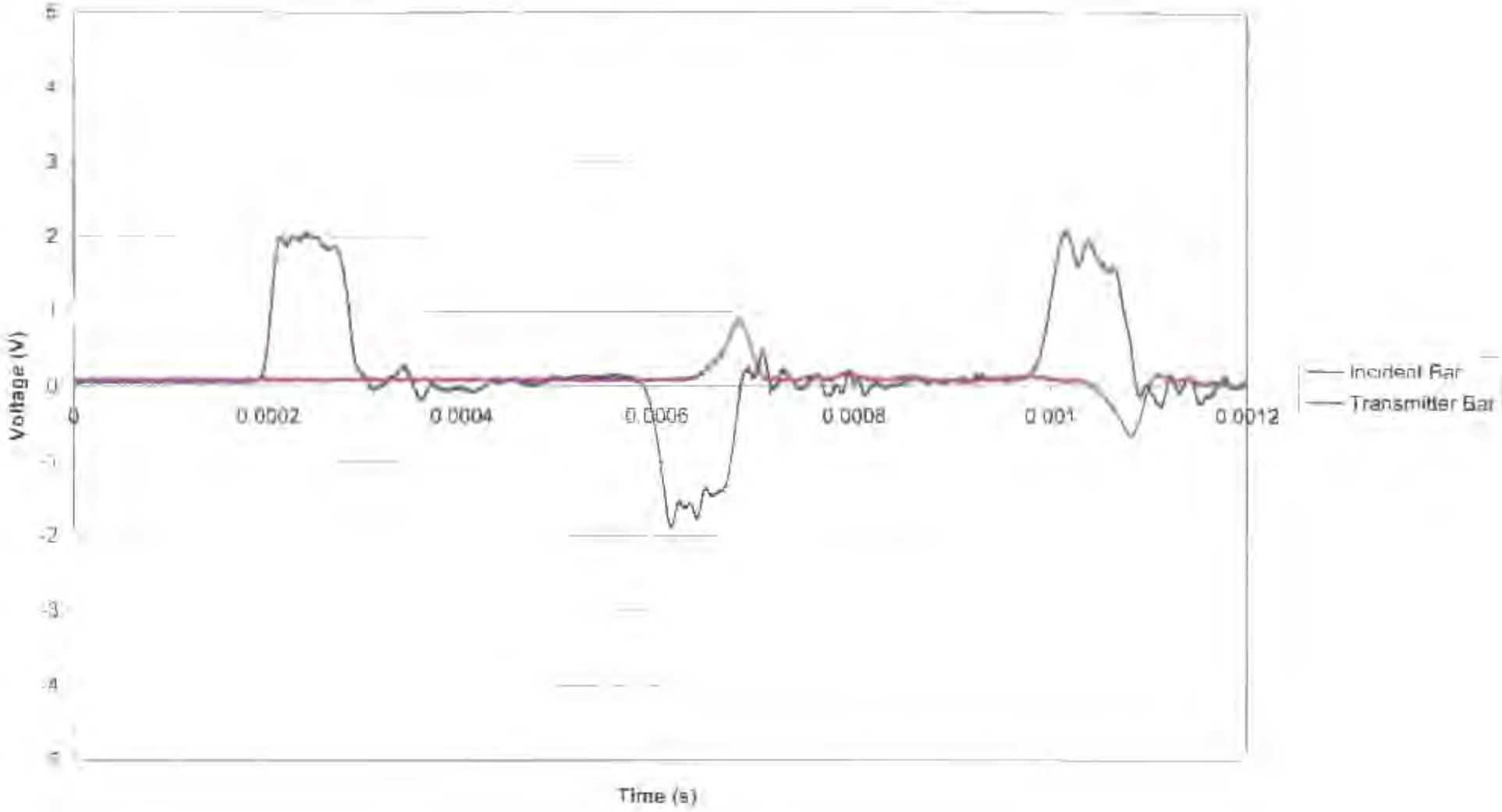
Voltage vs Time - 200 mm Striker Bar
Voltage (V)
Time (s)
0
0.0002
0.0004
0.0006
0.0008
0.001
0.0012
Incident Bar
Transmitter Bar

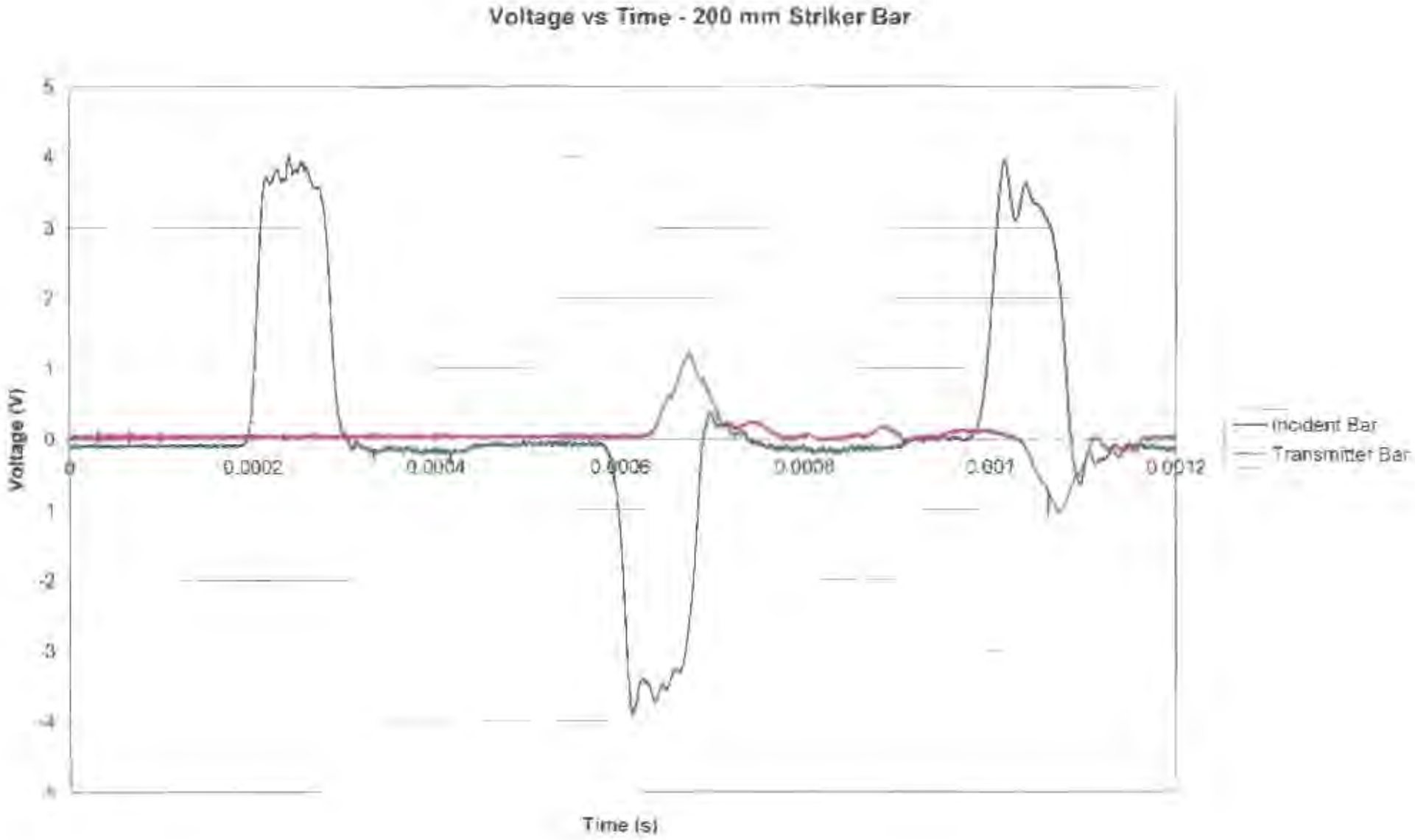
Voltage vs Time - 200 mm Striker Bar
Voltage (V)
5
4
3
2
1
0
-1
-2
-3
-4
-5
0
0.0002
0.0004
0.0006
0.0008
0.001
0.0012
Time (s)
Incident Bar
Transmitter Bar

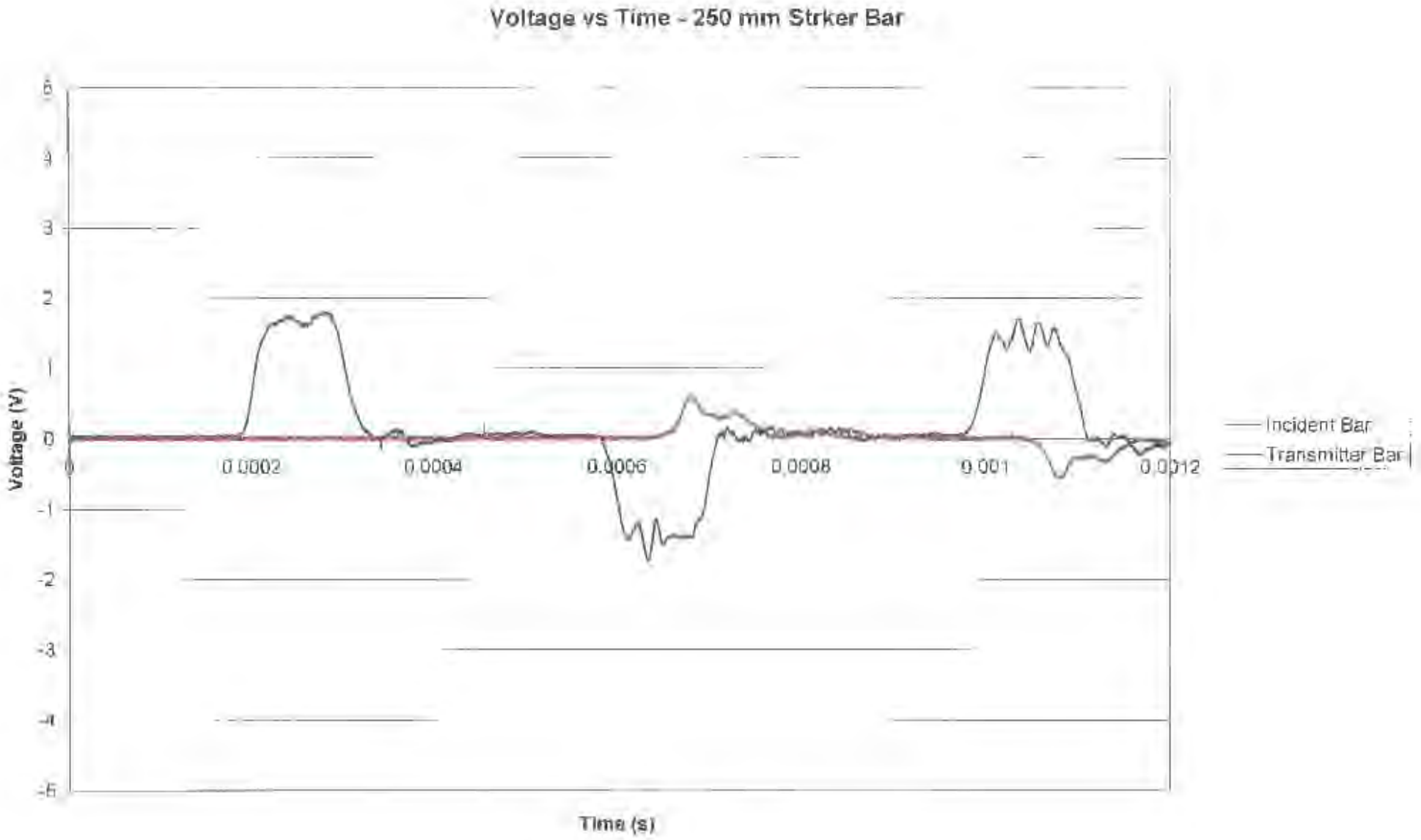
Voltage vs Time - 250 mm Strker Bar
Voltage (V)
Time (s)
0
0.0002
0.0004
0.0006
0.0008
0.001
0.0012
Incident Bar
Transmitter Bar

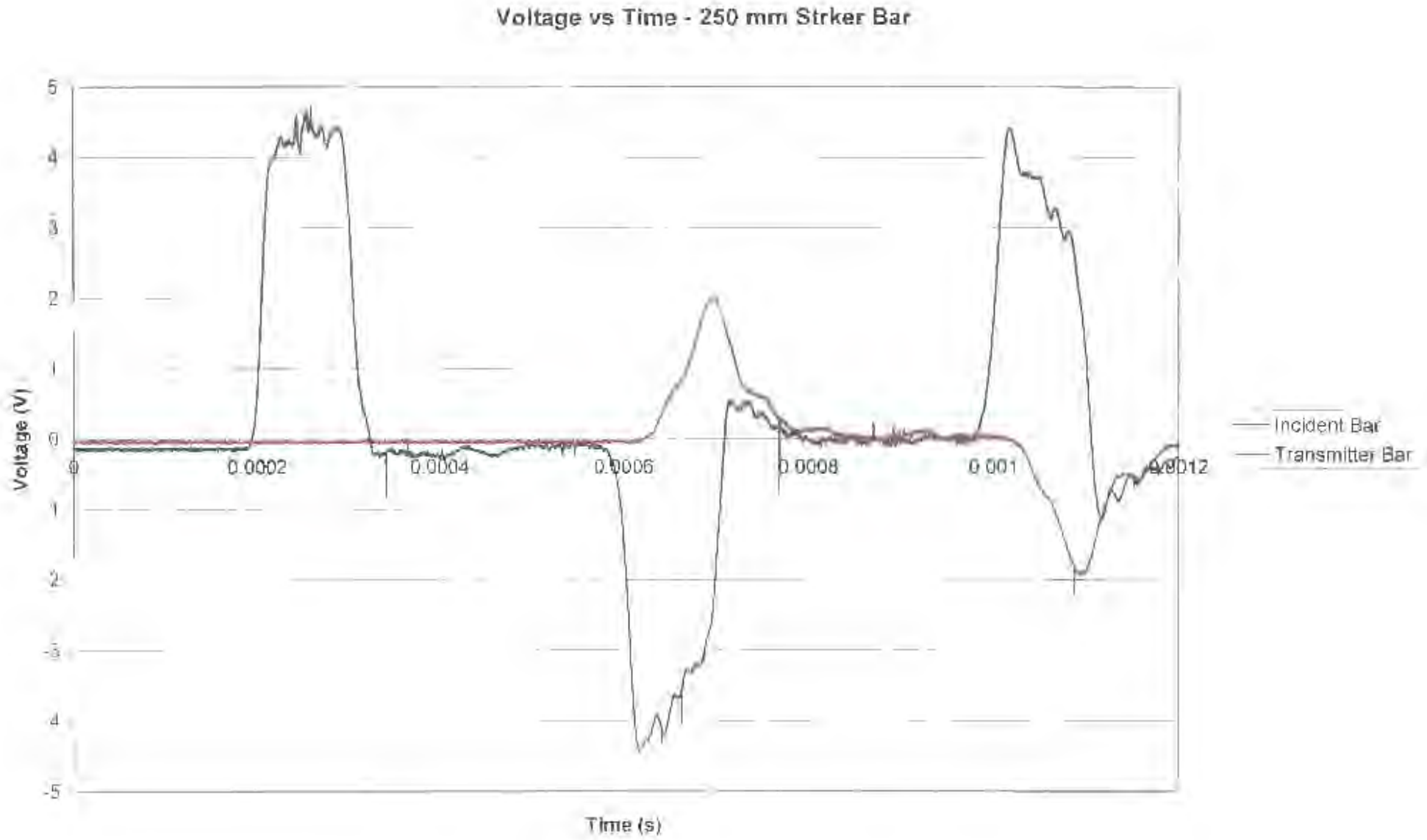
Voltage vs Time - 250 mm Strker Bar
Voltage (V)
5
4
3
2
1
0
1
2
3
4
-5
0
0.0002
0.0004
0.0006
0.0008
0.001
0.0012
Time (s)
Incident Bar
Transmitter Bar

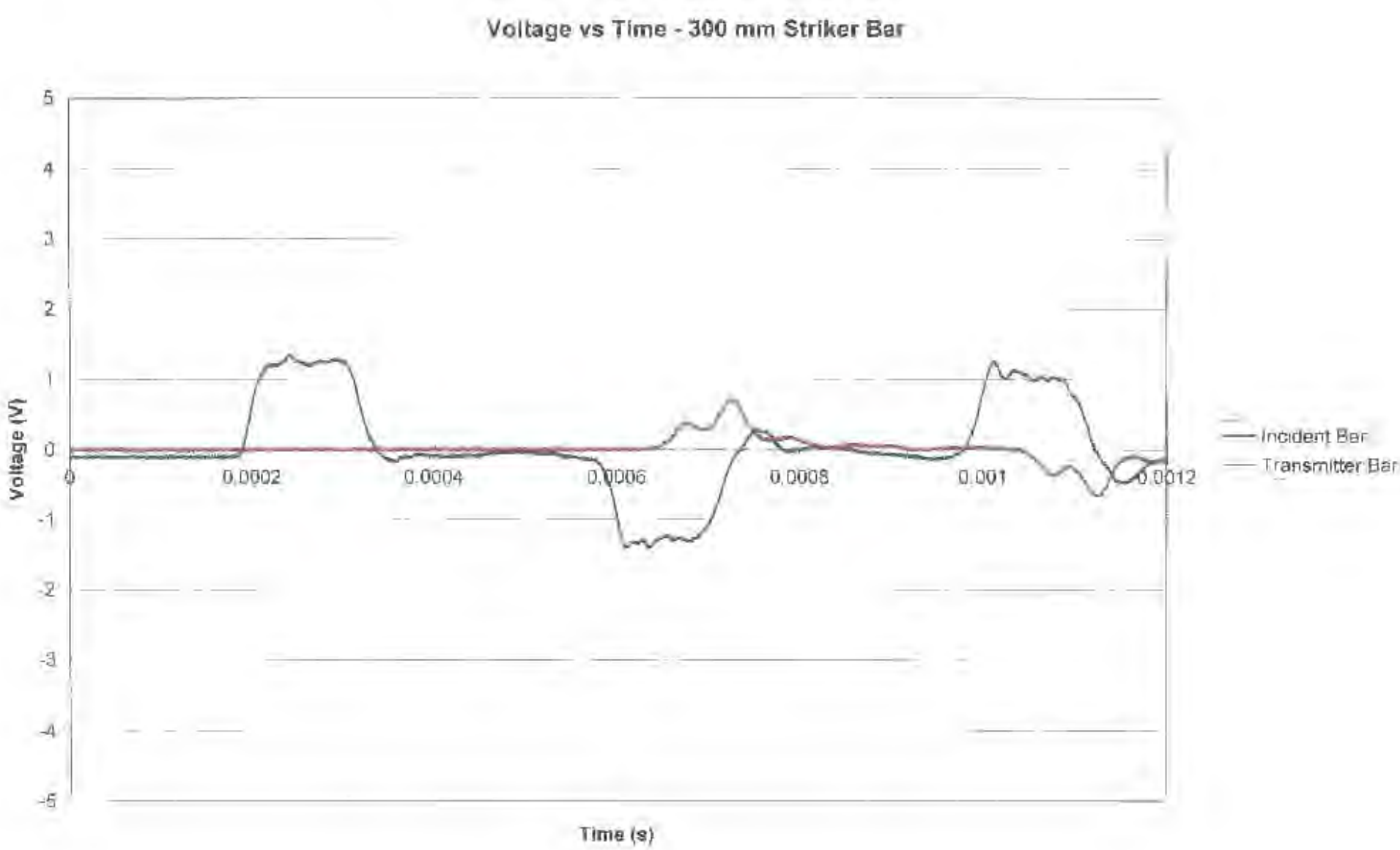
Voltage vs Time - 300 mm Striker Bar
Voltage (V)
5
4
3
2
1
0
-1
-2
-3
-4
-5
0
0.0002
0.0004
0.0006
0.0008
0.001
0.0012
Time (s)
Incident Bar
Transmitter Bar

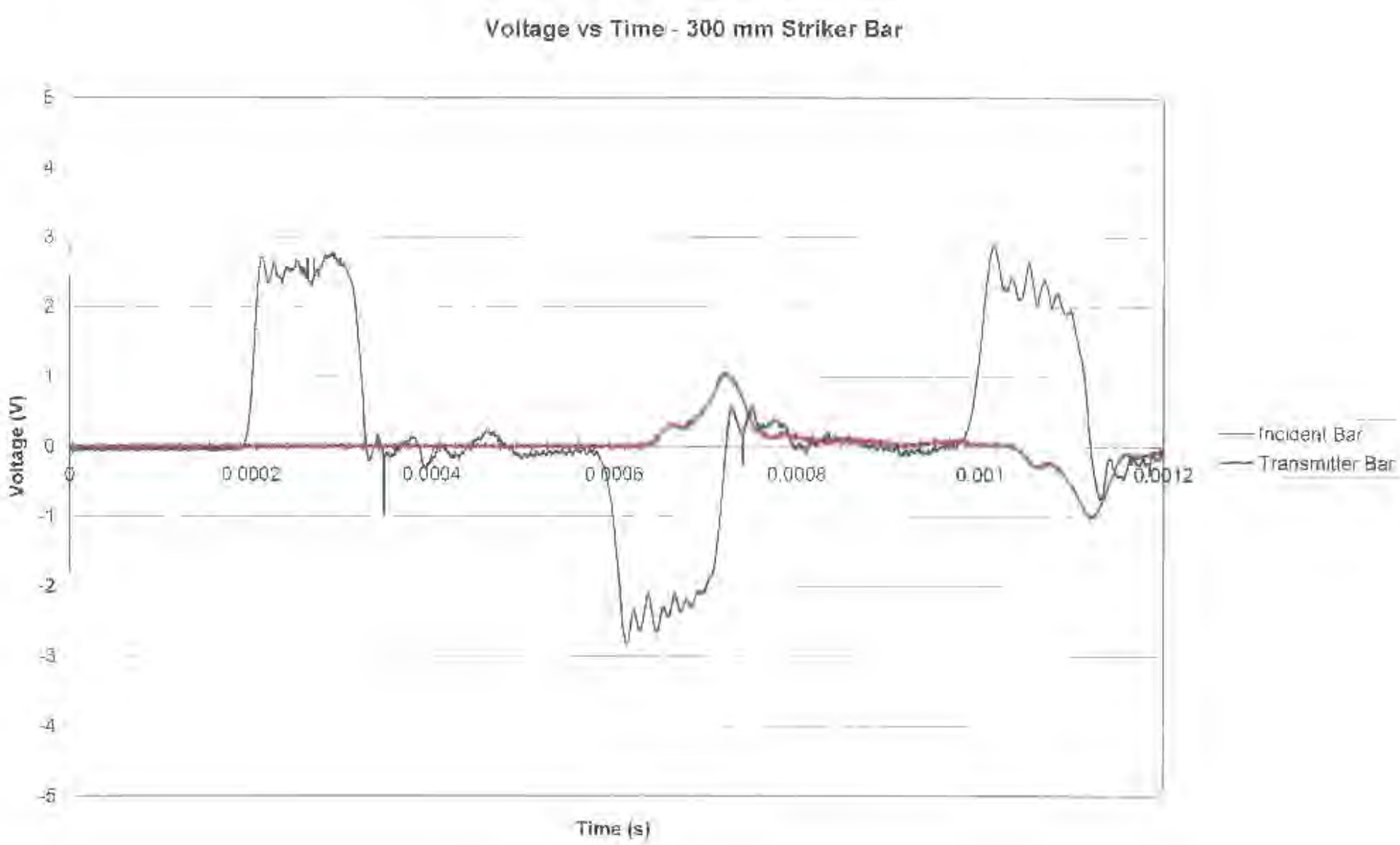
Voltage vs Time - 300 mm Striker Bar
Voltage (V)
5
4
3
2
1
0
-1
-2
-3
-4
-5
0
0.0002
0.0004
0.0006
0.0008
0.001
0.0012
Time (s)
Incident Bar
Transmitter Bar